DOC.20041028.0004

OCRWM	DESIGN CALCULATION OR ANALYSIS COVER SHEET	1. QA: QA 2. Page 1

3. System	4. Document Identifier
Waste Isolation System	CAL-WIS-AC-000002 REV 00A

5. Title

Mechanical Assessment of the Drip Shield Subject to Vibratory Motion and Dynamic and Static Rock Loading

6. Group

Regulatory Integration Team

7. Document Status Designation

☒ Preliminary ☐ Final ☐ Cancelled

8. Notes/Comments

This calculation was checked by Tim Schmitt with the exception of Attachment A. Attachment A was checked by Ming Lin.

Attachments	Total Number of Pages
Attachment A (Compact Disk 1 of 1)	2 ~~N/A~~ PaBD MB 10/27/04

RECORD OF REVISIONS

9. No.	10. Reason For Revision	11. Total # of Pgs.	12. Last Pg. #	13. Originator (Print/Sign/Date)	14. Checker (Print/Sign/Date)	15. QER (Print/Sign/Date)	16. Approved/Accepted (Print/Sign)	17. Date
00A	Initial issue	154	A-2	Branko Damjanac SIGNATURE ON FILE 10/27/04	Tim Schmitt SIGNATURE ON FILE Ming Lin SIGNATURE ON FILE 10/27/04	D. J. Tunney SIGNATURE ON FILE 10/27/2004	MARK BOARD SIGNATURE ON FILE	10/27/04

INTENTIONALLY LEFT BLANK

CONTENTS

Page

FIGURES

Page

FIGURES (Continued)

Page

TABLES

Page

TABLES (Continued)

Page

ACRONYMS AND ABBREVIATIONS

DE	distinct element (software)
DS	drip shield
DSC	drip shield connector
EBS	engineered barrier system
FE	finite element (software)
MN	megaNewton
MT	metric ton (1 MT = 1,000 kg)
PGV	peak ground velocity
PSHA	Probabilistic Seismic Hazard Assessment
PWR	pressurized water reactor
RT	room temperature
Ti	Titanium
TSPA-LA	Total System Performance Assessment - License Application

1. PURPOSE

The purpose of the drip shield (DS) is to divert water that may seep into emplacement drifts from contacting the waste packages, and to protect the waste packages from impact or static loading from rockfall. The objective of this document is to summarize, into one location, the results of a series of supporting engineering calculations[1] that were developed to study the effect of static and dynamic loads on the mechanical performance of the DS. The potential DS loads are a result of:

- Potential earthquake vibratory ground motion, and resulting interaction of the DS, waste package and pallet, and drift invert
- Dynamic impacts of rockfall resulting from emplacement drift damage as a result of earthquake vibratory motion
- Static load of the caved rock rubble that may come to rest on the DS as a result of vibratory motion or from time-dependent yielding of the rock mass surrounding the emplacement drift.

The potential mechanical failure mechanisms that may result from these loads include:

- Overturning and/or separation of the interlocking DS segments
- Loss of structural integrity and stability of the DS, including excessive deformation or buckling
- Localized damage[2] to the top and side-wall plates of the DS.

The scope of this document is limited to summarizing results presented in the supporting calculations in the areas of analysis of the potential for DS collapse, and determination of the damaged surface area of the DS plates. New calculations are presented to determine whether or not separation of DSs occur under vibratory motion.

The results of the supporting calculations, in terms of damaged surface area of DS plates for a given value of peak ground velocity (PGV) are reported in *D&E /PA/C IED Interlocking Drip Shield and Emplacement Pallet* (BSC 2004 [DIRS 169220]). These data are used as input to the *Seismic Consequence Abstraction* (BSC 2004 [DIRS 169183]), which utilizes this information to address the potential for advective flux of seepage water through the DS. Additionally, the new calculations presented in this document provide the technical basis for exclusion of separation of

[1] Most of the results reported here were previously reported in the following calculations: *Structural Calculations of Drip Shield Exposed to Vibratory Ground Motion* (BSC 2003, [DIRS 163425]); *Drip Shield Structural Response to Rock Fall* (BSC 2004, [DIRS 168993]); and, *Structural Stability of a Drip Shield Under Quasi-Static Pressure* (BSC 2004, [DIRS 170791]). This calculation provides new information on analysis of the potential for DS separation.

[2] The "damaged area" is defined in this document as the area where the residual first (major) principal stress exceeds a certain limit. The stress limit used throughout this document is defined as 50 percent of yield strength of the DS plate material, Titanium Grade 7 (Ti-7) (SB-265 R52400), at temperature of 150°C (see Assumptions 3.12 and 3.18 and Section 5.2.3.1.4).

DSs under vibratory ground motion from consideration in the Total System Performance Assessment-License Application (TSPA-LA). The exclusion arguments for DS separation are summarized in *Features, Events, and Processes: Disruptive Events* (BSC 2004 [DIRS 170017], Sections 6.2.1.5 and 6.2.1.3) (FEP 1.2.03.02.0A – Seismic Ground Motion Damages EBS Components) and the *Seismic Consequence Abstraction* (BSC 2004 [DIRS 169183]). The *Seismic Consequence Abstraction* subsequently provides the abstraction for the seismic scenario class used in support of the Total System Performance Assessment–License Application (TSPA-LA).

This document is prepared in accordance with the applicable technical work plan: *Technical Work Plan For: Regulatory Integration Modeling of Drift Degradation, Waste Package and Drip Shield Vibratory Motion and Seismic Consequences* (BSC 2004 [DIRS 171520]), which directs the work identified in work package ARTM05. The technical work plan was prepared in accordance with AP-2.27Q, *Planning for Science Activities.* This calculation was performed under the Repository Integration Project, in cooperation with the Waste Package and Components group of Design and Engineering. This document was developed in conformance with procedure AP-3.12Q, *Design Calculations and Analyses*. The DS is classified as a Safety Category item (BSC 2004 [DIRS 168361], p. A-5). Therefore, this calculation is subject to the *Quality Assurance Requirements and Description* (DOE 2004 [DIRS 171539]).

The DS design considered in the calculations summarized in this document is not presented in detail. Design drawings and material specifications can be found in *D&E / PA/C IED Interlocking Drip Shield and Emplacement Pallet* (BSC 2004 [DIRS 169220]) as well as in the calculations that support this summary document (BSC 2003 [DIRS 163425]; BSC 2004 [DIRS 168993] and BSC 2004 [DIRS 170791]). The dimensions and materials for the design of the 21-PWR (pressurized water reactor) waste package and emplacement pallet (pallet, for brevity, throughout the document) used in this calculation are also provided in *Emplacement Pallet* (BSC 2003 [DIRS 161520]) and *D&E/PA/C IED Typical Waste Package Components Assembly* (BSC 2004 [DIRS 169472]). The 21-PWR waste package was used as a basis for the calculations summarized in this document since it is the most commonly-occurring of the various waste package designs. More than 38 percent of all waste packages are 21-PWR waste packages, and the second most frequent design, the 44-boiling water reactor waste package (approximately 26 percent), has similar dimensions and mass as the 21-PWR waste package (BSC 2004 [DIRS 169472], Table 11).

2. METHOD

The DS calculations presented in this summary are conducted using commercial finite element (FE) and distinct element (DE) software. The FE method is a numerical technique in common use for analysis of engineering problems in structural dynamics. The method requires discretization of the structure (the DS in this case) into a number of elements (the FE mesh) that are interconnected by nodal points. The governing equations of motion, subject to imposed boundary and initial conditions, are solved to provide the solution of the transient mechanical response of the DS. The boundary and initial conditions are a result of the constraints supplied by the emplacement drift, waste package and pallet and from the applied static and dynamic loading conditions. The FE analysis is used primarily to examine damage to the DS surface plates and structure in response to vibratory motion, rockfall and quasi-static pressure from rock rubble resulting from possible drift collapse. Results of the FE analysis are given in terms of the transient induced stresses, strains and displacements of the finite element mesh. Three-dimensional graphical representation of the motion of the structure as well as the stress and strain states are used to aid in interpretation of the analysis results. The stability of the structure and damage to the surface plates can be inferred from this information. The DE method is a numerical technique used for analysis of mechanical interaction of a large number of solid (deformable or rigid) bodies, which can undergo large displacements and interact with each other in arbitrary ways. If the bodies are deformable, they are discretized into elements, which are interconnected by nodal (grid) points. The equations of motion are solved for each grid point using an explicit numerical integration scheme, and are subject to the applied initial and boundary conditions. The DE method is used to examine the potential for DS separation when subjected to vibratory motion. The time history of relative vertical offset of the DSs as well as axial forces generated in interlocking portions of the DSs are used to determine whether DSs separate.

The DS FE mesh is created by using either the commercially available software ANSYS V5.6.2 (STN: 10364-5.6.2-01, [DIRS 159357]) or TrueGrid V2.1.5 and TrueGrid V2.2. The FE calculations were then performed by using the commercially available LS-DYNA V960.1106 (STN: 10300-960.1106-00, [DIRS 158898]) and LS-DYNA V970 D MPP-00 (STN: 10300-970.3858 D MPP-00, [DIRS 166918]) FE codes. The LS-DYNA explicit solver uses the central difference method (Belytschko et. al. 2000 [DIRS 153664], Section 6.2.1 and Hallquist 1998 [DIRS 155373], Section 21.2) for time integration of the governing equations. The DE calculations were performed using the commercially available software UDEC V3.1 (STN: 10173-3.1-00, [DIRS 160331]). This software has integral mesh development and post processing graphical display capability.

After the FE and DE calculations are completed, results of the analyses are presented in terms of separation of the DSs, collapse of the DS and damage to the surface plates and support beams and bulkheads. Separation of the DSs is determined by comparison of the time history of relative vertical separation of adjacent DSs and by comparison of axial forces generated in the interlocking mechanism of adjacent DSs to their estimated load limit. Damage results are provided in terms of the damaged area of the DS plates or maximum vertical deflection of the DS apex node at the vertical symmetry plane (for comparison with clearance of DS to waste package separation). The damaged area is estimated based on the residual first principal stress plot for the DS plates. It is important to acknowledge the conservatism of the criterion used to

define the damaged area (conservatism independent of the choice of the residual stress threshold). Namely, the failure criterion (see Section 1 and Assumption 3.18) does not account for the possibility of crack arrest once the crack is nucleated (i.e., the area "fails" regardless of the residual stress distribution across the thickness of the DS plates). Damage to the structural bulkheads and supporting columns is defined in terms of the plastic yield of the structural element cross section which may lead to formation of a plastic hinge, and thus loss of load-bearing capacity.

3. ASSUMPTIONS

In the course of developing this document, the following assumptions are made regarding the structural calculation.

3.1 The density and Poisson's ratio are not available for Titanium Grade 7 (Ti-7 [SB-65 R52400]), Titanium Grade 24 (Ti-24 [SB-265 R56405]), and Alloy 22 (SB-575 N06022), except at room temperature (RT) (20 ºC). (Note: In regard to Unified Numbering System designation for Ti-24, notice that Ti-24 has the same mechanical properties as Ti-5 since the compositions are almost identical; see ASME 2001 [DIRS 158115], Section II, Part B, SB-265, Table 2.) The RT density and RT Poisson's ratio are assumed for these materials. The impact of using RT density and RT Poisson's ratio is anticipated to be negligible. The rationale for this assumption is that the material properties in question do not have dominant impact on the calculation results. This assumption is used in Section 5.2.3 and corresponds to paragraph 5.2.8.6 of Mecham (2004 [DIRS 170673]).

3.2 The temperature-dependent material properties are not available for TSw2 (Topopah Spring Welded welded, lithophysal-poor) rock except at RT. The TSw2 is used to represent the essentially unyielding invert, drift walls and rock blocks impacting the DS (Section 5.2) and the material properties are necessary only for the contact definitions. The corresponding RT material properties are assumed for this material. The impact of using RT material properties is anticipated to be negligible. The rationale for this assumption is that the material properties of the rock do not have a significant impact on the calculation results. This assumption is used in Section 5.2.3 and corresponds to paragraph 5.2.16.1 of Mecham (2004 [DIRS 170673]).

3.3 The rate-dependent material properties are not available for Ti-7, Ti-24, Alloy 22, and TSw2 rock mass at any strain rate. The material properties obtained under the static loading conditions are assumed for these materials. The impact of using material properties obtained under static loading conditions is anticipated to be negligible. The rationale for this assumption is that the change of mechanical properties of subject materials (Nicholas 1980 [DIRS 154072], Figure 28) at the peak strain rates that typically occur during the earthquake simulation and rockfall does not have significant effect on the results presented in this calculation. The maximum plastic-strain rate in the DS plates observed in the calculation of vibratory ground motion is 185 s-1 (as indicated by maximum slopes of the effective-plastic-strain time histories presented in *Structural Calculations of Drip Shield Exposed to Vibratory Ground Motion*, BSC 2003 [DIRS 163425], Figure IV-9). It is important to recognize that this strain rate is the maximum among all 1×10^{-6} realizations among all DS-plate elements; the typical strain rate is significantly lower. The average strain rate is approximately 85 s-1 (BSC 2003 [DIRS 163425], Figure IV-10b). It should be noted that realization 9 is conspicuous among the 1×10^{-6} realizations for a large number of high-intensity waste

package-pallet impacts (BSC 2004 [DIRS 167083], Table 6.1.3-3) resulting in exceptionally large damaged area of the DS (Table 5-18). More typically, the next two largest strain rates among 1×10^{-6} realizations appear to be the strain rates in realizations 6 and 11, and they do not exceed 15 s-1 (BSC 2003 [DIRS 163425], Figures IV-11 and IV-12). The maximum strain rate during rockfall is approximately 40 s-1 as indicated by maximum slope (0.2/0.005 s) in *Drip Shield Structural Response to Rock Fall* (BSC 2004 [DIRS 168993], Figure II-3). This assumption is used in Section 5.2.3 and corresponds to paragraph 5.2.5 in Mecham (2004 [DIRS 170673]).

3.4 The Poisson's ratio of Alloy 22 is not available in the literature. The Poisson's ratio of Alloy 625 (SB-443 N06625) is assumed for Alloy 22. The impact of this assumption is anticipated to be negligible. The rationale for this assumption is that the chemical compositions of Alloy 22 and Alloy 625 are similar (ASME 2001 [DIRS 158115], Section II, Part B, SB-575, Table 1 and ASM 1980 [DIRS 104317], p. 143, respectively). This assumption is used in Section 5.2.3 and corresponds to paragraph 5.2.8.2 of Mecham (2004 [DIRS 170673]).

3.5 The uniform strains (the strains corresponding to the uniaxial tensile strengths) of Ti-7 and Ti-24 are not available in literature. Therefore, it is assumed that the uniform strain is equal to the elongation. The rationale for this assumption is that a small change in tangent modulus does not significantly affect the results of this calculation. This assumption is used in Section 5.2.3.1.2 and corresponds to Section 5.2.6.5 of Mecham (2004 [DIRS 170673]).

3.6 The modulus of elasticity and Poisson's ratio of the TSw2 are characterized by significant scatter of data. For the purpose of the present calculation modulus of elasticity is assumed to be 33 GPa, and Poisson's ratio 0.21. The rationale for this assumption is that these values represent the mean values of the middle nonlithophysal zone (Tptpmn) the uppermost interval of the TSw2 unit (BSC 2004 [DIRS 170583]), Tables 6 and 5, respectively, DTN: MO402DQRIRPPR.003 [DIRS 168901]). This assumption is used in Section 5.2.3.3 and corresponds to paragraph 5.2.16.3 of Mecham (2004 [DIRS 170673]).

3.7 The density of the TSw2 is assumed to be 2,370 kg/m. The rationale for this assumption is that this value represents the mean saturated bulk density value for the TSw2 unit determined from mechanical property measurements on core samples (DTN: SNL 02030193001.027 [DIRS 108410], Table S98487 007, Data for Tptpmn, Rows 82-89 and 128-132). It should be noted that this assumption has no effect on the calculation results since density of the rock affects only masses of the essentially rigid invert and the rigid drift walls. This assumption is used in Section 5.2.3.3 and corresponds to paragraph 5.2.16.4 of Mecham (2004 [DIRS 170673]).

3.8 The friction coefficients for metal-to-metal contact and metal-to-rock contact are considered random parameters in the calculation of vibratory motion because these parameters have a profound effect on calculation results. The range of values for both of these friction coefficients is 0.2 to 0.8. The following is the rationale for this assumption.

Avallone and Baumeister (1987 [DIRS 103508], Table 3.2.1, p. 3-26), provide coefficients of static and sliding friction for various metals and other materials. However, coefficients of friction for the materials used in this calculation are not specifically mentioned in this or other handbooks. The potential for long-term corrosion to modify the sliding friction must also be considered in defining the friction coefficient. In this situation, the appropriate coefficients of friction for the repository components have high uncertainty. It is then appropriate to pick a distribution of values for the coefficients of friction that encompass a range of materials and a range of mechanical responses from little or no sliding between components to substantial sliding between components.

A distribution of values for the friction coefficient between 0.2 and 0.8 will achieve these goals (see Table 5-17 and DTN: MO0301SPASIP27.004 [DIRS 161869], Table I-4). First, this distribution is broad enough to encompass typical values of the dry sliding friction coefficients for a wide variety of metals and other materials (Avallone and Baumeister 1987 [DIRS 103508], Table 3.2.1, p. 3-26). Second, the appropriateness of this range is independently confirmed by seismic analyses for spent fuel storage racks (DeGrassi 1992 [DIRS 161539]). This distribution is also broad enough to represent a range of mechanical response for the DS. A friction coefficient near 0.2 maximizes sliding of the DS on the invert. Similarly, a friction coefficient near 0.8 minimizes that sliding. This assumption is used in Section 5.2.3.2.

3.9 The friction coefficient for contact between Alloy 22 (DS base plate material, which is excluded from FE representation, see Assumption 3.17) and stainless steel is not available in literature. It is, therefore, assumed (in calculations of impact by the rockfall) that the dynamic (sliding) friction coefficient for this contact is 0.5. The rationale for this conservative assumption is that this friction coefficient represents a mean value for most dry nickel-on-steel contacts (Avallone and Baumeister 1987 [DIRS 103508], Table 3.2.1, p. 3-26), nickel being the dominant component in Alloy 22 (ASME 2001 [DIRS 158115], Section II, Part B, SB-575, Table 1). The sensitivity analysis of the impact of friction coefficient on the calculation results is not necessary (in calculation of impact by the rockfall), because the calculation results due to impact are not expected to be significantly affected by the friction coefficient between the rock and drip shield. This assumption is used in Section 5.2.3.2.

3.10 The friction coefficient for contacts occurring between the rock and Ti-7 or invert and Alloy 22 is not available in literature. It is, therefore, assumed (in all calculations except vibratory ground motion) that the dynamic (sliding) friction coefficient for this contact is between 0.4 and 0.5. The rationale for this assumption is that this friction coefficient represents a reasonable estimate based on available information for metal-on-stone contacts which is between 0.3 and 0.7 (Beer and Johnston 1977 [DIRS 145138], Table 8.1, p. 306). This parameter does not have a significant effect on the results since the relative surface-to-surface movement of these components is not a significant determining factor in the amount of deformation during impact or static load of caved rock mass. The sensitivity analysis of the impact of friction coefficient on the calculation results is not necessary (for different loading cases than the vibratory ground motion), because the calculation results are not expected to be significantly affected by the friction coefficient. In the case of vibratory ground motion, the friction coefficient between the invert and the DS is the major factor in transfer of the load from the invert to the DS. In cases of vertical rockfall impact or static load by the caved rock, which are critical for estimate of damage, the friction coefficient between the DS and the invert, or between the rock and the DS during the impact has no effect on results. This assumption is used in Sections 5.2.2 and 5.2.3.2.

3.11 The variation of functional friction coefficient between the static and dynamic value as a function of relative velocity of the surfaces in contact is not available in literature for the materials used in the calculations (Section 5.2.3.2). Therefore, the effect of relative velocity of the surfaces in contact is neglected in these calculations by assuming that the functional friction coefficient and static friction coefficient are both equal to the dynamic friction coefficient. The impact of this assumption on results presented in this document is anticipated to be negligible. The rationale for this conservative assumption is that it maximizes the relative motion of unanchored repository components by minimizing the friction coefficient within the given FE analysis framework. This assumption is used in Sections 5.2.2 and 5.2.3.2 and corresponds to paragraph 5.2.14.2 of Mecham (2004 [DIRS 170673]).

3.12 The temperature of the DS is assumed to be 150°C for temperature-dependent material properties. The rationale for this assumption is that this temperature is conservative for most of the regulatory period for high-temperature operating modes and strictly conservative for low-temperature operating modes. The waste package temperature in an open drift remains below 150°C for approximately 97 percent of the regulatory time period of 10,000 years (BSC 2001 [DIRS 156276], Figure 6-3) and the DS temperature is less than the waste package temperature. The drip shield temperature of 150°C is also considered appropriate for the case of potential drift collapse that could accompany a low-probability seismic event or from time-dependent strength loss of the surrounding rock mass. In either case, the drip shield could be partially or completely surrounded by rock rubble. The Multiscale Thermohydrologic Model was used to conduct a parameter study of the

impact of thermohydrologic parameters on the in-drift environment (BSC 2004 [DIRS 169565], Section 6.3.7 and Table 6.3-8). The results show that the peak waste package temperature in a collapsed drift for the base case thermal conductivity of the rubble is greater than 200°C for a very brief period of time – less than 100 years – and the waste package temperature drops below 150°C within approximately 350 years after collapse, even for the "hottest" waste package considered in the parameter study. These results are for the case of a collapse occurring coincident with the closure of the repository. It follows that 150°C is a reasonable and conservative value for evaluation of material properties in a collapsed drift over 96.5 percent of the regulatory period. This assumption is used in Sections 1 and 5.2.3.

3.13 The thickness of the Ti-7 and Ti-24 plates are reduced by 2 mm. For Ti-7, this thickness reduction results from using the 95th percentile general corrosion rate values used in TSPA-LA for both sides of the titanium plate (BSC 2004 [DIRS 169845], Section 6.5.5; DTN: MO0408MWDGLCDS.002 [DIRS 171486]). For the outside and inside plates, the 95th percentile general corrosion rate values (a reasonably conservative estimate) are 1.12E-4 mm/yr and 8.59E-5 mm/yr, respectively. Therefore in 10,000 years, about 1.12 mm is removed from the outer surface by general corrosion and about 0.86 mm are removed from the inner surface (i.e., a total loss of about 2 mm of thickness). Alternatively, the highest measured general corrosion rate from the 5-year exposed Ti samples used for validation of the TSPA-LA general corrosion distributions is 77 mm/yr (BSC 2004 [DIRS 169845], Table 23; DTN: MO0408MWDGLCDS.002 [DIRS 171486]). Using this value for both sides of the drip shield, a total loss of about 1.54 mm of thickness can be calculated over an exposure period of 10,000 years. Therefore, a thickness reduction of 2 mm is a reasonable estimate of the total thickness loss for Ti-7 due to general corrosion in 10,000 years. For Ti-24, the thickness reduction over a 10,000 year period was determined to be about 0.75 mm per exposed surface in the *Aqueous Corrosion Rates for Waste Package Materials* report (BSC 2004 [DIRS 169982], Section 6.5.2). Therefore, a thickness reduction of 2 mm is a reasonable estimate of the total thickness loss for Ti-24 due to general corrosion in 10,000 years.

3.14 The rock shape is assumed to be a rectangular prism. The rationale for this assumption is that the rock block data (BSC 2004 [DIRS 168550]) show that some of the rock blocks are essentially rectangular prism. An FE representation of the rock with an inclined rectangular prism provides a conservative approach from the perspective that the rock center of gravity and the point of impact are on the line parallel with direction of the impact, transferring the maximum linear momentum to the DS. Impact by the sharp edge of the prism also results in maximum strain on the DS plate. The vertex coordinates of the prism are obtained from DTN: MO0301MWD3DE27.003 (*Block Geometry Information.doc*) in order to calculate the enveloping dimensions (DTN: MO0301MWD3DE27.003 provides details). This

assumption is used in Section 5.4.2.1 and corresponds to paragraph 5.2.16.6 of Mecham (2004 [DIRS 170673]).

3.15 A value of rock compressive strength of 290 MPa is assumed in the calculation. The mean value determined from uniaxial compression tests on small, 25.4 mm diameter cores of the Tptpmn is 207.2 MPa; however, the range of the data is 38.4 to 326 MPa with a standard deviation of 61.2 MPa (Cikanek, et. al 2004 [DIRS 169642], Table 5; DTN: MO0311RCKPRPCS.003 [DIRS 166073]). The compressive strength of rock blocks in nonlithophysal rock mass is a function of block size (BSC 2004 [DIRS 166107], Figure E-22). The asymptotic value of about 70 MPa for large block sizes is representative of the block sizes predicted in the rockfall analysis. However, since the damage induced by rock block impact to the drip shield will be a partial function of the strength of the rock block, a conservative value of 290 MPa for rock compressive strength, which is near the high end of the measured data, is assumed. The rationale for this assumption is that it leads to bounding set of results. This assumption is used in Section 5.2.3.3.

3.16 The DS side-walls are assumed to be unconstrained in the lateral direction during the 10,000 year regulatory period in the calculation of static and dynamic loading by the rockfall (with the exception of the lateral constraint provided by the pallet used in the calculation of the static load in lithophysal rock mass). The rationale for this assumption is that the gantry rail is made of steel sets (BSC 2004 [DIRS 169776]), which are not anticipated to remain intact (eventually corrode away) during the 10,000-year regulatory period. This assumption is used in Sections 5.2.1 and 5.2.2.

3.17 The Alloy 22 base is excluded from the FE representation in the rockfall calculation for simplicity. The rationale for this assumption is that the effect of a thin plate at the bottom of the long side wall on the calculation results is negligibly small during rockfall. This assumption is used in Section 5.2.2.

3.18 The residual stress threshold for the DS damaged area evaluation is assumed to be a constant value, equal to 50 percent of the yield strength of Ti-7. The rationale for this assumption is the data provided in DTN: MO0303SPARESST.000 [DIRS 162030] and Section 5.2.3.1.4. This assumption is used in Sections 1, 2, 5.3.3.2, and 5.2.3.1.4.

3.19 The lifting feature, and DS connector assembly are excluded from the FE representations for simplicity (The DS connector assembly and base were included in the analysis of vibratory ground motion.). The rationale for this assumption is that the effect of these DS components on the calculation results is negligibly small. This assumption is used in Section 5.2.2.

3.20 The kinematic calculation of DS separation is two-dimensional in the vertical plane that is oriented along the axis of the DS. Consequently, only the vertical

component and one component of horizontal ground motion were considered. The kinematic calculation was used for assessment of the potential of DS separation. The main mechanism that causes DS separation is unlocking of the DSs by vertical shear displacements of the connection. The horizontal component of the ground motion perpendicular to the "chain" of the DSs (i.e., the out-of-plane component) is not expected to cause vertical shear deformation of the connections between the DSs. The other possible mechanism of DS separation is by excessive deformation of the structural components in the connection or by shearing off of the welds in the connection interlocking mechanism. The out-of-plane component of the ground motion will contribute to deformation and strain of the chain of the DS, and consequently to the loads taken by the structural components and welds in the connection. The axial loading on the welds is assumed to be uniformly distributed along the entire length of the weld which is represented as two contact locations between adjacent DSs – one upper and one lower contact. One half the weld strength is assumed to be lumped at each of the two contacts. The ground motions that can cause separation of the DSs (1×10^{-5}, 1×10^{-6} and 1×10^{-7} probability of annual occurrence) result in at least some level of rockfall and rubble accumulation on the invert between the DSs and the drift walls. Even the limited amount of rubble on the sides of the DS will constrain the motion of the DS relative to the emplacement drift in the plane of the drift cross-section (i.e., the DS will move together with the emplacement drift). The out-of-plane deformation of the chain of the DSs will thus be small and the resulting bending deformation that will cause straining of the DS connections can be neglected. This assumption is used in Sections 5.2.2, 5.2.3.2 and 5.3.1.1.

3.21 The DS is represented in the kinematic DE calculations as a rectangular, deformable solid body with mass and outline dimensions (i.e., the length and height) equal to those of the actual DS. The mass is assumed to be uniformly distributed over the area of the geometrical representation of the DS. The separation of the DSs (which is analyzed by the kinematic calculation) is mainly affected by the differential rigid-body motion of adjacent DSs. The parameters that govern the rigid-body motion of the bodies are their mass and dimensions. This assumption is used in Sections 5.2.2 and 5.3.1.1.1.

3.22 Density of the rubble created by rockfall in the emplacement drift is assumed to be 2,000 kg/m^3. The density of the rubble is a function of the volume of the caved rock, which includes the porosity between rock particles. The bulking factor, B, defined as the percentage increase in volume of the rock in going from an in situ rock mass to a granular rubble, is used to determine the rubble density. If the density of the in situ rock mass is assumed to be 2,370 kg/m^3 (Assumption 3.7), the density of the rubble of 2,000 kg/m^3 corresponds to bulking factor of 18.5 percent (using the relation $\rho_r = \rho/(1+B)$, where ρ_r is the rubble density, ρ is the in situ rock mass density, and B is the bulking factor), which is approximately equal to

the lower bound of the bulking factor usually observed in the mining operations (BSC 2004 [DIRS 166107], Section 6.4.2.5.2). This assumption is used in Section 5.2.3.5.

3.23 The analyses summarized and conducted in this document assume that there is no ground support present in the emplacement drifts that would prevent rockfall or drift degradation from occurring. The rock support, consisting of stainless steel rock bolts and thin, perforated stainless steel sheeting, will continue to provide support for some indeterminate time after repository closure (BSC 2004 [DIRS 165425]). This assumption applies to most of the postclosure period and the calculations are run with and without rockfall effects. This assumption is used in Sections 5.2.3.5.

3.24 In the kinematic analyses of the vibratory motion of a chain of interlinked drip shields (Section 5.2.3.2.2.1), the drip shields are represented as deformable blocks that rest on a rigid invert. It is necessary to estimate the stiffness of the contact between the drip shield and invert for normal and shear loading. The normal and shear stiffnesses of the interface between the DS and the invert are considered to be 3 MPa/m as a base condition in the majority of the kinematic simulations for drip shield vibratory motion in an open drift. The tangent modulus (E) of the crushed rock at low confinement is on the order of 10,000 psi, or approximately 70 MPa, according to Marachi et al. (1972 [DIRS 157883])[3]. Considering the width of the DS base (BSC 2003 [DIRS 166897], $l = 2 \times 75\,\text{mm} = 150$ mm) and the thickness of the crushed tuff in the invert (d = 86 cm; see Figure 5-6), the normal stiffness of the contact is calculated as

$$k_n = \frac{El}{1.0 \times d} = \frac{70 \times 0.15}{1.0 \times 0.86} = 12.2 \text{ MPa/m} \qquad \text{(Eq. 3-1)}$$

In the majority of the calculations, a lower stiffness of 3 MPa/m was used to account for the effect of localized pressure at the base of the DS and nonlinear deformation of the invert during strong impacts. The value of 3 MPa/m was selected because it results in relatively small overlap of the simplified kinematic blocks that represent the DS and the invert, considering the load due to the weight of the DS only. This assumption is used in Section 5.2.3.2.2.1.

[3] The data supporting the value of tangent modulus (E) of tuff rock rubble is derived from laboratory triaxial compression testing of large (36 inch diameter by 7.5 feet in height) samples of crushed basalt at the Rockfill Testing Facility at the University of California at Berkeley. This data is reported in the Journal of the Soil Mechanics and Foundation Division, Proceedings of the American Society of Civil Engineers, a peer-reviewed journal. The reliability of this data source is considered high. The size-gradation curves for the crushed basalt tested are similar to the small rock fragments expected from lithophysal rock rubble, and the strength of the constituent grains from tuff and basalt are of similar magnitude as both are high strength volcanic rocks. For these reasons, this data source, used as direct input, is considered to be suitable for its intended use, which is to provide an approximate value for the Young's modulus of rock rubble.

3.25 In the simplified kinematic model of DS synchronous motion, the DSs are represented as deformable blocks that interact with one another via shear and normal contacts at their ends. Two contacts are used between these DS blocks – one at the top and one at the bottom of the block. The maximum axial force that can be taken by the welded interlocking DS connection is assumed to be half of the maximum value given in Equation 5-9, or 7.05 megaNewtons (MN) (Assumption 3.20). This estimate of the maximum axial force in the contact between the DSs is approximate, since the complex processes of nonlinear and inelastic deformation of different components of the DS structural connection are ignored. To take these effects into account, engineering judgment is used to reduce the maximum axial force used in the calculations by 50 percent, to 3.5 MN.

INTENTIONALLY LEFT BLANK

4. USE OF COMPUTER SOFTWARE

This document provides a summary of several calculations, as described in Section 1, in which software was utilized to derive the results summarized here. In this present calculation, only the UDEC software was used to develop new results not previously reported in supporting calculations. The computer software used to develop results summarized in this calculation, but developed in the supporting calculations is also reviewed in this section for completeness. The computer software cited in Section 4 of the supporting structural calculations (BSC 2003 [DIRS 167083]; BSC 2004 [DIRS 168993]; and BSC 2004 [DIRS 170791]) is also listed in Table 4-1.

Table 4-1. Computer Software Used in Structural Calculations

Software	STN	Operating system	Computer Type	Computer Number[a]
ANSYS V5.6.2 (BSC 2002 [DIRS 159357])	10364-5.6.2-01	HP-UX 11.00	Hewlett-Packard (HP) 9000 series UNIX workstations	117162, 151324, 151325, 151664, and 151665
LS-DYNA V960.1106 (BSC 2002 [DIRS 158898])	10300-960.1106-00	HP-UX 11.00	HP 9000 series UNIX workstation	117162, 151324, 151325, 151665, 151664, 150691, 150689, 150690, 150688
LS-DYNA V970.3858 D MPP-00 (BSC 2003 [DIRS 166918])	10300-970.3858 D MPP-00	HP-UX 11.22	HP Itanium2 (IA64) series UNIX workstations	501711
UDEC V3.1 (BSC 2002 [DIRS 161949])	10173-3.1-00	Windows 2000	PC	NA
TrueGrid V2.1.5	exempt of the requirements defined in LP-SI.11Q-BSC (Section 2.1.2)	HP-UX 11.00	HP 9000 series UNIX workstation	150689
TrueGrid V2.2	exempt of the requirements defined in LP-SI.11Q-BSC (Section 2.1.2)	HP-UX 11.00	HP 9000 series UNIX workstation	150689
LSPOST V2	exempt of the requirements defined in LP-SI.11Q-BSC (Section 2.1.2)	HP-UX 11.00	HP 9000 series UNIX workstation	117162, 151324, 151325, 151665, 151664, 150691, 150689, 150690, 150688
LS-PREPOST V1.0	exempt of the requirements defined in LP-SI.11Q-BSC (Section 2.1.2)	HP-UX 11.22	HP Itanium2 (IA64) series UNIX workstations	501711
LS-PREPOST V2.0	exempt of the requirements defined in LP-SI.11Q-BSC (Section 2.1.2)	HP-UX 11.22	HP Itanium2 (IA64) series UNIX workstations	501711

[a] Yucca Mountain Project property tag numbers for computers located in Las Vegas, Nevada.

The FE meshes of the DS developed in the supporting calculations were constructed using either ANSYS V5.6.2 (BSC 2002 [DIRS 159357]) or TrueGrid V2.1.5 and TrueGrid V2.2 (XYZ Scientific Applications, Inc.). These software programs were used solely to mesh geometric representations of the domain (i.e., for the development of FE mesh), and are therefore exempt from the requirements defined in procedure LP-SI.11Q-BSC, which defines software qualification requirements.

The qualified FE analysis computer codes used for this calculation are Livermore Software Technology Corporation LS-DYNA V960.1106 (BSC 2002 [DIRS 158898]) and LS-DYNA V970.3858 D MPP-00 (BSC 2003 [DIRS 166918]) (LS-DYNA V960 and LS-DYNA V970, respectively[4]). Both LS-DYNA codes are obtained from Software Configuration Management in accordance with the appropriate procedure (LP-SI.11Q-BSC). The FE calculations performed herein are fully within the range of the validation performed for LS-DYNA V960 code (BSC 2002 [DIRS 168545], Sections 4 and 5) and LS-DYNA V970 code (DOE 2003 [DIRS 168558], Sections 4 and 5). LSPOST V2, LS-PREPOST V1.0 and LS-PREPOST V2.0 (Livermore Software Technology Corporation) are postprocessors[5] used for visual display and graphical representation of results.

The qualified DE analysis computer code used for this calculation is UDEC (BSC 2002 [DIRS 161949]). UDEC is obtained from Software Configuration Management in accordance with the appropriate procedure (LP-SI.11Q-BSC). The DE calculations performed herein are fully within the range of the validation performed (BSC 2002 [DIRS 171617]).

The data files and saved file states to recreate the parametric kinematic analyses conducted with UDEC V3.1 are provided in Attachment A. Files for each case listed in Table 5-19 are listed in Section 7 of this document and provided in Attachment A. The file extensions have the following meaning: *.dat are primary input data files, *.fis and *.fin are macro files called by *.dat in setting up and running the problems, *.vel are input velocity ground motion time history records (H signifies horizontal and up signifies vertical velocity components), *.sav are the saved files used for the initial model geometry (before application of the ground motion time histories) and at the end of the analysis, *.lnk are shortcut files for execution of the UDEC program, and *.pcx are bit map graphics files of the model geometry and results.

[4] LS-DYNA V960 and LS-DYNA V970 are referred to as LS-DYNA when it is unnecessary to make a specific distinction.

[5] Note that LS-PREPOST V1.0 and LS-PREPOST V2.0 also have preprocessing capabilities, which were not used in the calculations documented in the supporting calculations.

5. CALCULATION

5.1 BACKGROUND INFORMATION

Figure 5-1 illustrates the major components of the engineered barrier system (EBS) in a typical emplacement drift. The major EBS components are the waste package, the DS, and the fuel rod cladding (the cladding is not shown in Figure 5-1). These components provide barriers to the release of radionuclides from the EBS into the unsaturated zone. The effectiveness of these barriers is potentially compromised by the direct effects from an earthquake, including vibratory ground motion, fault displacement, and rockfall induced by ground motion or some other effects. Other, non-seismic mechanical effects could include rockfall resulting from time-dependent degradation of the emplacement drift. The effectiveness of these barriers is also potentially compromised by indirect effects after an earthquake, including changes in seepage, temperature, and relative humidity if an emplacement drift collapses completely during a very low probability earthquake.

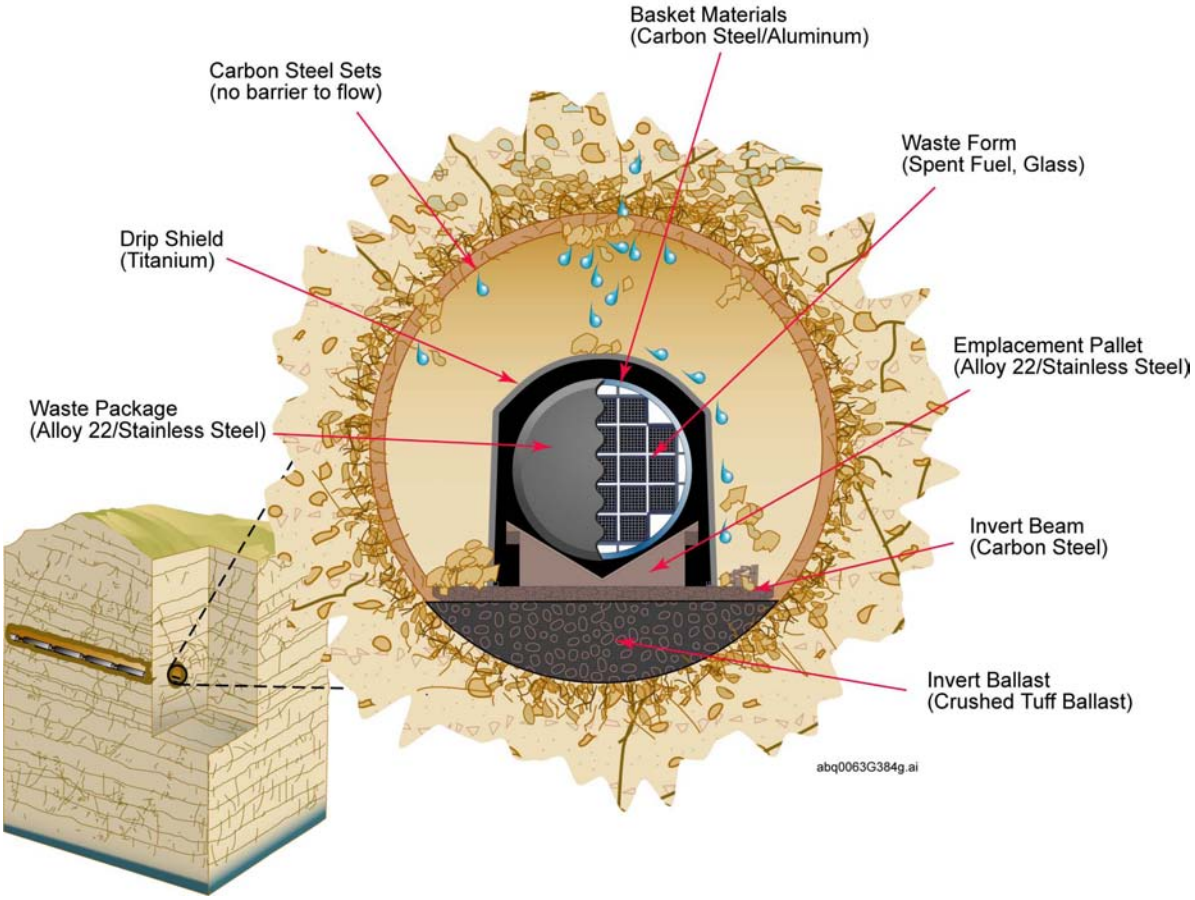

Figure 5-1. Schematic Diagram of the EBS Components in a Typical Emplacement Drift

The DS is a free-standing structure, constructed of titanium bulkheads and overlying sheets, whose legs rest on the invert of the tunnel. The invert is constructed of carbon steel beams with crushed tuff compacted between them. Initially the weight of the DS is borne by the steel beams. As corrosion of these beams occurs over time, the weight will be transferred to the compacted, crushed tuff invert. The purpose of the DS is to prevent direct seepage of water on the waste packages, and to protect the waste packages from direct impacts by rockfall (illustrated in Figure 5-1). Specifically, effectiveness of the DS could be affected by the following mechanical processes:

- Relatively large rigid-body displacements of the DSs that would overturn the DS or create a gap between the neighboring DSs (The DSs are designed to overlap each other creating a continuous shielded area underneath them. This potential separation is an important consideration because it impacts the function of the DS as a flow and rockfall barrier.)

- Loss of structural integrity due to mechanical collapse or buckling of the main structural elements (e.g., the support beam and the bulkhead)

- Puncture, tearing or damage that would accelerate the stress corrosion rate of the DS plates (other corrosion mechanisms are accounted for in the calculation by a uniform thickness reduction of the DS as discussed in Assumption 3.13 and Section 5.2.3.1.5).

The DS could be subjected to static and dynamic loads during the postclosure period. Static load that could potentially have an effect on structural integrity of the DS is due to the weight of caved rock rubble that may rest on the top of the DS or between the DS and the walls of the emplacement drift. Emplacement drift failure, and resulting caving and expansion of the tunnel profile can occur as a result of thermally induced stresses, seismic loading, time-dependent strength degradation, or different combinations of these factors. The dynamic loads on the DS, which are primarily due to the seismic ground motion, include inertial forces and impacts of the falling rock blocks. The inertial forces can result in motion of the DSs relative to each other, and relative to the drift walls and other objects inside the drift (e.g., the waste packages and pallet). Consequently, inertial forces can cause separation of the DSs and impact to other DSs and objects inside the emplacement drifts. The impacts of the falling blocks can take place during seismic ground motion and as a result of drift degradation due to time-dependent strength loss.

The calculations summarized in this document determine potential for separation of the DSs and loss of the structural integrity and stability, but also the damaged areas on the DS (i.e., those areas that exceed the residual stress threshold for Ti-7) from impacts between the DS and the waste package, pallet, invert, drift wall, and by rockfall. The damaged area estimates to the DS surface plates as a function of peak ground velocity (PGV) are used as input to the *Seismic Consequence Abstraction* (BSC 2004 [DIRS 169183]), which provides damage abstractions to the TSPA-LA. In the *Seismic Consequence Abstraction* (BSC 2004 [DIRS 169183]), the physical interpretation of the damaged areas is a resulting network of stress corrosion cracks through which seepage water could potentially pass to the waste package. A discussion of the physical morphology of the stress corrosion cracks, and the potential for advective flux through the DS is provided in the *Seismic Consequence Abstraction* (BSC 2004 [DIRS 169183]).

5.1.1 Scope of Calculation

Integrity and stability of the DS were analyzed for the following loads, which are expected to be the bounding loading cases during the operation of the DS during the postclosure period:

- Static pressure of the rock rubble that covers the DS following collapse or partial collapse from seismic effects or from time-dependent degradation
- Vibratory motion of the DS induced by the seismic ground motion
- Impacts by the falling rock from rockfall due to seismic effects.

5.1.1.1 Loading from Static Pressure of Rock Rubble

Static pressure of rock rubble resting on the DS is derived from two basic sources as described in *Drift Degradation Analysis* (BSC 2004 [DIRS 166107], Section 6.4). These are: 1) low probability seismic events with large peak ground velocity and 2) the combined effects of thermal stresses, time-dependent strength degradation and repeated higher probability seismic events.

Complete or Partial Drift Collapse from Low Probability Seismic Events – Low probability postclosure seismic events are predicted to result in extensive collapse of emplacement drifts in lithophysal rock and partial collapse of nonlithophysal rock, with resulting rubble either completely or partially covering the DS. Drifts located in lithophysal rock are expected to undergo collapse sufficient to cover the DS for seismic events characterized by a PGV of approximately 2 m/s or higher. Approximately 25 percent of the ground motions associated with the 1×10^{-5}, and all of the 1×10^{-6} and lower annual frequency of occurrence show complete collapse in lithophysal rocks. Ground motions associated with 1×10^{-6} and lower annual frequency of occurrence show extensive damage that either covers the DS or fills the area between the DS and drift walls in the nonlithophysal rocks (BSC 2004 [DIRS 166107]). Dynamic discontinuum analyses presented in *Drift Degradation Analysis* (BSC 2004 [DIRS 166107]) show that the collapse of the drifts in response to the ground motion occurs simultaneous with the arrival of the strong ground motion. Thus, within a few seconds after beginning of seismic ground motion, the drift collapses and restrains the DS with broken rubble.

Rockfall from Thermal Stress, Time-Dependent Effects and Higher Probability Seismic Events – In the absence of low probability seismic events, the emplacement drifts are expected to be largely stable over the postclosure period. For the assumed base case scenario (i.e., rock mass loading resulting from thermally induced stresses and higher probability, preclosure ground motions [i.e., those with 5×10^{-4} or 1×10^{-4} annual frequency of occurrence]) some lesser amount of rockfall is expected. This rockfall, derived from the drift sidewalls, will occur primarily in the lithophysal rocks and will vary along the drifts depending on the local quality of the rock mass. The lithophysal rock comprises approximately 85 percent of the total length of the emplacement drifts, while approximately 15 percent occurs within the stronger nonlithophysal rocks. Within the lithophysal rocks and in the absence of low probability seismic events, it is expected that at most, approximately 3 percent of the total length of the emplacement drifts can completely

collapse covering the DS with broken rock[6]. The rockfall along the remaining length of the emplacement drifts will be limited with some accumulation of the broken rock on the sides or on the top (less than 1 m height of the broken rock) of the DS.

5.1.1.2 Loading from Vibratory Motion

The effect of seismic ground motion on damage from vibratory motion of the DS was analyzed for ground motions with 5×10^{-4}, 1×10^{-6} and 1×10^{-7} annual frequency of occurrence. The effect of seismic ground motion on potential for separation of the DSs was analyzed for ground motions with 1×10^{-6} and 1×10^{-7} annual frequency of occurrence. Although the caved rock mass inside the emplacements drifts (surrounding the DS) could potentially restrict motion of the DS as a rigid body, it was assumed conservatively in a number of the calculations that the drifts were stable during the entire simulation (as stated in Section 5.1.1.1, collapse of the drifts in lithophysal rock and nonlithophysal rock masses is expected for seismic ground motions with 1×10^{-6} and 1×10^{-7} annual frequency of occurrence). The seismic motion is transmitted from the invert (which has the identical motion of the far-field rock mass in these calculations – see Section 5.2.3.4) to the DS through the frictional interface in the contacts between the invert and the DS.

5.1.1.3 Loading from Rockfall Impacts

Rockfall, which can occur as gradual drift degradation or can be seismically induced, may impact the DS. The seismically induced impacts of the rockfall, which will have greater energy (because of larger impact velocity) than the impacts resulted from slow, quasi-static drift degradation, are considered in the analysis. The size distribution of the unstable blocks will be different in the lithophysal and nonlithophysal rock masses. Spacing of the rock mass fractures and lithophysae is expected to control the size of the blocks in general, and the size of those blocks that are detached under seismic load. The nonlithophysal rock mass is characterized by four sets of naturally-occurring fractures, with spacings that average, in general, between 0.5 m and 3 m (BSC 2004 [DIRS 166107], Section 6.1). The ubiquitous fracture fabric of relatively short fractures in the lithophysal rock mass have average spacing of less than 0.1 m. The median and maximum block sizes produced in the nonlithophysal rock mass are larger as a result of the wider fracture spacing. The rockfall in lithophysal rock mass is estimated to consist of blocks with edge length of, on average, a few tens of centimeters, in contrast to the largest blocks destabilized by the strong ground motions (1×10^{-6} and 1×10^{-7}) in nonlithophysal rock mass with mass in excess of 25 metric tons. Impact of blocks in nonlithophysal rock mass is analyzed as a bounding scenario in *Drip Shield Structural Response to Rock Fall* (BSC 2004 [DIRS 168993]) and summarized in Section 5.4.2.

[6] The lithophysal rock mass has been subdivided into 5 rock strength categories, with category 1 being of the lowest quality or strength. This category, representative of lithophysal rock with lithophysal porosity greater than about 25 percent comprises roughly 3 percent of the repository host horizon (BSC 2004 [DIRS 166107], Appendix E).

5.2 DRIP SHIELD GEOMETRY

5.2.1 Description of the Drip Shield Design

The geometry of the DS is shown in perspective views in Figures 5-2 and 5-3. All details and dimensions of the geometry of the DS can be found in *D&E / PA/C IED Interlocking Drip Shield and Emplacement Pallet* (BSC 2004 [DIRS 169220]) as well as in the calculations that support this summary document (BSC 2003 [DIRS 163425], BSC 2004 [DIRS 168993] and BSC 2004 [DIRS 170791]). The components of the DS structure are indicated in these figures. The main structural (load bearing) elements of the DS, the bulkheads and the support beams, will be manufactured of Ti-24. They form 4 typical frames spaced at 1,072 mm along the DS. Two peripheral frames (at the ends of the DS) have a different geometry than the bulkhead and support beams. The DS plates 1 (on the top) and 2 (on the sides), which are placed continuously over the bulkheads and the support beams, will be manufactured of Ti-7, as well as the external and internal support plates that strengthen the DS plates 1 and 2 in the region of their junction. The plates provide the ultimate functionality of the structure—i.e., to prevent: a) dripping of water from the drift roof and walls onto the waste packages, and b) impacts of loose blocks from the drift roof and the walls directly onto the waste packages. Each DS is 5,805 mm in length, and 2,886 mm in height, and its total mass is 5,000 kg (BSC 2004 [DIRS 169220]). The DSs will be installed, prior to closure of the repository, over the waste packages and pallets. Adjacent DSs partially overlap one another using the drip shield connector (DSC) assembly on one DS, which is placed over and interlocks the DSC Guide of the next DS to provide continuous shielding of the waste packages. In order to separate (unlock) two DSs (or to lock them together) without significantly deforming the support beams, bulkheads or plates, or shearing off the welds, it is necessary to lift one DS relative to another by at least 40 inches (approximately 1 m; shown in Figure 5-4). This is because the DS side plates are inclined 2 degrees with respect to the invert surface normal (BSC 2004 [DIRS 169220]).

The DS and other structures inside the emplacement drift after its installation are shown in the cross-section in Figure 5-5. The details of the invert structural support for the DS and its relationship to the emplacement drift are shown in Figure 5-6. The DS will be placed between the edge of the pallet (inside) and the gantry crane rail and the associated structures (outside). However, in the calculations, it is assumed (Assumption 3.16) that the gantry crane rail and the associated structure do not exist—i.e., that in the postclosure period they have corroded in such a way that they do not provide any mechanical resistance or obstacle to motion of the DS. The DS will be resting on the invert by its own weight. Initially, the weight of the DS, waste package and pallet is borne by a framework of structural steel that is bolted to the floor of the emplacement drift. Compacted, crushed tuff is placed between the structural steel members during the construction process and prior to emplacement. In the postclosure period, as the steel framework corrodes and looses its load bearing capacity, the weight of the DS, waste package and pallet will be borne by the compacted crushed tuff invert. As shown in Figure 5-6, the maximum thickness of the crushed tuff is approximately 86 mm (2 ft 10 in) beneath the waste package. There is no additional resistance to lifting the DS off the invert than the weight of the DS. The only resistance to lateral movement of the DS (before it hits the pallet or the drift wall) is friction between the DS and the invert.

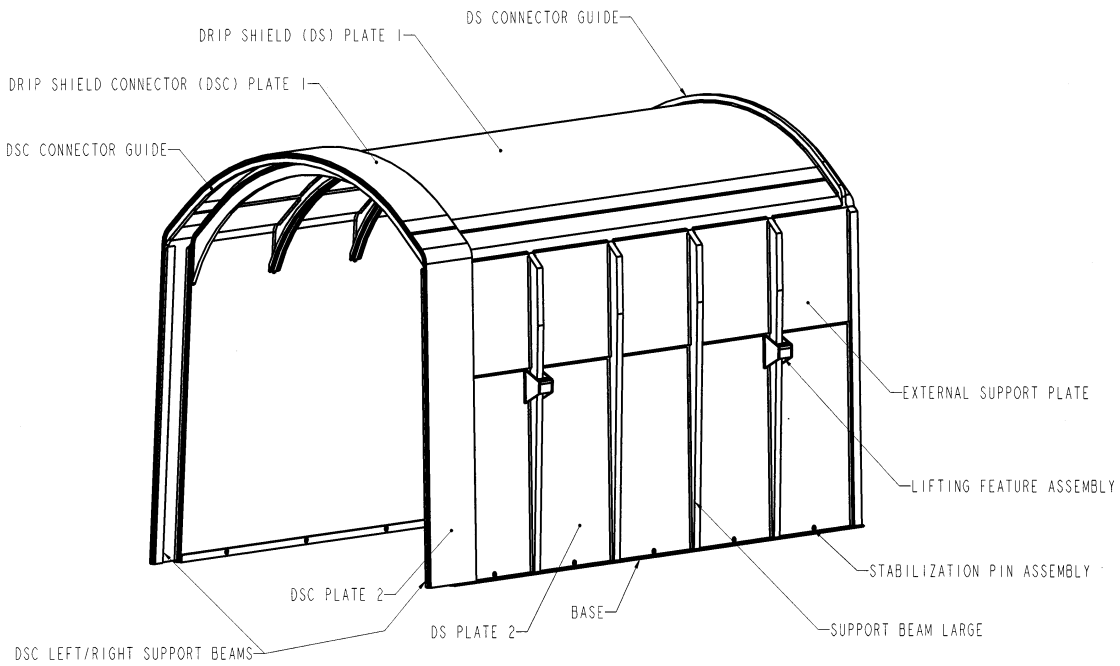

Source: BSC 2004 [DIRS 168275].

Figure 5-2. Geometry of the Drip Shield – Side View

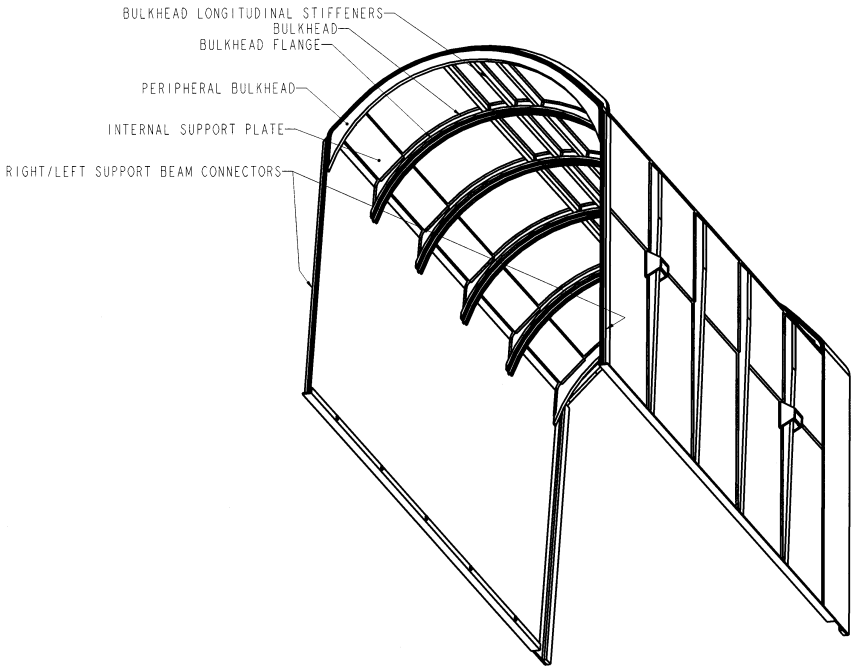

Source: BSC 2004 [DIRS 168275].

Figure 5-3. Geometry of the Drip Shield – View from Below

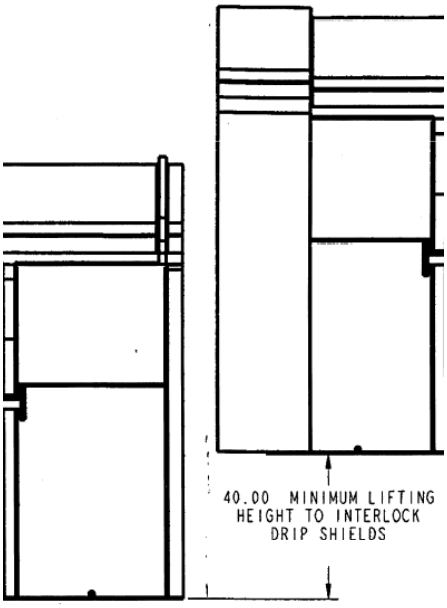

NOTE: The indicated dimension is in inches.

Source: BSC 2003 [DIRS 165038].

Figure 5-4. Interlocking of the Drip Shields

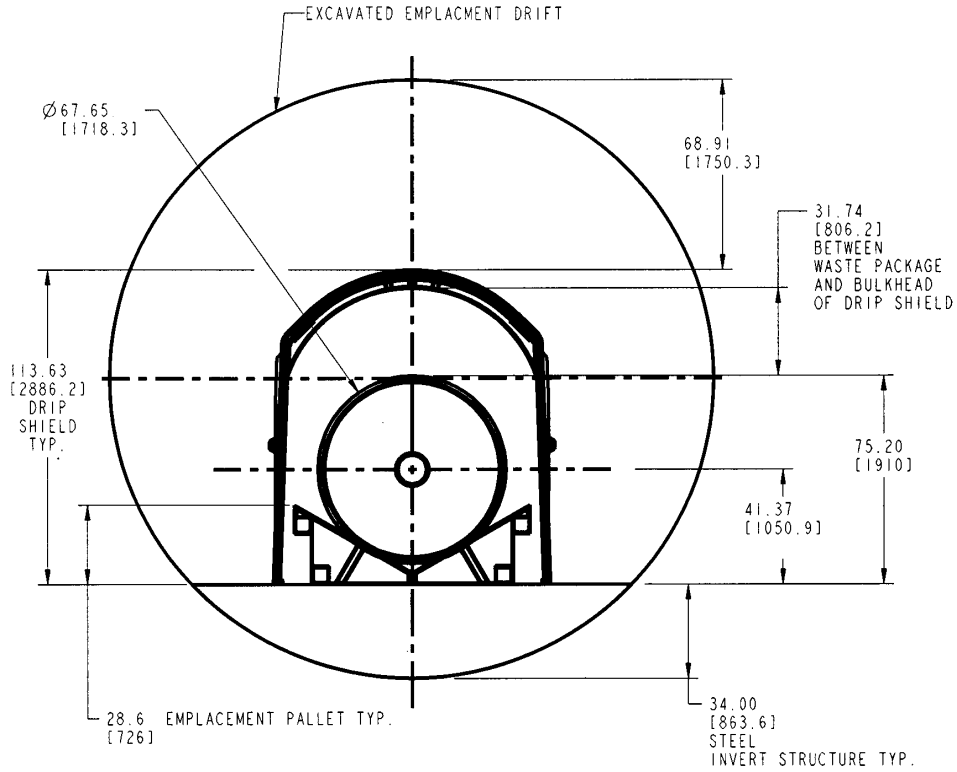

Source: BSC 2004 [DIRS 170074].

NOTE: Dimensions: inches [millimeters]; Dimensions are utilized as references only.

Figure 5-5. Configuration Inside the Emplacement Drift During the Postclosure Period

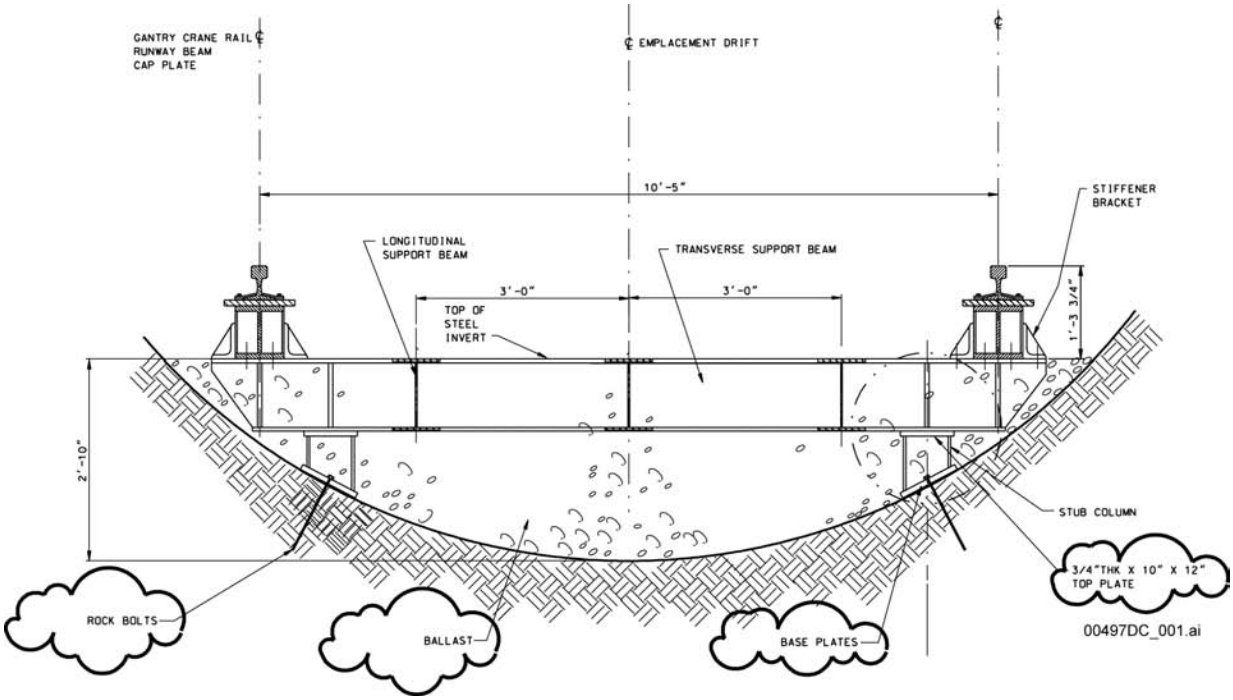

Source: BSC 2004 [DIRS 169776].

NOTE: Dimensions in feet and inches are utilized as references only.

Figure 5-6. Detail of the Steel Invert Structure and Crushed Tuff Ballast at the Bottom of the Emplacement Drift

5.2.2 Drip Shield Numerical Representation

Different numerical representations of the DS are used for the various loading conditions and analysis requirements. Because these calculations are computationally intensive (in terms of computer memory requirements and computer simulation run-time), it is necessary that the numerical representation be optimized for the particular loading case and objectives of the calculation.

Assumptions 3.16, 3.17 and 3.19 are used in development of FE representations of the DS. Assumptions 3.20 and 3.21 are used in development of DE representation. The invert is represented in all calculations as rigid. The DS is designed to be free standing on the invert, and is represented in the calculations as freely resting on the invert with a coefficient of friction between the DS footing and the invert specified as appropriate (Assumptions 3.8, 3.10 and 3.11). As illustrated in Figures 5-5 and 5-6, the only constraints to the DS motion are the drift walls, pallet and gantry rail. It is assumed (Assumption 3.16) that the gantry rail, manufactured of carbon steel, will corrode away and present no restrain to motion of the DS. Because it is assumed that the life of standard carbon steel rail is on the order of hundreds of years, this assumption is adequate for most of the duration of the regulatory period. The accumulated rockfall (due to seismic shaking or time-dependent drift degradation), if present, provides a lateral constraint to motion of the DS. Sensitivity of the calculation as a result of the presence of the lateral constraint provided by rockfall is examined in the DE kinematic analyses. The impact of lateral constraints on damage to drip shield plates under vibratory motion subsequent to the rockfall is not assessed. The largest damaged area of surface plates is predicted (Tables 5-26 and

5-27) for the vertical impact by rockfall, in which case the lateral constraints are inconsequential. It is not expected that the lateral constrain would affect significantly the results of calculations for the side impacts.

The DSC assembly, lifting feature, and base were excluded from the FE representation (Assumption 3.19) (the DSC assembly and base were included in the analysis of damage from vibratory ground motion). The benefit of this simplification is to reduce the computer execution time while preserving the features of the problem most relevant to the structural response of the DS.

5.2.2.1 Representations for Vibratory Ground Motion

An objective of this calculation was to investigate the effect of vibratory ground motion on the potential for separation of the DS and to determine the areas of residual first principal stress that exceed 50 percent of the Ti-7 yield strength (Section 5.2.3.1.4). For analysis of DS separation, it is necessary to consider motion and interaction of a large number of DSs. To conduct such an analysis using a detailed representation of the DS geometry (required for proper analysis of impact-induced damage) would be demanding computationally. Instead, two different approaches were used:

- Simplified DE kinematic calculations of motion of a large number of DSs to investigate the potential for DS separation
- FE calculation of interaction of 3 DSs (with detailed representation of the DS geometry) to analyze impact damage.

Two-dimensional DE kinematic calculations using the UDEC software (BSC 2002 [DIRS 161949]) were conducted to investigate the effect of vibratory ground motion on potential for DS separation only. Because the dominant mode of deformation of the DSs that affects their separation and interaction during seismic ground motions is their rigid body motion, the DS is represented as a rectangular (in two dimensions), deformable body with the overall DS dimensions (i.e., length, height and mass [Section 5.2.1]). Normal and shear contact relations are used to represent interaction of the DSs (Section 5.2.3.2.2.2). The DSs may become separated when limiting shear (relative vertical) displacement or limiting axial force is exceeded. If the limiting shear displacement is exceeded, the DSs become unlocked, and if the limiting axial force between two interlocked DSs is exceeded, welds of the interlocking feature are sheared and the connection is broken. The DSs will not separate as long as they move synchronously. The loss of synchronicity in DS motion is primarily a result of the following factors:

- Differential motion of the invert along the drift resulting in variable normal and shear impulse transferred to the DSs along the interconnected “chain” of DSs. If the incoming seismic wave propagates as a plane wave traveling vertically upward, all points with the same elevation move synchronously. If the incoming wave is not propagating vertically upward, there is an effect of the traveling wave along the emplacement drift that will cause a differential motion of the DSs, resulting in strain in the chain of the DSs and potential separation.

- Variability in friction coefficient (between the DS and the invert) along the chain, resulting in variable shear impulse transferred to the DSs.

- Variability of the conditions of interaction with the neighboring DSs. The DSs at the ends of the chain are always the source of the perturbation because of the asymmetric conditions of interaction—i.e., the end DS interacts with a DS on one side and is free on the other side.

The DE kinematic analysis employs a simplified representation of the DS. This analysis is supplemented by analysis of an extreme case regarding the potential for DS separation and damage due to vibratory motion impacts using a detailed FE representation of three adjacent DSs (only the central DS of those three is deformable). In this case, a rigid longitudinal boundary is assumed on both sides of the chain of three DSs. The main objective of the FE calculations is to estimate damage due to interacting impacts of adjacent DSs.

5.2.2.1.1 Representation for Kinematic Analysis

The kinematic analysis was carried out using the two-dimensional DE code UDEC. Only two components of ground motion were considered: one horizontal (along the axis of the drift) and one vertical (Assumption 3.20) applied to a longitudinal section of the drift. The lateral motion of the DSs in the plane perpendicular to the emplacement drift axis was not considered (Assumption 3.21).

Each DS is represented as a rectangular deformable body defined by 5 grid points (and 4 elements) representing the DS. Rigid-body motion is the dominant mechanism for motion and separation of the DSs within the framework of this analysis. The entire geometry of the numerical representation is discretized into elements, but the portions of the domain that represent the invert and the roof of the drift are rigid because their motion is controlled to be coincident with the input ground motion time history during the simulation. The dimensions and weight of the DS listed in Section 5.2.1 are used in the calculations. Because the DSs overlap in reality, the length of the DS in this simplified representation is reduced for the length of the overlap (i.e., BSC 2004 [DIRS 169220], 320 mm). The geometry of the DS representation in the UDEC calculation, for the case of an open emplacement drift is shown in Figure 5-7.

Numerical simulations indicate that the drifts in the lithophysal rock mass collapse completely for a PGV larger than approximately 2 m/s (BSC 2004 [DIRS 166107], Section 6.4.2.2.2). In the nonlithophysal rock mass, the amount of rockfall predicted in the drifts at this level of PGV approximately fill the region between the DS and the drift wall (BSC 2004 [DIRS 166107], Section 6.4.2.2.2). Some ground motions from the set of 1×10^{-5} ground motions and all 1×10^{-6} and 1×10^{-7} ground motions have a PGV larger than 2 m/s. It is shown in the *Drift Degradation Analysis* (BSC 2004 [DIRS 166107], Section 6.4.2.2.2) that most of the predicted rockfall takes place within about two seconds after strong ground motion begins. Different levels of rockfall (but not complete drift collapse) are predicted for ground motions with a PGV less than 2 m/s. If the drift completely collapses, the DS will be covered with at least 5 m of rubble. The rubble will also fill the space between the DS and the drift walls.

Figure 5-7. UDEC Representation of a Chain of 20 Drip Shields Linked Together at Their End Contacts

Two different approaches were used to account for the effect of the rockfall on the rigid body movement of the DS and the potential for DS separation. Sensitivity cases in which rubble covers the DS were analyzed using the geometrical representation illustrated in Figures 5-8 and 5-9. The collapsed rock that accumulates on top of the DS is represented as a layer of material of a given thickness (Young's modulus and density, see Section 5.2.3.5 on discussion of rubble properties). Different combinations of rubble properties and dimensions are analyzed (Table 5-19). In the first step of a simulation, the layer of the collapsed rock is completely unrestrained and rests on the DSs. Simulation of seismic shaking is carried out after the equilibrium stresses caused by the weight of the rubble and the DSs are generated. During the seismic shaking, the top boundary of the rubble layer is moved rigidly in synchronous motion with the far-field ground motion. In the two-dimensional analysis, the calculation is conducted for a unit thickness, i.e., 1 m in the out-of-plane direction. Although the mass of the DS representation in the UDEC calculation is 5,000 kg, which is the total mass of the DS, the pressure and reactive stresses of the caved rock are accounted for in only 1 m of the model out-of-plane thickness (the width of the DS is approximately 2.5 m). Because this approach also does not account for the frictional forces between the DS and the rubble accumulated between the DS and the drift walls, the calculations are conservative in nature.

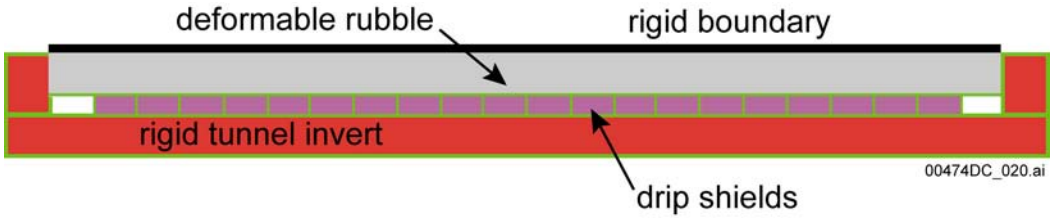

NOTE: The analysis depicted above has a simplified representation of the rubble as a coherent block of elastic material that rests on the drip shields. No rubble is represented at the ends of the DS chain.

Figure 5-8. UDEC Representation of Chain of 20 Drip Shields Covered with Rubble

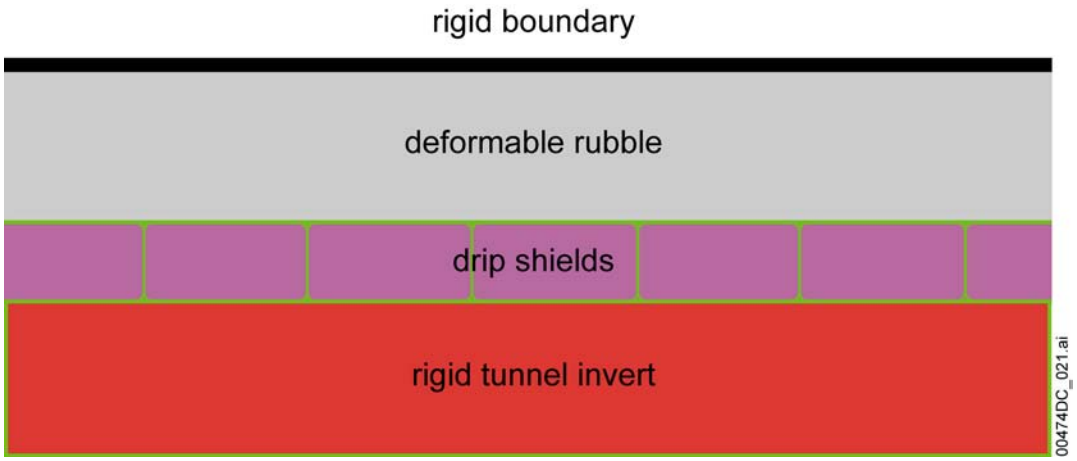

Figure 5-9. Detail of UDEC Representation of Drip Shields Covered with Rubble

The effect of the friction between the DS and the rubble on the sides of the DS (when a limited amount of rockfall does not cover the top of the DS, but rests between the DS and tunnel wall) is simulated using the geometrical representation shown in Figure 5-7. The frictional forces, applied at the 4 corners of each of the blocks that represent the DS, are calculated using the following relation:

$$F_{\text{fric}} = 0.25\, f_{m\text{-}r}\, l_{ds}\, h_{ds}\, p_{av}\,, \qquad \text{(Eq. 5-1)}$$

where l_{ds} and h_{ds} are DS length and height (Section 5.2.1), f_{m-r} is the metal-to-rubble friction coefficient, and p_{av} is the average horizontal static pressure of the broken rubble. The pressure of the rubble can be estimated using the formula for the active ground pressure in cohesionless materials (e.g., Sowers 1979 [DIRS 107479], page 385, equation 9:3b):

$$p(h) = \rho_r g h \tan^2(45^\circ - \phi_r / 2)\,, \qquad \text{(Eq. 5-2)}$$

where ρ_r is the density of the rubble, h is the height, g is gravitational acceleration, and ϕ_r is the angle of internal friction of the rubble. If the rubble height, h, is equal to the height of the DS (2,886 mm), the maximum horizontal pressure is 12,551 Pa for a typical angle of internal friction of 40 degrees (Section 5.2.3.5). The pressure varies linearly from a maximum value at the invert to zero at the top of the DS. Because the pressure is acting on both sides of the DS, the average horizontal pressure is 12,551 Pa. The force F_{fric} acts always in the direction opposite to the relative velocity between the DS and the far-field.

The parts of the calculation domain and the boundaries indicated as rigid in Figures 5-7, 5-8, and 5-9 are subjected to prescribed velocities throughout the simulations. The velocity histories are functions of the prescribed far-field velocity histories and the angle of incidence of the incoming seismic waves. The seismic waves are considered to propagate as plane (normal and shear) body waves. The effect of interactions between the seismic waves and the emplacement drifts, or any other excavations in the vicinity, is neglected.

The velocity of point x_i can be derived in the coordinate system aligned with the direction of the incident seismic wave, taking into account the phase change as a function of distance (Figure 5-10):

$$\tilde{v}_1(x_i,t) = \begin{cases} 0, & \text{for } t - \dfrac{d}{C_p} \le 0 \\ v_n\left(t - \dfrac{d}{C_p}\right), & \text{otherwise} \end{cases} \qquad \text{(Eq. 5-3)}$$

$$\tilde{v}_2(x_i,t) = \begin{cases} 0, & \text{for } t - \dfrac{d}{C_s} \le 0 \\ v_s\left(t - \dfrac{d}{C_s}\right), & \text{otherwise} \end{cases} \qquad \text{(Eq. 5-4)}$$

where $v_n(t)$ and $v_s(t)$ are prescribed vertical and horizontal velocity histories; and C_p and C_s are P- and S-wave velocities, respectively. A simple coordinate transformation was used to calculate the velocity components in the original coordinate system:

$$\begin{aligned} v_1(x_i,t) &= \tilde{v}_1(x_i,t)\sin(a_{inc}) - \tilde{v}_2(x_i,t)\cos(a_{inc}) \\ v_2(x_i,t) &= \tilde{v}_1(x_i,t)\sin(a_{inc}) + \tilde{v}_2(x_i,t)\cos(a_{inc}) \end{aligned} \qquad \text{(Eq. 5-5)}$$

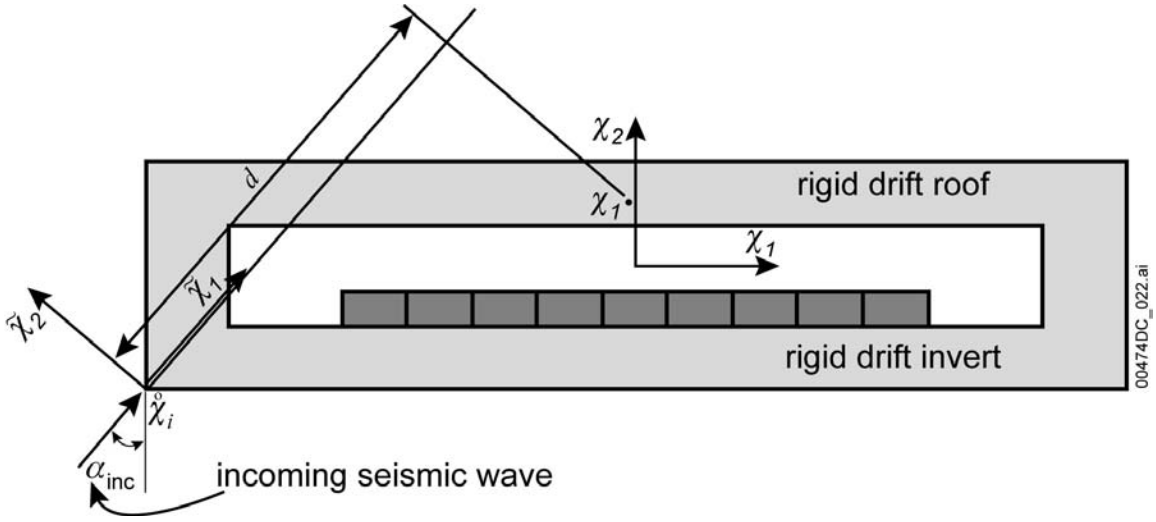

Figure 5-10. Nomenclature for Far-Field Velocity Calculation

5.2.2.1.2 Detailed Finite Element Representation

The three-dimensional FE representation, used for the vibratory ground-motion simulations, is developed in ANSYS V5.6.2, by using the DS dimensions provided in Attachment I of (BSC 2004 [DIRS 167083]). The FE representation is shown in Figure 5-11. A corresponding cutaway view (portions of various parts are removed for viewing inside the outer model boundary) is presented in Figure 5-12. As seen in these figures, the FE representation consists of three interlocking DSs, the waste package-pallet assembly, the invert surface, and the lateral and longitudinal boundaries.

Three interlocking DS's have identical geometry. However, the purpose of three interlocking DS's in the calculation is different, based on the detail to which yield mechanisms are to be represented. The finely meshed middle DS is analyzed using a bilinear elastoplastic constitutive representation for the Ti-7 and Ti-24 (Section 5.2.3.1.4). All results presented in this document are evaluated exclusively for the DS plates of the middle DS. The other two, more coarsely meshed DSs (called "peripheral DSs"), are represented as rigid (with exception of their DSC plates). The purpose of the peripheral DSs is to ensure realistic boundary conditions for the middle DS.

The boundary conditions for the DS representation used for surface plate damage are shown in Figure 5-11. The longitudinal fixed, rigid end boundary, representing the neighboring waste package pallet assemblies and DSs (which are moving synchronously with the far-field), provides constraints for the unanchored repository components in the longitudinal direction. The lateral boundary (perpendicular to the drift axis) represents the walls of the emplacement drift. The lateral and longitudinal boundaries are both rigid and fixed to the invert by tied-interface contacts (for the tied-interface contacts, LS-DYNA V960.1106, Livermore Software Technology Corporation 2001 [DIRS 159166], p. 6.29). Thus, the motion of the boundaries and the invert is completely synchronous.

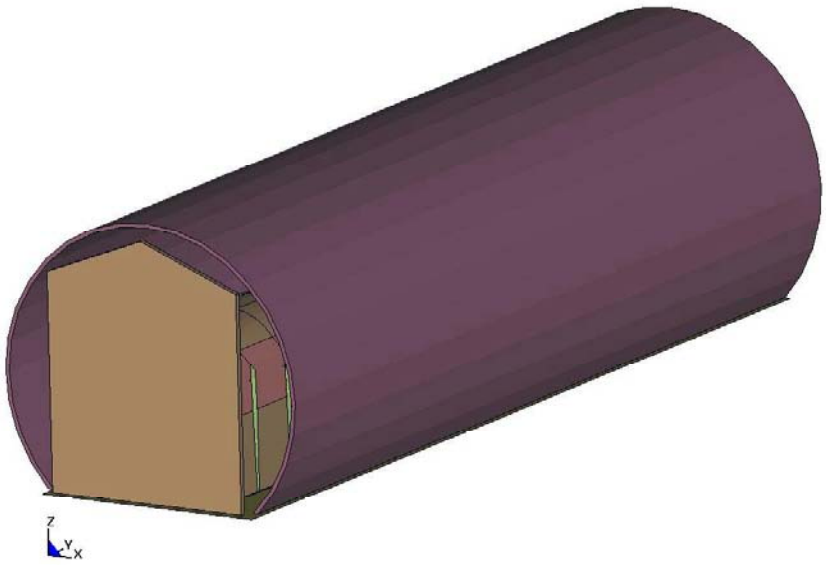

Source: BSC 2003 [DIRS 163425], Figure 1.

Figure 5-11. Setup for DS Vibratory Simulations

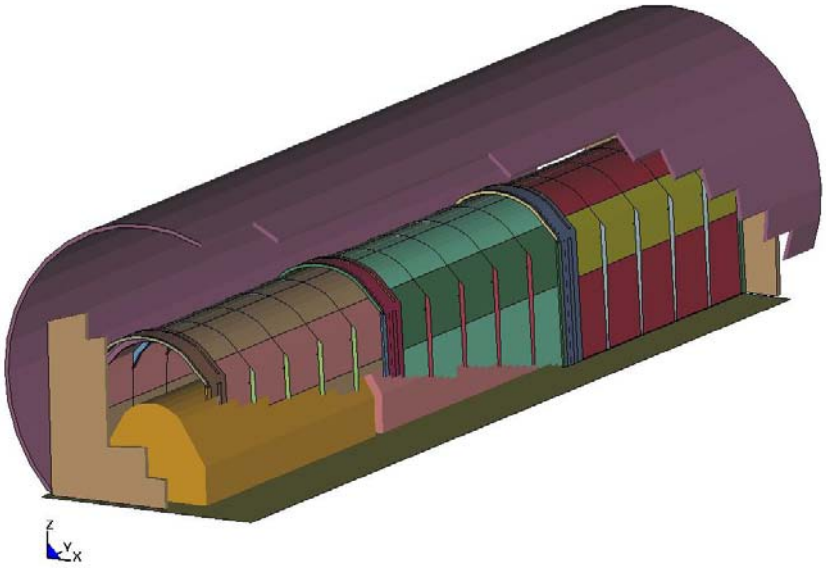

Source: BSC 2003 [DIRS 163425], Figure 2.

Figure 5-12. Cutaway View of Setup for DS Vibratory Simulations Showing Drip Shields and Internal Waste Package–Pallet Assembly

The waste package pallet assembly is a structure developed to represent the physical size, shape and mass of the waste package and pallet, but represented crudely for computational convenience. The main purpose of waste package pallet assemblies is to impose proper boundary conditions on the DSs (most importantly, the middle DS) in both a conservative (from the standpoint of the DS damaged area) and time-efficient manner. Thus, the structure of the 21-PWR waste package[7] and pallet is simplified by reducing their FE representation to a rigid thick-wall structure of uniform density (waste package pallet assembly). The geometry of the waste package pallet assembly is defined based on the contour of the waste package mounted on the pallet (Figure 5-13). The most relevant outside dimensions of the waste package mounted on the pallet are matched by FE representation and kept unchanged during the vibratory simulation (since the waste package in this FE representation cannot move relative to the pallet [see Section 5.3.2.2 for detailed discussion]). The thickness of the waste package pallet assembly is determined by using the material properties (including density) of Alloy 22, and matching the total masses of the waste package and pallet as presented in *D&E/PA/C IED Typical Waste Package Components Assembly* (BSC 2004 [DIRS 169472]) and *Emplacement Pallet* (BSC 2003 [DIRS 161520]). The initial longitudinal distance between the neighboring waste package pallet assemblies, 0.1 m, is based on the initial longitudinal distance between the neighboring waste packages (Williams 2002 [DIRS 159916], Table 2). The benefit of using this approach is to reduce the computer execution time while preserving the features of the problem most relevant to the structural response of the middle DS. (for further discussion of the waste package pallet assembly see Section 5.3.2.2.).

[7] The 21-PWR assembly is used here as it is the most common type of waste package assembly to be emplaced in the repository (roughly 38 percent – BSC 2004 [DIRS 169472], Table 11).

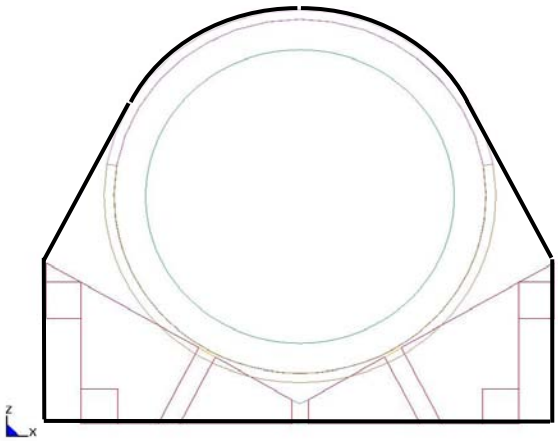

Source: BSC 2003 [DIRS 163425], Figure 3.

Figure 5-13. Contours of Waste Package Pallet Assembly and Waste Package Mounted on Pallet

Three components of the ground-motion acceleration time history are simultaneously applied on the platform representing the invert surface, which is unyielding (elastic)[8]. Externally applied momentum is transferred to all freestanding (unanchored) objects solely by friction and impact.

The DSC support beams, the DSC connector guides, the DSC guides, the support beam-connectors, the peripheral bulkheads, and the boundary walls are represented by eight-node solid (brick) elements. All other parts are represented by four-node shell elements. In general, the shell elements are adequate for representation of structural components as long as their dominant mode of deformation is bending. It is important to note that this analysis is focused on the DS plates; the stress state in other DS parts is of interest only to the extent it affects the DS plates results. The damage in other structural elements is not essential for overall performance of the DS as long as the structure remains stable. Time-dependent stress corrosion of the structural elements other than the DS plates will not significantly affect potential for water seeping through the DS on the waste packages. A possible effect of time-dependent stress corrosion would be weakening of the structure for any subsequent seismic events, but this is felt to be a second-order effect and is not analyzed here. The shell element used for representation of the DS plates is fully integrated four-node shell element with Gauss integration and five integration points through the shell thickness (Livermore Software Technology Corporation 2003 [DIRS 166841], p. 26.22). The use of shell elements in the FE representation of DS is further discussed in Section 5.3.2.1.

The FE representation is used in LS-DYNA to perform a transient dynamic analysis of the interlocking DSs exposed to vibratory ground motion. The simulation is performed in two steps. The first step is simulation of vibratory motion. During this computational phase the three components of ground-motion acceleration time history are simultaneously applied to all invert nodes. In the course of this vibratory simulation, neither system damping nor contact damping (between the unanchored objects) is applied. This conservative approach is used in order to prevent unwanted interference of the damping with the rigid-body motion of unanchored structures that could affect the results. The second step of the simulation is the post-vibratory

[8] This is a formal LS-DYNA requirement; the same acceleration time history applied to all platform nodes result in zero deformation by definition, thus, the invert is essentially rigid.

relaxation. During this computational phase the motion of the invert nodes is constrained in all three directions, and the only load applied to freestanding objects is the acceleration of gravity. In the course of this phase, the system damping is applied globally (to all objects). The goal of this step is to obtain steady-state results (and residual stresses in the DS plates) in a reasonable time, while the purpose of the global system damping is to reduce the convergence time (see Section 5.2.6 for details). The specified duration (0.5 s) of this post-vibratory relaxation part of the simulation is to allow for the steady-state stresses to equilibrate, which can be verified by visual inspection of the residual stress distributions by the post-processing graphical software program, LS-POST V2.

The mesh of the FE representation is appropriately generated and refined in appropriate regions according to standard engineering practice. This practice calls for use of finer meshing in areas of potential contact and/or stress concentration. Thus, the accuracy and representativeness of the results of this calculation are acceptable (see Section 5.2.2.4.1 for discussion of results). The uncertainties are taken into account by random sampling (from appropriate probability distributions) of the calculation inputs that are inherently stochastic (uncertain) and characterized by a large scatter of data (namely, ground-motion time histories and friction coefficients as discussed in more detail in Section 5.3.1.2).

5.2.2.2 Finite Element Representation for Rock Impact in Nonlithophysal Rock Mass

The objective of this calculation is to determine the DS damaged areas after impact by rockfall in nonlithophysal rock mass (Section 1). These areas are calculated using the postprocessor LS-PREPOST V1.0, and verified by visual inspection and measurement of the FE representation.

The three-dimensional FE mesh representations of the DS and the impacting rock blocks are developed in ANSYS V5.6.2 for six different rock sizes. Based on the nonlithophysal rockfall estimates presented in *Drift Degradation Analysis* (BSC 2004 [DIRS 168550], Section 6.3), three different rockfall-DS impact orientations have been considered: vertical, DS corner, and DS side-wall (described in Section 5.4.2.1). The FE representations of the DS are developed by using the dimensions provided in *Drip Shield Structural Response to Rock Fall* (BSC 2004 [DIRS 168993], Attachment I).

All of the DS components are represented by constant stress eight-node solid (brick) elements (Livermore Software technology Corporation 2003 [DIRS 166841], p. 26.30). One-point Gaussian quadrature is used for the solid element (Hallquist 1998 [DIRS 155373], Section 3). Because the DS top plate and the side-walls are the most important DS components in this calculation, all damaged areas are reported exclusively for these parts. To capture the details of stress concentration at the rock block impact location, the FE representation of the DS consists of one finely-meshed region where rock impact takes place, and coarsely-meshed regions elsewhere. The FE representation of the DS top plate has five layers of brick elements through the thickness. Furthermore, the FE mesh is refined in the impact regions in both axial and circumferential directions. The geometry of the FE representations used in this calculation is illustrated in Figures 5-14 and 5-15.

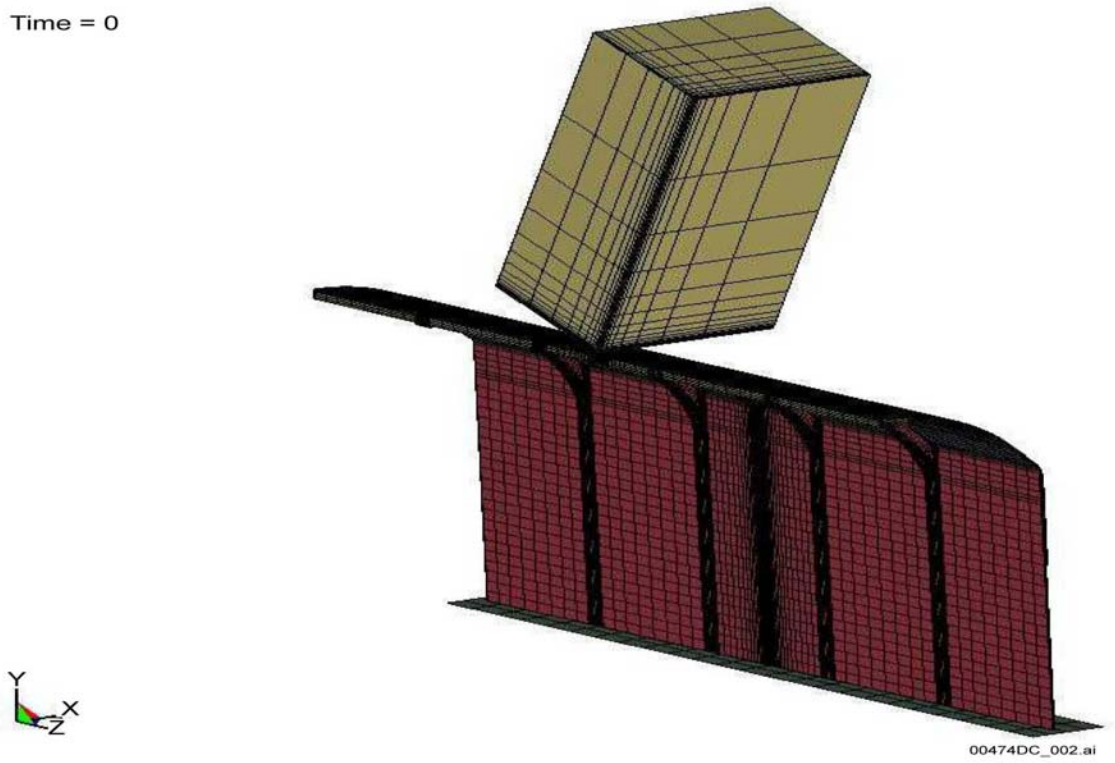

Source: Derived from BSC 2004 [DIRS 168993], Table 8-1, c1mesh4.

Figure 5-14. View of the Finite Element Representation Used for Analysis of Rock Impact

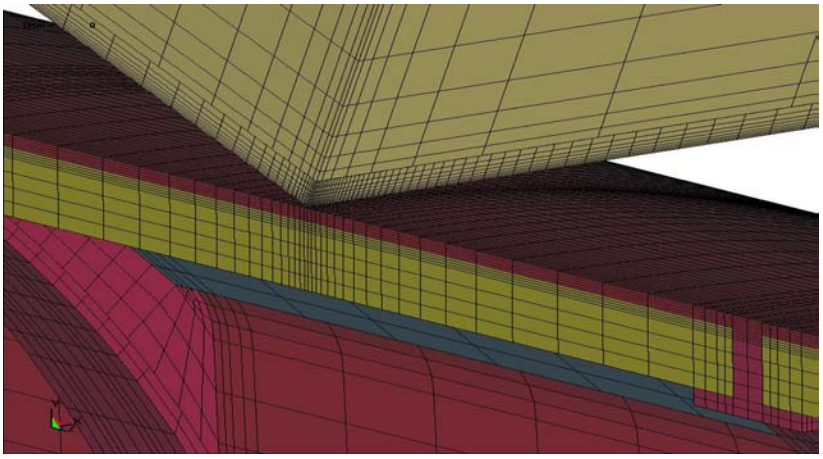

Source: Derived from BSC 2004 [DIRS 168993], Table 8-1, c1mesh4.

Figure 5-15. Detailed View of the Finite Element Representation Used for Analysis of Rock Impact

The DS corner and side-wall rockfall FE representations include an idealized waste package positioned next to the DS side-wall inside surface. The waste package is represented by rigid shells, which is used to provide a rigid boundary condition and bounding stress results for the DS.

The full-length of the DS is represented in the FE solutions. The rockfall is imposed at the mid-length of the DS, which receives no additional support from the connector plates; and hence, provides bounding stress results. Furthermore, the Alloy 22 base plate is excluded from the FE representation (Assumption 3.17). The benefit of using this assumption is to reduce the computer execution time while keeping the essential parts of the structure.

The FE representation of the impacting rock block is divided into two regions: a small, finely meshed impact region and coarsely meshed region representing the remaining part of the rock block. The continuity of deformation between these two differently meshed regions of the rock is ensured by a tied-interface contact. The fine mesh in the impact region is essential for accurate representation of the rock deformation. The elastic-ideally-plastic constitutive representation (Section 5.2.3.3) in the finely meshed region ensures realistic rock deformation and yield in the impact zone compared to the elastic rock defining the remainder of the rock block. This approach attempts to capture the localized crushing of the rock in the contact region and the consequent load distribution over the larger DS top plate area (Section 5.2.3.3).

The specified termination times of rock-fall simulation are such to allow the rock to bounce off of the DS top plate after the impact, and for steady state to establish.

The mesh of the FE representation was appropriately generated and refined in the contact regions according to standard engineering practice. Thus, the accuracy and representativeness of the results of this calculation are deemed acceptable (Section 5.2.2.4.2).

5.2.2.3 Finite Element Representation for Static Load by the Caved Rock Mass

The objective of this calculation is to investigate stability of the DS under static load of the caved rock mass, and to determine an approximate value for the factor of safety of the DS for the applied vertical and lateral static load. The three-dimensional FE representation that is used to perform the structural stability calculations is developed in TrueGrid V2.2 (Figures 5-16 through 5-18). This FE representation is limited to one segment of the DS (Figure 5-17); thus, it is referred to as the one-segment FE representation. Appropriate boundary conditions are specified at the end-sections A-A and B-B of the one-segment representation (Figure 5-17) to account for the removed part of the DS. One calculation was also performed by using the full FE representation of the DS (Figure 5-16) to verify the results obtained by using the one-segment FE representation (Section 5.4.3.2).

In the FE representations, the DS is free to move laterally with the exception of the constraint provided by the pallet (Figure 5-17) (Assumption 3.16). Note that this calculation is concerned with the quasi-static pressure induced by rock rubble. The rock rubble pressure distribution on the DS is calculated in a separate model (which couples rock mass deformation and rockfall with elastic deformation of the DS) for the DS that is in static equilibrium. The details of the modeling of emplacement drift collapse, rubblization of the rock mass and loading of the DS is presented in *Drift Degradation Analysis* (BSC 2004 [DIRS 166107], Section 6.4), and reviewed

in Section 5.2.5.1 of this document. The final deformed DS configuration, corresponding to static equilibrium under the specific rubble pressure distribution, is different from the DS configuration before the pressure application. The DS equilibrium configuration could be affected by the pallet lateral constraint depending on the pressure distribution.

All DS nodes belonging to end-sections A-A and B-B (Figure 5-12) are constrained from translating in the longitudinal (*z*-) direction and from rotating about the *x*-axis and *y*-axis. The following are reasons for these boundary conditions: (1) the DS (as represented in Figure 5-11) has a plane of longitudinal symmetry and its geometry for the most part consists of the repeating segments, and (2) the pressure distribution is independent of the longitudinal (*z*-) coordinate.

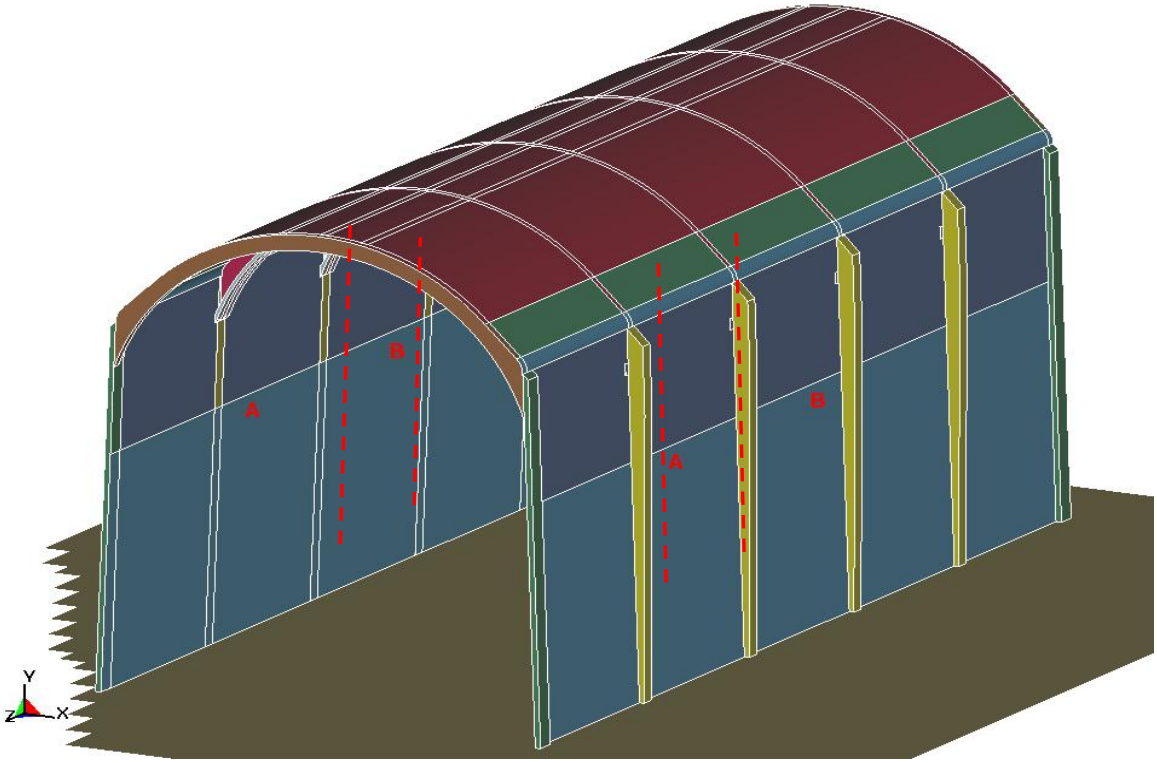

Source: BSC 2004 [DIRS 170791], Figure 1.

Figure 5-16. Full Finite Element Representation of the Drip Shield

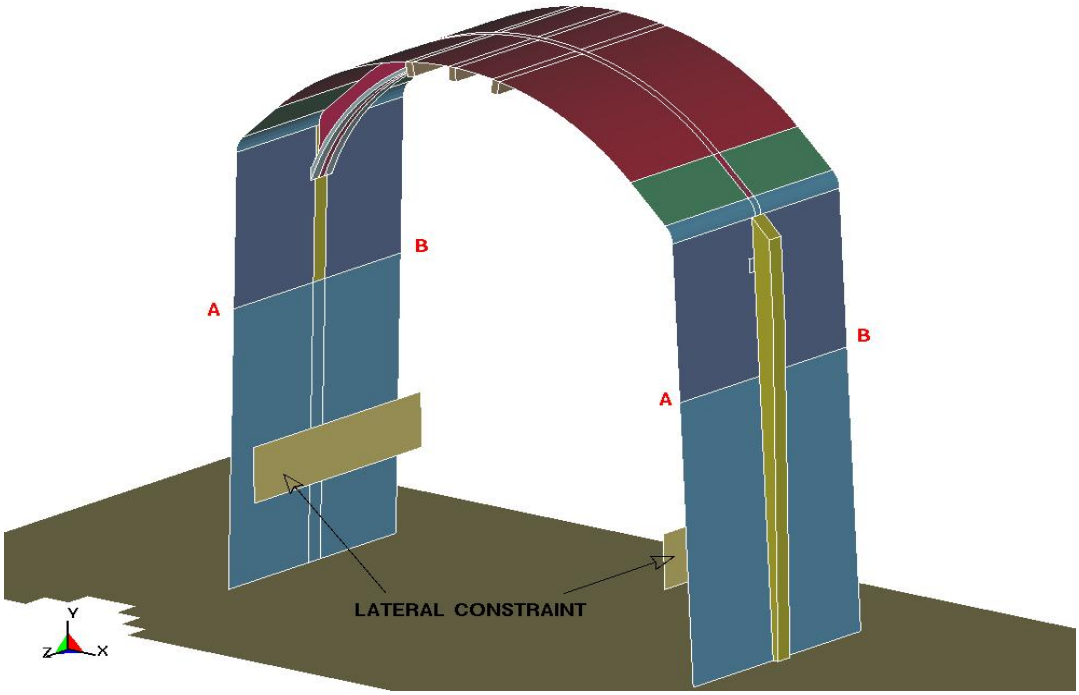

Source: BSC 2004 [DIRS 170791], Figure 2.

Figure 5-17. One-Segment Finite Element Representation of the Drip Shield

The FE representations are developed by using shell elements for the DS plates (specifically, DS plate-1, DS plate-2, and support plates), and solid (brick) elements for the rest of the structure (i.e., the support beams, bulkheads, bulkhead longitudinal stiffeners, etc.; see BSC 2004 [DIRS 170791], Attachment I). The details of the FE representation are illustrated in Figure 5-18. The fully-integrated four-node shell element (Livermore Software Technology Corporation 2003 [DIRS 166841], p. 26.22) and the constant-stress eight-node solid element (Livermore Software Technology Corporation 2003 [DIRS 166841], p. 26.30) are used for all calculations. Gauss integration and five through-thickness integration points (Livermore Software Technology Corporation 2003 [DIRS 166841], p. 26.23) are specified for the shell element. One-point Gaussian quadrature is used for the solid element (Hallquist 1998 [DIRS 155373], Section 3).

5.2.2.4 Mesh Objectivity

The objectivity (mesh insensitivity of the calculations) of the meshes used for the calculations is verified in this section. The approach used is presented in detail in Mecham (2004 [DIRS 170673], Section 6.2.3). Two different meshes of the DS are generated and used in the FE simulation. The first mesh is obtained by following the standard engineering practice and guidance in Mecham (2004 [DIRS 170673], Section 6.2.3). The second mesh is a refined version of the first mesh. The results obtained by the first mesh are considered mesh-objective (i.e., mesh-insensitive) if the relative difference of results (e.g., damaged area) between the first and the second mesh are much smaller (approximately an order of magnitude smaller) than the relative difference of areas (or volumes) of their representative (average, typical) elements.

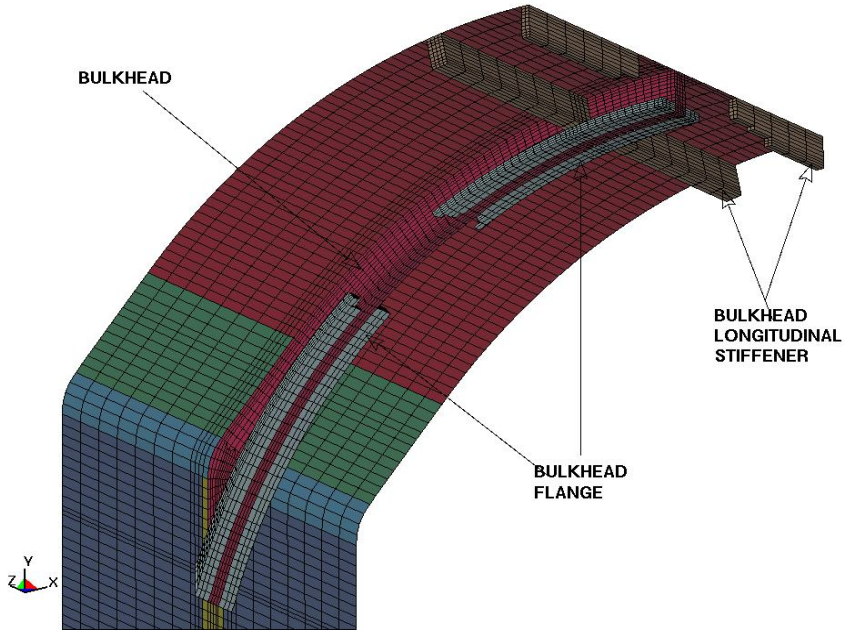

(a)

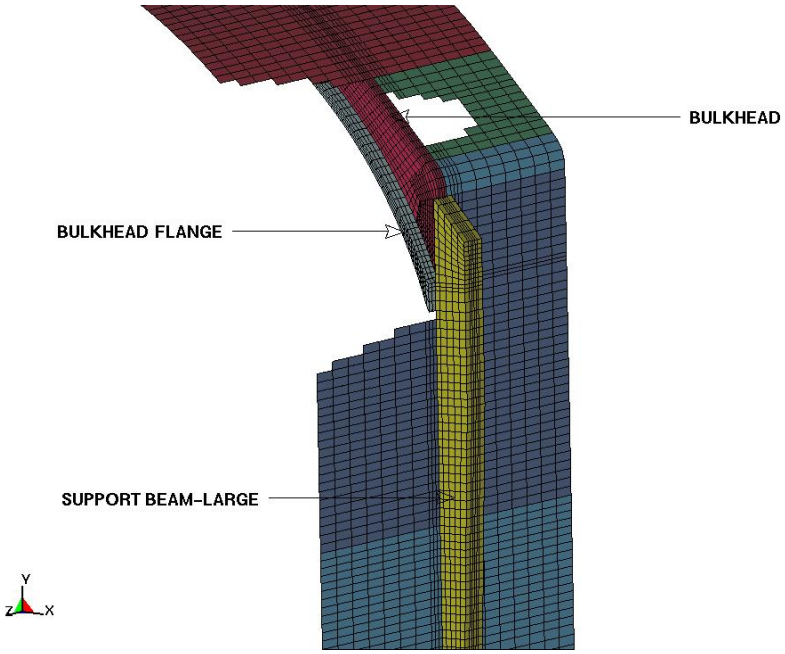

(b)

Source: BSC 2004 [DIRS 170791], Figure 3.

NOTE: Some DS parts are partially removed from Figure 5-13 to improve visibility; (a) top (inside view) and (b) side (outside view).

Figure 5-18. Details of Finite Element Representation of the Drip Shield

5.2.2.4.1 Vibratory Ground Motion

The typical DS shell element area of the first mesh is 300 percent (four times) larger than the area of the corresponding element in the second mesh. Element number 6442 of the first mesh and element number 9617 of the second (refined) mesh can be compared as typical elements for the two FE representations.

The mesh sensitivity of the DS damaged area is studied for realization 10 (Table 5-17) at 1×10^{-6} annual frequency of occurrence. The results are presented in Table 5-1.

Table 5-1. Damaged DS Area for Two Different FE Meshes for Realization Number 10 (1×10^{-6} Annual Frequency of Occurrence)

Mesh	Damaged Area (m^2; % of DS plate area)
First Mesh $A = 4A_0$	0.192; 0.502
Second Mesh $A = A_0$	0.169; 0.441

Source: BSC 2003 [DIRS 163425], Table III-1.

According to results presented in Table 5-1 the reduction of typical element size by 300 percent for realization 10 results in decrease of the damaged area by 12.0 percent.

The decrease of the damaged area in the case of the refined mesh can be explained by more localized DS deformation (following the impacts between DS and waste package pallet assembly) for the refined mesh compared to the one for the coarser mesh. Thus, the results obtained by using the first mesh meet the mesh-objectivity criterion from Mecham (2004 [DIRS 170673], Section 6.2.3). Namely, a coarse mesh is inherently less capable of accommodating localized deformation (it is less flexible to do so). Consequently, the impact energy delivered to the DS plate is smeared over a larger area. In other words, the redistribution of the impact energy over a larger area is caused by the inherent inability of the (less flexible) coarse mesh to capture the localized deformation. In the case of a relatively low damage threshold, the results of fine mesh calculations leads to overestimation of the damaged area by the coarse mesh model. The stress averaging within a relatively coarse constant-stress element is, consequently, likely to overestimate the damaged area.

5.2.2.4.2 Rock Impact in Nonlithophysal Rock Mass

The values of two stress invariants (stress intensity and the maximum first principal stress) are presented for two different meshes in Table 5-2. The DS top plate element volume at the point of impact in the first mesh is 67 percent larger than the corresponding element in the second mesh ($5.148\times10^{-8}/3.089\times10^{-8}$ = 1.67). Specifically, the numbers of divisions in the axial, tangential, and thickness directions are increased from 14 to 16, from 4 to 5, and from 5 to 6, respectively. The calculation results presented in Table 5-2 indicate that the reduction of the element volume by 67 percent in the contact region results in negligible effect on the stress intensity. The difference in the first principal stress values between the two meshes is a little bit

more pronounced, but still meets the mesh-objectivity requirements in Mecham (2004 [DIRS 170673], Section 6.2.3). The original FE mesh is, therefore, deemed acceptable and all remaining calculations are performed with the coarser mesh.

Table 5-2. Stress Intensity and First Principal Stress for Two Different FE-Representation Meshes (14.5 MT Vertical Rockfall)

	Stress Intensity (MPa)	First Principal Stress (MPa)
First Mesh V = 1.67 V0	346	340
Second Mesh V = V0	352	363
Difference (%)	1.7	6.3

Source: BSC 2004 [DIRS 168993], Table 6-1.
MT: metric tons (1 MT = 1000 kg)

5.2.2.4.3 Static Load by the Caved Rock Mass

The volumes of the typical elements for the support beam and bulkhead for two different meshes are presented in Table 5-3. The numbers presented in Table 5-3 in parentheses represent the number of the element that is considered typical.

As described in Section 5.2.5.1, the rock rubble loads derived from 6 realizations of drift collapse provided in *Drift Degradation Analysis* (BSC 2004 [DIRS 166107], Section 6.4.2.5), are applied to the outer surface of the DS to investigate structural stability and damage. As a part of this study, the ultimate load-bearing capacity of the DS is examined by artificially increasing the density of the rubble to force increasing loads until failure of the DS occurs. The rubble density was increased in a number of steps from 1 to 4 times, with 6 realizations conducted at each density step. The mesh sensitivity was studied in particular for the case in which the average loads from all 6 realizations with a density multiplication factor of 2.5 was used (discussed in Section 5.4.3.1). The choice of this realization is arbitrary: the mesh-objectivity results should not depend on the particular pressure distribution. The calculation with the density of the surrounding rock multiplied by 2.5 is interesting because it illustrates an approximate stability safety margin for the DS for that pressure distribution (Section 5.4.3.2). The results are presented in Table 5-4.

According to results presented in Tables 5-3 and 5-4, the calculation results are not mesh-sensitive.

Table 5-3. Volume of Typical Element for Two Different Finite Element Meshes

DS Component	Volume of Typical Element ($1 \cdot 10^{-6}$ m^3)		
	First Mesh	Second Mesh	Relative Difference (%)
Bulkhead	1.38 (e# 6453)	0.85 (e# 15798)	62
Support Beam	2.47 (e# 4800)	1.46 (e# 12614)	69
	5.21 (e# 4888)	1.92 (e# 12854)	171

Source: BSC 2004 [DIRS 170791], Table V-1.

Table 5-4. Maximum Vertical Displacement of Drip Shield Top for Two Different Finite Element Meshes

Maximum Vertical Displacement ($1 \cdot 10^{-3}$ m)		
First Mesh	Second Mesh	Relative Difference (%)
19.08	18.92	0.8

Source: BSC 2004 [DIRS 170791], Table V-2.

5.2.2 Material Properties

Material properties used in these calculations are discussed in this section. The basic material properties required as input to these analyses include the mechanical properties of Ti-7 and Ti-24, as well as the mechanical properties of the rock blocks (termed TSw2). The DS temperature is assumed to be 150°C (Assumption 3.12). Some of the temperature-dependent and rate-dependent material properties are not available for Ti-7, Ti-24 and TSw2 rock. Therefore, RT Poisson's ratio, elongation, and modulus of elasticity obtained under the static loading conditions are used for these materials (Assumptions 3.1 through 3.3).

5.2.3.1 Titanium

Typical stress-strain curves for Ti-7, Ti-24 and Alloy 22, and their idealizations used in numerical analyses are shown in Figure 5-19. Material properties of Ti-7 (SB-265 R52400) are given in Table 5-5.

Material properties of Ti-24 (SB-265 R56405) are similar to those of Ti-5 because the compositions are almost identical (ASME 2001 [DIRS 158115]), Section II, Part B, SB-265, Table 2). These material properties, given in Table 5-6, are specified using the nominal composition, 6Al-4V.

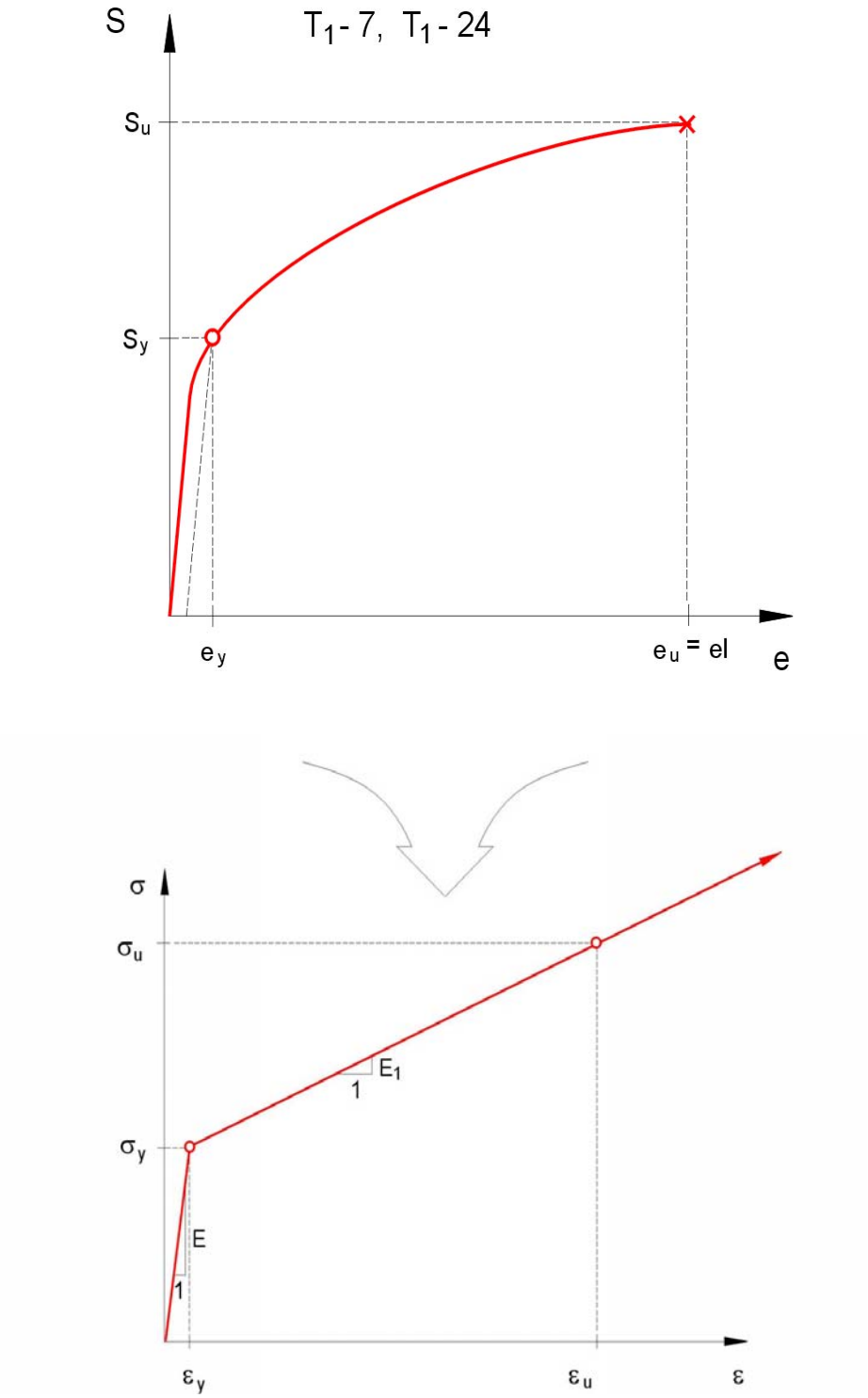

Figure 5-19. Typical and Idealized Stress-Strain Curves for Titanium Grades 7 and 24

Table 5-5. Material Properties of Ti-7 (SB-265 R52400)

Property	Temperature [°C]/[°F]	Range	Value	Source
Young's Modulus E [GPa]*	149/300	—	101	MO0003RIB00073.000 [DIRS 152926], page 3
	204/400	—	97	MO0003RIB00073.000 [DIRS 152926], page 3
Density ρ [kg/m^3]*	RT	4500-4540	4520	MO0003RIB00073.000 [DIRS 152926], page 1
Poisson's Ratio ν	RT	—	0.32	MO0003RIB00073.000 [DIRS 152926], page 3
Yield Strength s_y [MPa]*	RT	275-450	363	MO0003RIB00073.000 [DIRS 152926], page 2
	204/400	138-152	145	MO0003RIB00073.000 [DIRS 152926], page 2
Tensile Strength s_u [MPa]*	RT	—	345	MO0003RIB00073.000 [DIRS 152926], page 2
	204/400	207-228	218	MO0003RIB00073.000 [DIRS 152926], page 2
Elongation e_u	RT	—	0.2	MO0003RIB00073.000 [DIRS 152926], page 2
	204/400	0.38-0.45	0.42	MO0003RIB00073.000 [DIRS 152926], page 2

NOTE: An average value is used in the calculations described in this document, as the number of data points available does not justify the assumption of a distribution of values.

*Values rounded to nearest whole number.

RT = room temperature

Table 5-6. Material Properties of Ti-24 (SB-265 R56405)

Property	Temperature [°C]/[°F]	Range	Value	Source
Young's Modulus E [GPa]*	RT	107-122	115	TIMET 2000 [DIRS 160688], table 2
	230/450	95-111	103	TIMET 2000 [DIRS 160688], table 2
Density ρ [kg/m^3]*	RT	—	4430	ASM 1990 [DIRS 141615], page 620
Poisson's Ratio ν	RT	—	0.34	ASM 1990 [DIRS 141615], page 621
Yield Strength s_y [MPa]*	RT	—	910	TIMET 1993 [DIRS 157726], page 11
	204/400	—	683	TIMET 1993 [DIRS 157726], page 11
Tensile Strength s_u [MPa]*	RT	—	1000	TIMET 1993 [DIRS 157726], page 11
	204/400	—	772	TIMET 1993 [DIRS 157726], page 11
Elongation e_u	RT	—	0.18	TIMET 1993 [DIRS 157726], page 11
	204/400	—	0.17	TIMET 1993 [DIRS 157726], page 11

NOTE: An average value is used in the calculations described in this document, as the number of data points available does not justify the assumption of a distribution of values.

*Values rounded to nearest whole number.

RT = room temperature

5.2.3.1.1 Calculation for Material Properties at Elevated Temperature

Some of the material properties of Ti-7 and Ti-24 are not available at $T_{\max} = 150\ ^oC$ (Section 5.2.3.1). They are, therefore, obtained (Table 5-7) by linear interpolation using the following relation:

$$P = P(T) = P_l + \left(\frac{T - T_l}{T_u - T_l} \right) \cdot (P_u - P_l), \qquad \text{(Eq. 5-6)}$$

where subscripts *u* and *l* denote the bounding values of the property (*P*) at the corresponding bounding temperatures (*T*).

Table 5-7. Interpolated Mechanical Properties for Titanium

Property	Temperature [ºC]	Ti-7	Ti-24
Young's Modulus E [GPa]	20	—	115
	150	101	108
	204	97	—
	150*	101	108
Yield Strength s_y [MPa]	20	363	910
	204	145	683
	150*	209	750
Tensile Strength s_u [MPa]	20	345	1000
	204	218	772
	150*	255	839
Elongation e_u	20	0.2	0.18
	204	0.42	0.17
	150*	0.36	0.17

Source: BSC 2004 [DIRS 168993], Section 5.1.1.

NOTE: All input parameters listed in Section 5.2.3.1. The calculated values are for 150ºC, marked with *.

5.2.3.1.2 Calculations for True Measures of Ductility

The material properties in Section 5.2.3.1 were derived from static tensile strength tests and refer to quantities of *engineering* stress, s, and strain, e, defined as: $s = P/A_0$ and $e = L/L_0 - 1$ (Dieter 1976 [DIRS 118647], Chapter 9), where *P* stands for the force applied during a static tensile test, *L* is the length of the deformed specimen, and L_0 and A_0 are the original length and cross-sectional area of the specimen, respectively. The engineering stress-strain curve does not give a true indication of the deformation characteristics of a material during plastic deformation since it is based entirely on the original dimensions of the specimen. In addition, ductile metal that is pulled in tension becomes unstable and necks down during the course of the test. Hence, LS-DYNA code requires input in terms of *true* stress, σ, and strain, ε, definitions, i.e.: $\sigma = P/A$ and $\varepsilon = \ln(L/L_0)$ (Dieter 1976 [DIRS 118647], Chapter 9).

The relations between the true stress and strain and the engineering stress and strain, $\sigma = s \cdot (1+e)$ and $\varepsilon = \ln(1+e)$, can be readily derived based on constancy of volume (i.e., $A_0 \cdot L_0 = A \cdot L$) and strain homogeneity during plastic deformation (Dieter 1976 [DIRS 118647], Chapter 9). These expressions are applicable only in the hardening region of the stress-strain curve that is limited by the onset of necking.

In absence of data on the uniform strain in the available literature, it is estimated based on the material elongation (strain corresponding to rupture of the tensile specimen, see Assumption 3.5).

Table 5-8. True Tensile Strength and Elongation for Titanium

Property	Ti-7	Ti-24
Engineering Elongation e_u	0.36	0.17
Engineering Tensile Strength s_u [MPa]	255	839
True Elongation ε_u	0.31	0.16
True Tensile Strength σ_u [MPa]	347	982

Source: BSC 2004 [DIRS 168993], Section 5.1.2.

NOTE: All properties are estimated for 150ºC (Section 5.2.3.1.1).

The calculated true measures of ductility are given in Table 5-8. Note that there is no practical difference between the true and engineering yield strength, $s_y \approx \sigma_y$, or between the true and engineering strain corresponding to yield strength, $e_y \approx \varepsilon_y$, because $e_y \approx 1$.

5.2.3.1.3 Calculations for Tangent Moduli

As previously discussed, the results of the simulations described in this report are required to include elastic and plastic deformations for Ti-7 and Ti-24. When the materials deform plastically, the slope of the stress-strain curve continuously changes as shown in Figure 5-14. A ductile failure is preceded by a protracted regime of hardening and substantial accumulation of inelastic strains. Thus, a simplification for stress-strain curve is needed to incorporate plasticity into the FE analysis. A standard approximation commonly used in engineering is to use a straight line that connects the yield point and the tensile strength point of the material as indicated in Figure 5-19. The parameters used in the subsequent calculations in addition to those defined in Section 5.2.3.1.2 are modulus of elasticity (*E*) and tangent (hardening) modulus (E_1). The tangent modulus, which represents the slope of the stress-strain curve in the plastic region, is calculated using the following relation.

$$E_1 = \left(\sigma_u - \sigma_y\right) \Big/ \left(\varepsilon_u - \sigma_y / E\right) \qquad \text{(Eq. 5-7)}$$

The calculated values of the tangent moduli are listed in Table 5-9.

Table 5-9. Titanium Tangent Moduli

Property	Ti-7	Ti-24
Yield Stress σ_y [GPa]	0.209	0.750
Young's Modulus E [GPa]	101	108
Ultimate Stress σ_u [GPa]	0.347	0.982
Elongation ε_u	0.31	0.16
Tangent Modulus E_1 [GPa]	0.448	1.516

Source: BSC 2004 [DIRS 168993], Section 5.1.3.

NOTE: All properties are for 150ºC (Sections 5.2.3.1.1 and 5.2.3.1.2).

5.2.3.1.4 Failure Criteria

Mechanical processes that occur during a seismic event may compromise the functionality of the DSs as barriers to seepage of water and rockfall on the waste package. These mechanical processes include impacts caused directly by vibratory ground motion during an earthquake, impacts caused by rock blocks and rockfall induced by vibratory ground motions, and mechanical loading from rockfall rubble.

Under vibratory ground motions, impacts can occur between the DS and the waste package, the pallet, the invert, and even the drift wall. Rockfall induced by vibratory ground motions can result in impacts on the DS in the postclosure period. Rockfall induced by vibratory ground motion in the lithophysal zones may collapse the drifts, resulting in static loads from the mass of rubblized rock surrounding the DS.

These mechanical processes are associated with a number of potential failure mechanisms:

- Mechanism 1–Dynamic loads have the potential to result in immediate puncture (breach) or tearing of the DS plates if the localized strain exceeds the tearing failure threshold. A puncture provides a potential pathway for flow through the DS.

- Mechanism 2–Impact-related dynamic loads may dent the DS, resulting in permanent structural deformation with residual tensile stress. High levels of residual tensile stress may lead to local degradation from accelerated corrosion processes. Areas that are breached from corrosion processes provide a potential pathway for flow.

- Mechanism 3–Static loads from rockfall lead to (plastic) structural deformation and may collapse or buckle the DS's. Buckling or collapse represents a change in the physical shape of the DS, potentially compromising its ability to deflect seepage and rockfall away from the waste package.

The potential for immediate puncture (breach) or tearing of the DS plates (Mechanism 1) through tensile or shear failure is not excluded in the constitutive representation for the structural response calculations. Note however, that for the vibratory ground motion simulations, the computational meshes used for the damaged area calculations may be too coarse to realistically simulate a small, localized puncture. The maximum stresses during this event may, therefore, be mesh-sensitive and underestimated; and, consequently, unreliable for the immediate breach evaluation (BSC 2003 [DIRS 165497]). Nonetheless, the immediate breach or tearing of the DS plates (Mechanism 1) is unlikely because Ti-7 is a ductile metal that requires very high dynamic loads to reach the tearing failure threshold. Additionally, the tearing failure of ductile materials is, in general, accompanied by large distortion and significant expenditure of energy. Consequently, a small tear (through-wall macrocrack) is likely to be encompassed by a much larger highly-distorted region that is preferable site for stress corrosion cracking. Therefore, the small tear would likely be encompassed, if not covered, by the deformed area; and thus, accounted for indirectly by Mechanism 2.

The presence of high residual tensile stress (Mechanism 2) has the potential to result in accelerated stress corrosion cracking. This combined mechanical-corrosion failure mechanism is

expected to be the most likely cause of failure for the DS from impact processes caused by vibratory ground motions and by rockfall induced by vibratory ground motions. The areas that exceed the residual tensile stress threshold are referred to as the damaged area.

Figure 5-20 is a simplified illustration of how residual stress is generated by permanent (plastic) deformation in a simple uniaxial strain model. The loading path in Figure 5-20 has three phases: (1) elastic loading until reaching the elastic yield limit, (2) plastic loading above the elastic yield limit, and (3) elastic unloading when the external load reduces the local stress. Figure 5-20 shows that plastic deformation does not always generate a damaged area because the final residual stress state may be compressive or, if tensile, may be below the tensile threshold to initiate accelerated stress corrosion cracking.

The static loads from rockfall (Mechanism 3) have the potential to produce plastic deformation of the DS, possibly initiating the buckling or collapse of the DS. The appropriate failure criterion for plastic structural deformation is the elastic yield strength (the point at the end of the elastic loading path in Figure 5-20). The physical configuration of the DS can change when local stresses exceed the elastic yield strength, resulting in plastic deformation of the structure. It is important to differentiate between the two failure criteria for the DS. For impact loading on the DS, an area is damaged when it exceeds the residual stress threshold of Ti-7. This failure is a combined mechanical-corrosion response of a cold-worked material to dynamic impacts. For static loading, the failure of the DS is determined by the elastic yield strength when plastic yielding begins. These criteria are applied separately and independently because the appropriate failure mechanisms are distinct physical responses to different loading conditions and failure modes (BSC 2004 [DIRS 169183], Section 6.6.2).

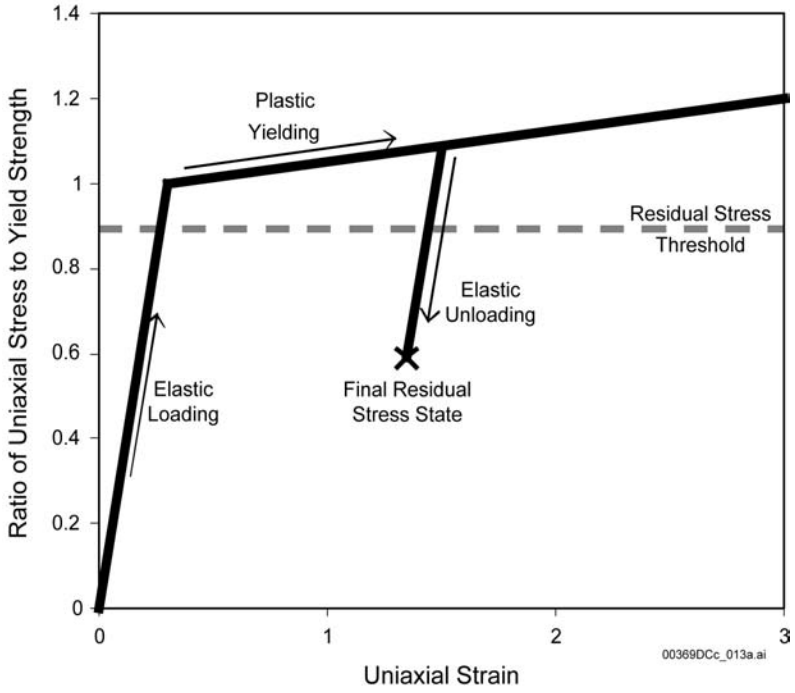

Source: BSC 2004 [DIRS 169183], Figure 6.3-1.

Figure 5-20. Permanent Deformation from Plastic Yielding Generates Residual Stress

In summary, accelerated stress corrosion cracking from high residual stress is expected to be the most likely cause of failure for the DS from impact. Since a residual stress threshold is the main failure criterion for vibratory ground motion and rockfall impact, this failure mechanism is described in detail.

For the DS, the residual stress threshold for failure is represented by a fixed lower bound of 50 percent of the yield strength of the DS plate material (Ti-7) (BSC 2004 [DIRS 169042], Section 6.2.1). There is a significant experimental database for Ti-7 that justifies the use of 50 percent of yield strength as a stress corrosion cracking initiation criterion (BSC 2004 [DIRS 169042]). These data include long-term constant load tests in a concentrated groundwater environment at 105°C (221°F), with specimens loaded to stresses of 110 percent to 140 percent of the yield strength. A second source of information comes from U-bend tests. Initiation of stress corrosion cracking is not observed in fixed deflection U-bend tests on Ti-7, exposed for 1 year, and Titanium Grade 16 (an analogous titanium–palladium alloy), exposed for 5 years, to a range of relevant aqueous environments at 60°C (140°F) and 90°C (194°F). These U-bend tests are more representative of secondary residual stress loading that might result from deformation following seismic loadings. A conservative value of 50 percent of yield strength is selected (Assumption 3.18) as a threshold criterion for Ti-7, even though the initiation of stress corrosion cracking is not observed for residual stresses greater than yield strength.

5.2.3.1.5 Effect of Corrosion

To account for the effect of corrosion during the postclosure period (other than stress corrosion) the thickness of Ti-7 and Ti-24 components is reduced by 2 mm (Assumption 3.13). It must be emphasized, though, that the objective of this calculation is not to rigorously evaluate the thickness reduction of the DS components due to corrosion or the corrosion-acceleration effects. A depth of corroded layer of 2 mm is, therefore, conservative within the stated objective of this calculation (Section 1). It should also be noted that the overall thickness of the parts of the DS plates covered by the internal and external support plates is conservatively reduced by 4 mm, implying the thickness reduction of 2 mm per plate at each location. The rationale for this conservative thickness reduction is that the welds connecting the DS support plates and the DS plates cannot guarantee hermiticity. Consequently, the general corrosion on the interface between the two plates cannot be excluded.

5.2.3.2 Frictional Contacts

5.2.3.2.1 Finite Element Calculations

Contacts are specified, in FE representations, between all DS, waste package pallet, drift walls and invert surfaces that can interact. In all calculations, except analysis of vibratory ground motion, it is assumed that the friction coefficient between interacting surfaces is 0.4 or 0.5 (Assumptions 3.9 and 3.10). In the analysis of vibratory ground motion, in which friction is essential for transfer of seismic ground motion from the invert to the DS, in absence of more specific data, the dynamic friction coefficients for all contacts are randomly sampled from a uniform distribution between 0.2 and 0.8 (Assumption 3.8). Different values for metal-to-metal friction coefficient and metal-to-rock friction coefficient are randomly sampled for each realization, and applied to all metal-to-metal and metal-to-rock contacts. Fifteen realizations

combine friction coefficients with 15 ground motions (Section 5.3.1.2). The friction coefficients of all metal-to-metal contacts have the same friction coefficient in a specific realization regardless of the contact pair; the same applies to metal-to-rock contacts.

The functional friction coefficient used by LS-DYNA code is defined in terms of static and dynamic friction coefficients, and relative velocity of the surfaces in contact (Livermore Software Technology Corporation 2001 [DIRS 159166], p. 6.9). The effect of the relative velocity of the surfaces in contact is introduced by way of a fitting parameter—exponential decay coefficient. The variation of friction coefficient between the static and dynamic value as a function of relative velocity of the surfaces in contact is not available in literature for the materials used in this calculation. Therefore, it is not possible to objectively evaluate the exponential decay coefficient. Hence, the effect of the relative velocity of the surfaces in contact is neglected in these calculations by assuming that the functional friction coefficient and the static friction coefficient are equal to the dynamic friction coefficient. This approach provides the bounding set of results by minimizing the friction coefficient within the given FE-analysis framework (Assumption 3.11). In case of quasi-static calculations the effect of the variation of friction coefficient between the static and dynamic value as a function of relative velocity of the surfaces in contact is not as important as in transient analysis.

5.2.3.2.2 Kinematic Model

5.2.3.2.2.1 Interaction Between the Drip Shield and the Invert

Two contacts (shown in Figure 5-21 as two vertical lines crossing the interface between the DS and the invert) represent the interaction between the DS and the invert in the kinematic calculations. The contacts in UDEC are characterized by both elastic and inelastic behavior. The elastic deformation (prior to yield) is controlled by the normal and shear stiffnesses. Inelastic deformation occurs if the stress along the contacts exceeds the tensile and shear strengths. The Coulomb slip condition, a function of cohesion and friction angle, defines the conditions when the interacting bodies slip relative to each other along the contact. The contact between the DS and the invert is considered to be frictional only (i.e., cohesion and tensile strength are considered to be zero). In all kinematic calculations, the friction coefficient between the DS and the invert is selected from a uniform distribution between 0.2 and 0.8 (Assumption 3.8). However, unlike the FE calculations (Section 5.2.3.2.1), each DS is assigned a different friction coefficient along the interface with the invert based on a random sampling of the uniform distribution. The variable friction coefficient is illustrated in Figure 5-22 as different colors of the DS blocks at the interface between the block and invert. The drift invert will be constructed from crushed tuff. Although there will be an effect of local conditions, the friction coefficient between the DS and the invert will likely be less variable than assigned here (i.e., between 0.2 and 0.8 corresponding to variation in friction angle between 11 degrees and 39 degrees.). This range of friction coefficient (0.2 to 0.8) represents a very wide range from ease of sliding to a high friction angle of contact. The friction coefficient between the DS and the invert is an important factor controlling relative horizontal motion of the DSs.

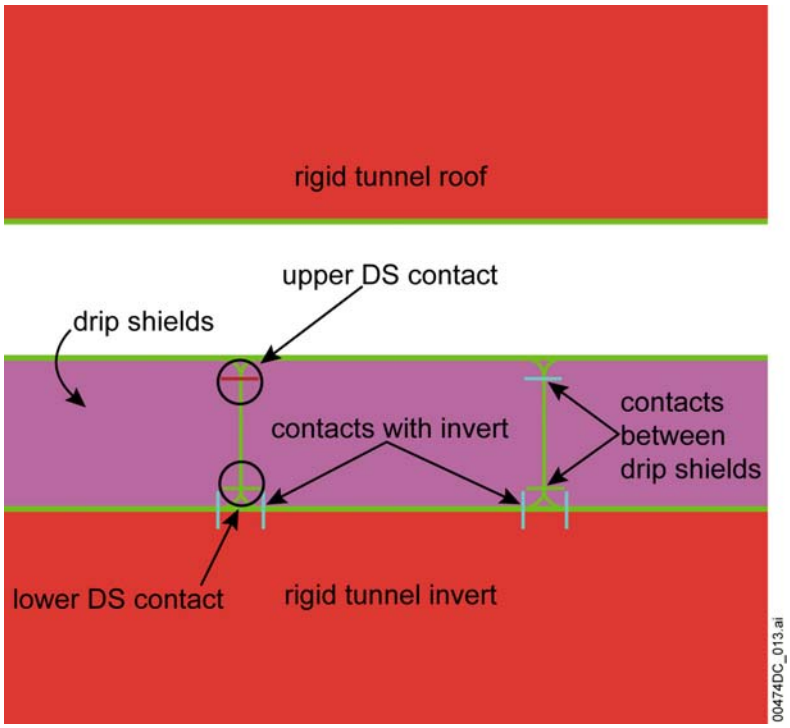

Figure 5-21. Detail of the Drip Shield and its Interaction with Neighboring Drip Shields and the Invert

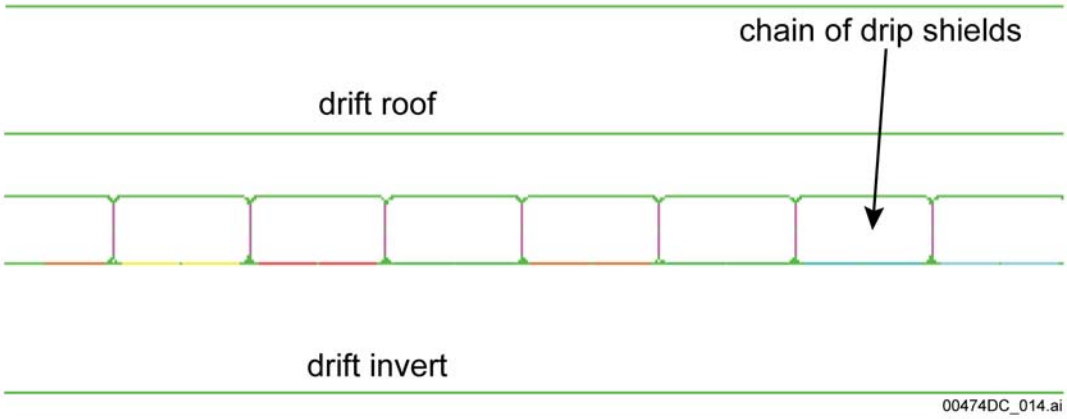

NOTE: Each drip shield boundary color signifies a different contact friction coefficient that varies via a uniform distribution between 0.2 and 0.8.

Figure 5-22. Contact Friction Coefficient Varies from DS to DS in UDEC Representation

The normal and shear contact stiffnesses of the interface between the DS and the invert are considered to be 3 MPa/m based on Assumption 3.24. The sensitivity of the calculation results of the invert contact stiffness is investigated here by considering cases in which the contact stiffness is assumed to be up to 10 times larger (i.e. 30 MPa/m) than in the base case (Table 5-19). All contacts are linearly elastic in the normal direction if the normal force is compressive. Consequently, the coefficient of restitution for all normal impacts is equal to unity. Energy dissipation during impacts takes place as a result of frictional sliding only.

5.2.3.2.2.2 Interaction Between the Drip Shields

Because of the adopted discretization, the kinematic simulation considers the interaction between the DSs to occur along two contacts (shown in Figure 5-21 as two horizontal lines crossing the interface between the DSs). A numerical idealization of the contact between the DSs, shown in Figure 5-23, deforms elastically, followed by plastic deformation after the peak shear and normal strengths are exceeded.

The contact normal (axial) and shear force-displacement relations have the form illustrated in Figures 5-24 and 5-25, respectively. Results indicate that the normal and shear stiffnesses (k_n and k_s as illustrated in Figures 5-23, 5-24 and 5-25) of the contact between the DSs do not significantly affect interaction and separation of the DSs. This is particularly the case for the shear stiffness. The majority of the analyses were carried out assuming the normal and shear stiffnesses of the contacts are equal to 100 MPa/m. This value was selected because it results in a small overlap or separation (compared to the size of the DS) of neighboring DSs before the contact breaks. In the simulations for 1×10^{-6} and 1×10^{-7} ground motions, the selected stiffness results in an axial elastic deformation of the contact of approximately a few centimeters only (Table 5-21). The sensitivity of results to the contact stiffness is examined through a parameter study in which the normal contact stiffness is increased by an order of magnitude to 1,000 MPa/m (Table 5-19).

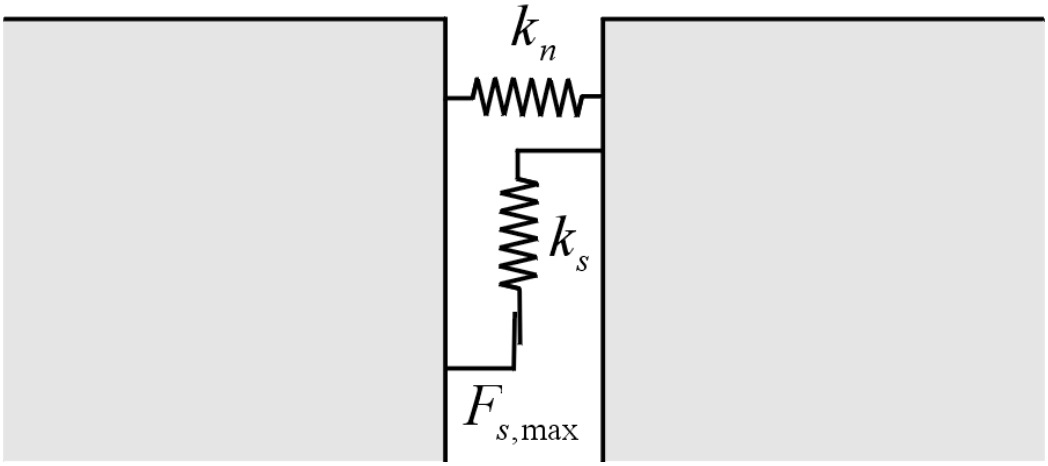

Figure 5-23. Mechanical Idealization of the Shear and Normal Contact between the Drip Shields

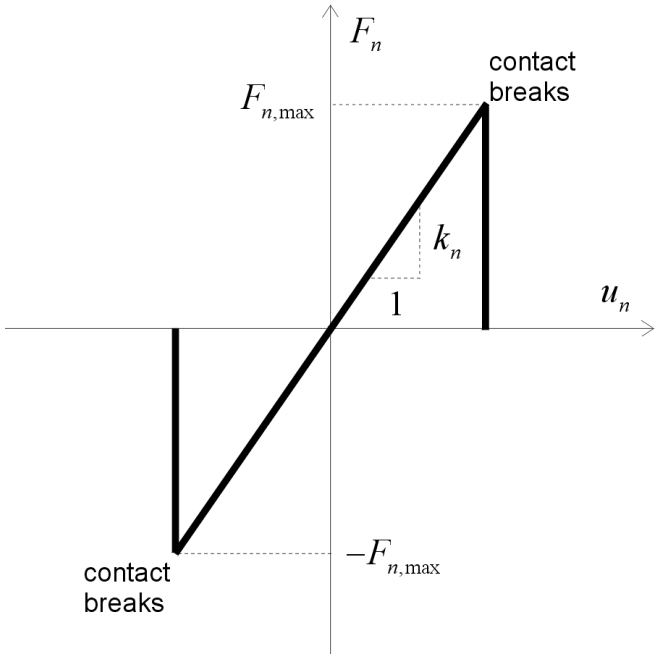

NOTE: k_n=Normal strengthen of the contact; F_n=axial force, U_n=axial displacement; $F_{n,\max}$=Maximum axial force.

Figure 5-24. Axial Force-Displacement Relation of the Contact between the Drip Shields

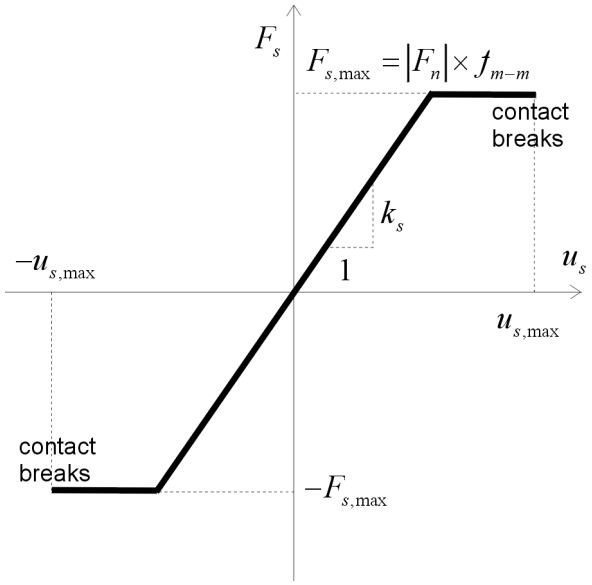

NOTE: k_s=Shear stiffness of drip shield contact; F_s=Maximum axial force; U_s=shear displacement; $F_{s,\max}$=Maximum shear force of contact.

Figure 5-25. Shear Force-Displacement Relation of the Contact between the Drip Shields

If the axial force exceeds the limit in tension or compression, $F_{n,\max}$ (illustrated in Figure 5-24), the contact is broken. The axial strength of the contact in tension and compression is considered the same. It is equal to the force required to shear off the welds on the DSC guide and connector support beams, or on the DSC guide and DSC support beams. The total length of the welds (both on the sides and the top) is approximately 7.5 m (BSC 2004 [DIRS 168275]). The area, A, of a 12.7 mm (shown Figures 5-26 and 5-27) angle weld is:

$$A = 7.5 \times 12.7 \times 10^{-3} \times \sin 45^{\circ} = 0.0674 \text{ m}^2. \quad \text{(Eq. 5-8)}$$

Only one weld per structural component is accounted for in the analysis. The strength of the welds is taken to be equal to the yield strength of Titanium Grade 7 (Ti-7) at 150°C, $\sigma_Y = 209$ MPa (Table 5-7), resulting in the maximum axial force taken by the entire connection between two DSs to be:

$$F_{n,\max} = \sigma_Y A = 14.1 \text{ MN}. \quad \text{(Eq. 5-9)}$$

Each connection is represented by two contacts between the DS blocks (shown in Figure 5-21) and thus the total strength of the welded connection is lumped at these two locations. The maximum force that can be taken by either contact is half of the maximum value given in Equation 5-9 or 7.05 MN (Assumption 3.20). To take into account the uncertainty in the strength of the welded connections, engineering judgment is used to reduce the maximum axial force used in the calculations by 50 percent, to 3.5 MN (Assumption 3.25).

The relative shear deformation of the DSs in the connection is controlled completely by metal-to-metal friction, f_{m-m}. The friction is activated when the connection is either in compression or in tension. Usually, friction is activated when contact is in compression only; however, in this case, even large-scale tension in the connection is carried by compression between the elements of the DS structure. The DSs can shear relative to each other while their connection still exists and can transmit an axial force until the shear deformation reaches the limiting value. In order to interlock adjacent DSs, it is necessary to lift one DS relative to another by at least 40 inches (~102 cm) as illustrated in Figure 5-4. Consequently, to unlock the DSs, it is necessary that shear deformation of the contact be approximately equal to 40 inches (~102 cm).

The reduction factor used for limiting axial force (50 percent) is not rigorously derived. However, the time histories of both the axial force and relative shear displacement are recorded during the dynamic simulations, and the extreme values of the histories can be used to assess the safety margin with respect to the nominal limiting values (i.e., 7.05 MN and 40 inches [~102 cm] for force and displacement, respectively). Therefore, the conservatism inherent in the selection of limiting values can be evaluated directly by the analysis.

If the connection is broken (by exceeding the maximum axial force) or unlocked, the DSs no longer interact with each other. They can separate or overlap without generation of interaction forces.

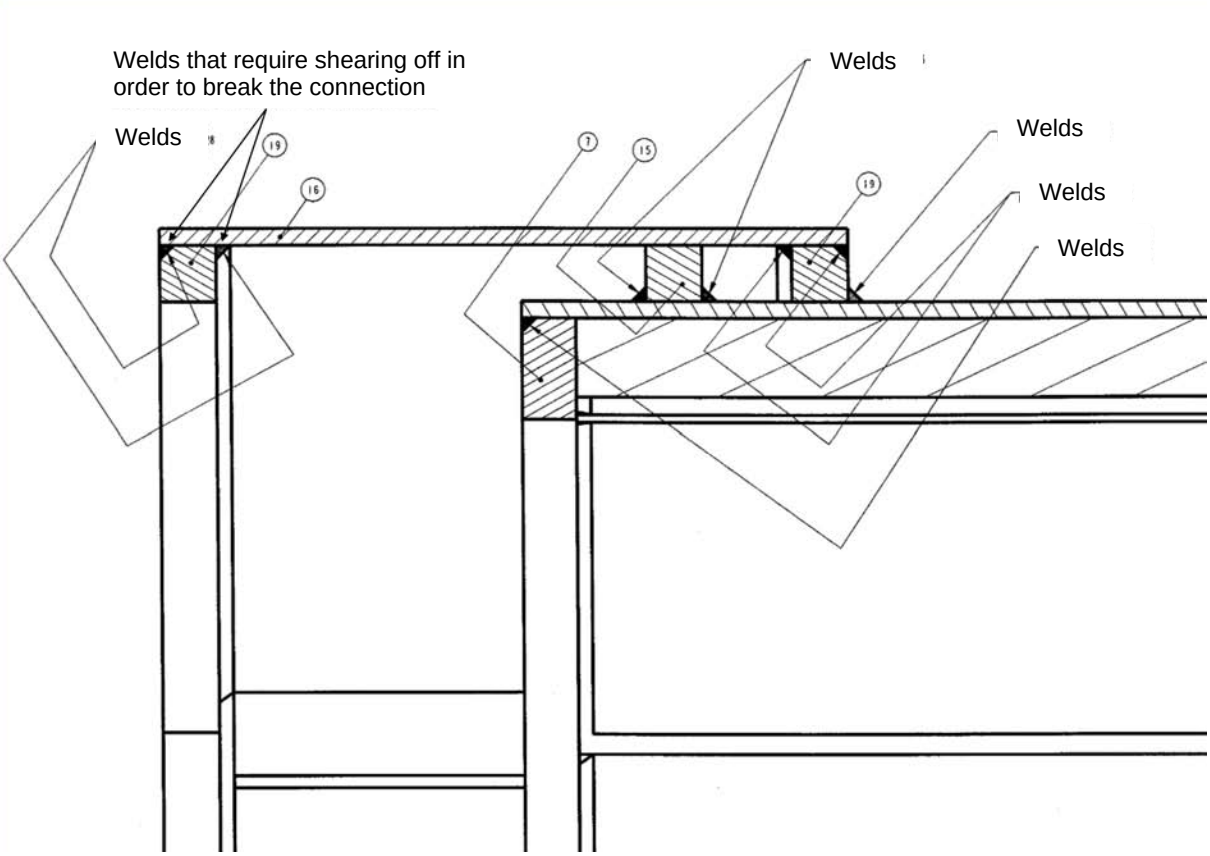

Source: BSC 2004 [DIRS 168275].

Figure 5-26. Vertical Cross-Section Through the Connector Assembly

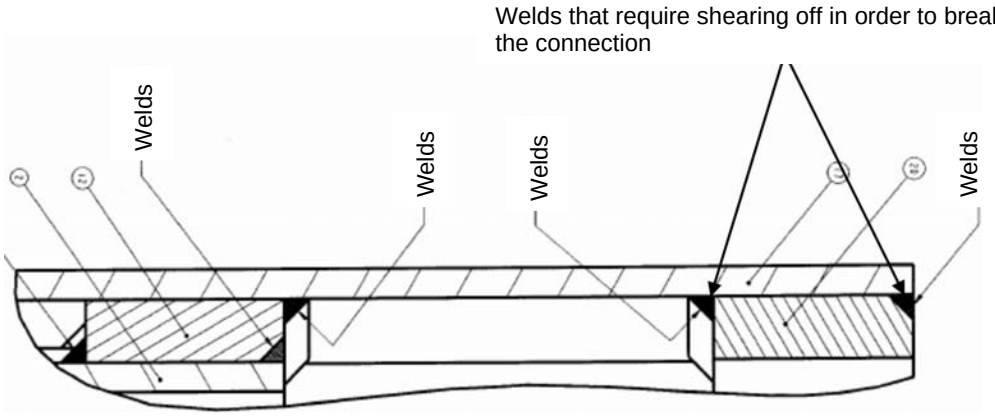

Source: BSC 2004 [DIRS 168275].

Figure 5-27. Horizontal Cross-Section Through the Connector Assembly

5.2.3.3 Rock Mass

Rock mass properties used in these calculations are listed in Table 5-10. The selected stiffness and strength are representative of the laboratory-determined properties of intact rock blocks of the middle nonlithophysal unit of the Topopah Spring tuff rock mass at the repository level. From the perspective of the DS calculations, these results will yield the upper bound results for damage in the structure.

Table 5-10. Material Properties of TSW2 Rock

Property	Value	Source
Density ρ [kg/m^3]	2370	Assumption 3.7
Young's Modulus E [GPa]	33	Assumption 3.6
Poisson's Ratio ν	0.21	Assumption 3.6
Unconfined Compressive Strength [MPa]	290	Assumption 3.15

Only the elastic rock properties were used for representing the emplacement drift walls and definition of corresponding contacts. Plastic deformation (fracturing) of the blocks impacting the DS in nonlithophysal rock mass is taken into account in the calculations. Neglecting inelastic deformation of rock during the impact leads to a conservative estimate of impact loads. In general, the constitutive representation of rock behavior (i.e., stress-strain relation) needs to address various complexities of rock deformation. The brittle materials in general, when subjected to compression, exhibit a wide range of nonlinear stress-strain behaviors due to the nucleation, propagation, and coalescence of microcracks under different boundary conditions (Jaeger and Cook 1979 [DIRS 106219], Sections 4.2 through 4.5). Moreover, the compressive strength of brittle materials (including rock) is significantly higher than their tensile strength. Finally, unlike engineering metals, the rocks may exhibit nonlinear behavior even under moderate hydrostatic compression, and significant effect of size on strength (Jaeger and Cook 1979 [DIRS 106219], Sections 4, 6, and 7 for detailed discussion). A variety of constitutive representations are developed to address the most prominent features of the behavior of brittle materials (Chen 1982 [DIRS 159153], pages 362 and 363). These complex constitutive representations require many input parameters. A reasonable simplification of rock constitutive behavior is deemed necessary for the analysis of the rock impact to the DS. As a first approximation, the constitutive representation of rock behavior should appropriately capture local crushing of the rock at the point of impact, resulting in dissipation of impact energy and distribution of impact energy over the larger contact area. It is considered appropriate to represent the rock behavior as elastic-ideally-plastic (Figure 5-28 and Jaeger and Cook 1979 [DIRS 106219], Section 9). This representation of nonlinear behavior offers obvious advantages compared to the elastic representation, while remaining relatively simple and conservative under the given loading conditions. The unconfined compressive strength of rock, used as the yield strength in the constitutive representation, is one of the parameters in this study that affects the results. The rock properties provided in Table 5-10 are derived from small-core laboratory tests. These strength and moduli are considered to be conservative, upper bound estimates, since it is well-known that the mechanical properties of rock decrease with increasing size of the specimen (BSC 2004 [DIRS 166107], Figure E-22).

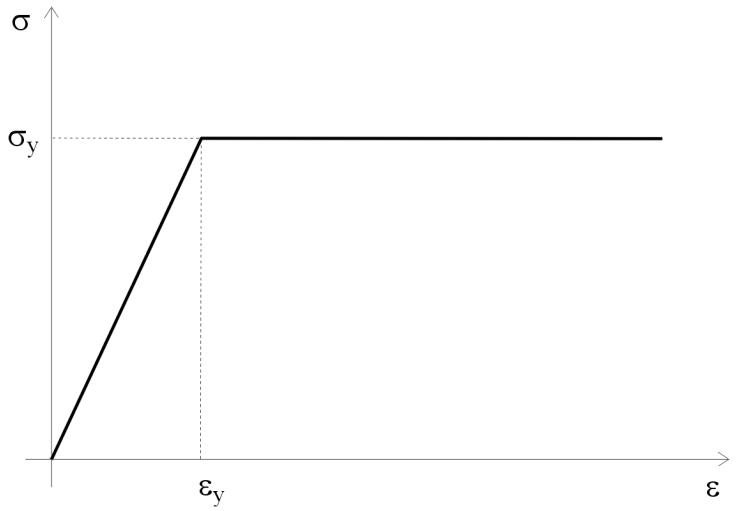

NOTE: σ_y and ε_y are the yield strength and strain, respectively.

Figure 5-28. Idealized Stress-Strain Behavior Defining Elastic-Ideally-Plastic Constitutive Representation for Rock

5.2.3.4 Invert Crushed Tuff

The structural response calculations use an idealized representation of the dynamic response of the invert to the ground motion. The invert is represented as an elastic body whose surface responds instantaneously and uniformly to the given ground motion. In other words, the ground motion time histories for the three components of motion are applied directly to the surface of the invert. This is a reasonable approach for small amplitude ground motions because the invert thickness is small and it is compacted under the weight of the waste package and DS and because any remaining steel framework in the invert will tend to provide some integrity. These effects will result in an invert that tends to move as a single unit. For high amplitude ground motions, the invert ballast is likely to be thrown up and redistributed, allowing the heavy EBS components to settle on the bottom of the drift, directly in contact with the rock floor. In this case, applying the ground motions directly to the surface of the invert is again a reasonable approach.

5.2.3.5 Collapsed Rubble Around the Drip Shield

The mechanical properties of the rubble created by the rockfall were used in the kinematic calculations of the rigid body motion of the DSs and assessment of the potential for separation of the DSs. It is assumed that the ground support used for drift support in the preclosure will have lost its supporting function as a result of corrosion early in the postclosure time frame (Assumption 3.23). The collapsed rock mass will accumulate on the invert between the DS and the drift walls and, in case of a large volume of rockfall, cover the DS. The density and stiffness (i.e., Young's modulus) of the rubble resulting from the rockfall are always smaller than the properties of the original rock mass. The rubble is a cohesionless, granular material with large porosity. The increase in porosity is a result of bulking of the rock mass as it collapses. The most important factor (besides the properties of the intact rock), which affects the mechanical properties of the rubble is the bulking factor or increase in porosity. The bulking will be smaller if the average block size is smaller and if the block size distribution is more uniform. It is

expected that the rubble in the lithophysal rock mass will have a smaller bulking factor than the rubble in the nonlithophysal rock mass, which will be composed of the blocks of relatively large size. A detailed discussion of bulking factor for collapsed rock in the repository host horizon can be found in *Drift Degradation Analysis* (BSC 2004 [DIRS 166107], Section 6.4.2.5). The pressure that the rubble exerts on the DS restrains the lateral motion of the DS, but also, due to friction between the DS and the rubble, it restrains the motion of the DS in the axial direction along the emplacement drift. The pressure of the rubble on the DS can act in an active mode, due to weight of the rubble (both vertical, on the top of the DS, and horizontal, on the sides of the DS), or reactive, due to elastic deformation of the rubble during interaction with the DS and the walls of the emplacement drift. The active pressure is controlled by the height, density and, in case of horizontal pressure, the angle of internal friction of the rubble (e.g., Equation 5-2 in Section 5.2.2.1.1). The reactive pressure is controlled by stiffness and thickness of the rubble. The material properties of the rubble used for the base-case calculations are listed in Table 5-11. To investigate the sensitivity of the calculation results to these parameters, a series of calculations were also carried out in which the rubble parameters were assumed to have conservative (and unlikely) values of modulus and density. Young's modulus was considered to be as low as 1 MPa, and rubble density as low as 20 kg/m^3 (Table 5-19).

Table 5-11. Base-Case Material Properties of Rock Rubble

Property	Value	Source
Density ρ_r [kg/m^3]	2000	Assumption 3.22
Young's Modulus E_r [MPa]	100	Assumption 3.24
Friction Angle ϕ_r [º]	40	Fruchtbaum J. 1988 [DIRS 161774]

5.2.4 Ground Motions

5.2.4.1 General Description

Site-specific ground motions for three levels of annual frequency of occurrence, 5×10^{-4}, 1×10^{-6}, and 1×10^{-7}, are included in this study[9]. The 5×10^{-4} ground motion is for preclosure consideration, while the 1×10^{-6} and 1×10^{-7} ground motions are for postclosure. The 5×10^{-4} preclosure level is provided only for comparison to the postclosure levels. For higher-frequency spectral accelerations (5 to 10 Hz) and an annual frequency of occurrence of 5×10^{-4}, results of the probabilistic seismic hazard analysis for Yucca Mountain indicate the ground motion hazard derives primarily from earthquakes in the magnitude range of 5.0 to 6.5 occurring at distances less than 15 km from the site. For lower-frequency spectral accelerations (1 to 2 Hz) at the same annual frequency of occurrence, the hazard shows, in addition to nearby sources, a significant

[9] The ground motions 1×10^{-6} were revised during the course of the project (BSC 2004 [DIRS 166107], Appendix X). The discussion in this section is for the original set of 1×10^{-6} ground motions in which all three components of the motion were scaled to a single value of PGV. The detailed FE calculation of the vibratory ground motion was conducted for the original set of 1×10^{-6} ground motions. The kinematic calculation to assess potential for DS separation ground motion was conducted for the revised set of 1×10^{-6} ground motions in which one component of the ground motion was scaled to a target value of PGV while the amplitudes of the other two components were allowed to vary, thus providing ground motions with intercomponent variability.

contribution from earthquakes in the magnitude range of 7.0 to 8.0 occurring at an epicentral distance of about 50 km. For annual frequency of occurrence of 1×10^{-6} and 1×10^{-7}, nearby earthquakes in the magnitude range 5.5 to 7.0 are the dominant sources contributing to ground motion hazard at both higher and lower spectral accelerations.

A total of 15 sets of Point B ground motions (i.e., ground motions developed at repository horizon) were selected for each annual postclosure hazard level. The multiple sets ensure a reasonable distribution of spectral shapes and time history durations, as described in *Sampling of Stochastic Input Parameters for Rockfall and Structural Response Calculations Under Vibratory Ground Motion* (BSC 2004 [DIRS 169999], Section 4.1). For each set of ground motions, two horizontal components (H1 and H2) and one vertical component (V) of acceleration, velocity, and displacement are supplied. Figure 5-29 shows the H1 velocity time history for all three annual hazard levels. Only one ground motion was provided for the preclosure hazard level because of the deterministic-based approach for preclosure consideration. The amplitudes of the peak ground acceleration, velocity, and displacement for one of the ground motion sets from each hazard level are provided in Table 5-12. This table is used to demonstrate the typical ground motion parameters for the three hazard levels considered. It is apparent that the preclosure ground motions have lower amplitude vibrations compared with the postclosure ground motions. The peak values for each ground motion set provided for postclosure hazard level varies. For example, the peak ground velocity in the vertical component for 1×10^{-7} hazard level ground motion set #3 reaches 1,634 cm/s.

Arias Intensity (An estimate of energy delivered to structures—for a definition see Kramer 1996 [DIRS 103337], Section 3.3.4) for each set of ground motions is listed in Table 5-13. A large variation of energy within the same hazard level is observed. All 15 sets of ground motions (for 1×10^{-6} and 1×10^{-7} annual frequency of occurrence) were randomly combined with friction coefficients of the contacts between different materials in the model for probabilistic analysis. The combining of ground motions and friction coefficients is described in Section 5.3.1.2.

Table 5-12. Peak Ground Motion Parameters

Annual Hazard Level	Ground Motion Component	Peak Acceleration (g)	Peak Velocity (cm/s)	Peak Displacement (cm)
5×10^{-4}	H1	0.19	19.00	12.86
	H2	0.18	17.72	12.37
	V	0.16	12.37	7.83
1×10^{-6} Ground Motion Set 1	H1	6.86	243.74	28.19
	H2	7.31	243.35	17.44
	V	10.46	229.79	14.26
1×10^{-7} Ground Motion Set 1	H1	16.28	535.26	58.68
	H2	14.79	428.42	58.72
	V	13.15	298.44	36.86

Source: BSC 2004 [DIRS 168550], Table 9.

In running the seismic simulation, the duration of the seismic time histories is commonly truncated to that portion of the records displaying the majority of the energy (discussed in Section 5.2.4.2). The strong ground motion is usually defined as duration bracketed by the 5 percent and 95 percent points in the energy buildup as measured by the Arias Intensity. For each three-component set of ground motions, these points were determined for each component (H1, H2, and V) and then the earliest 5 percent point and the latest 95 percent point were used to define the duration of strong ground motion for that set of ground motions.

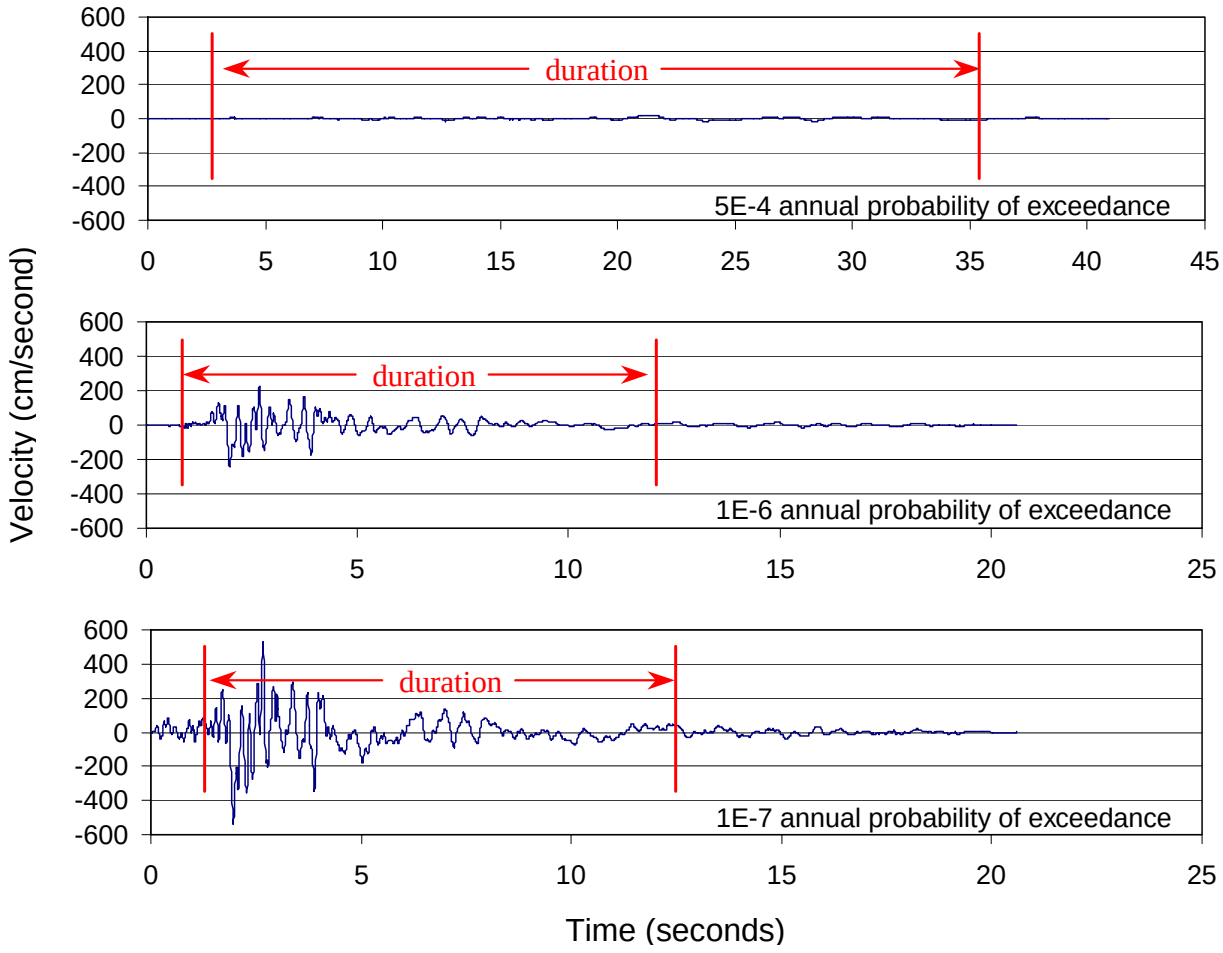

Source: BSC 2004 [DIRS 168550], Figure 42.

Figure 5-29. Examples of Ground Velocity Time Histories (H1) with Truncated Duration for Analysis

Table 5-13. Arias Intensity (m/s) for Each Ground Motion Set

Annual Hazard Level	Ground Motion Set[a]	H1	H2	V	Total Sum
1×10^{-6} annual frequency of occurrence	1	246	304	482	1032
	2	229	229	471	928
	3	139	23	33	195
	4	179	176	282	638
	5	58	81	150	288
	6	42	160	71	272
	7	65	58	217	339
	8	65	35	213	312
	9	174	39	91	303
	10	94	186	615	894
	11	63	74	146	283
	12	97	40	117	254
	13	82	131	56	269
	14	43	386	206	636
	16	24	42	86	151
1×10^{-7} annual frequency of occurrence	1	1128	1215	820	3163
	2	989	1202	2972	5163
	3	577	735	971	2283
	4	856	1052	1013	2921
	5	373	568	205	1146
	6	331	271	566	1168
	7	303	291	3357	3951
	8	343	524	437	1304
	9	813	1691	3340	5844
	10	282	125	409	816
	11	272	214	321	808
	12	277	284	332	893
	13	469	815	881	2165
	14	302	351	854	1507
	16	112	72	244	428
5×10^{-4} annual frequency of occurrence		0.59	0.67	0.46	1.72

Source: BSC 2004 [DIRS 168550], Table 10.

[a] A total of 17 sets of ground motions was developed for each postclosure level. Ground motion sets #15 and #17 were not used.

5.2.4.2 Ground Motion Time History Cutoff Used in FE Simulations

The FE simulations of the DS under vibratory motion are conducted to specifically examine damage to the DS surface plates and supporting structure resulting from vibration. These calculations are extremely computationally intensive because of the following reasons (BSC 2003 [DIRS 163425]):

- Complex FE representation (Section 5.2.2.1.2)
- Highly nonlinear nature of the problem (large deformation plasticity, friction, impacts, etc.)
- Small computational time step necessary to ensure convergence ($\approx 1\ \mu$ s or less)
- Long durations of the ground motion time histories ($\approx$ 30 – 40 s).

In order to obtain credible results in a reasonable time, it is necessary to reduce the duration of seismic excitation used in the simulation.

Therefore, most realizations at the 1×10^{-6} annual frequency of occurrence are terminated at a time corresponding to 95 percent of ground motion energy (For brevity, the maximum time corresponding to 95 percent of ground motion energy is, in the remainder of this document, called "95 percent time". Similarly the maximum time corresponding to 90 percent of energy of ground motion is called "90 percent time", and the minimum time corresponding to 5 percent of energy of ground motion is called "5 percent time". Note that all three time instances are determined by taking into account all three components of ground motion.). In two 1×10^{-6} realizations (11 and 15, see Table 5-20 in Section 5.3.1), the termination time is extended beyond this 95 percent energy cutoff to examine the effect of the cutoff (i.e., the ending time is larger than the 95 percent time).

The simulation for 5×10^{-4} annual frequency of occurrence was conducted from 3 s to 15 s of ground motion time history (i.e., from 5 percent to 65 percent of total energy). This approach was justified by the calculation results for this ground motion level (Section 5.3.3.1).

In Table 5-14, the duration of each simulation and characteristic times used to define the duration are listed for 1×10^{-6} realizations. The time in the fifth column is the starting time of the simulation. The starting time, for most realizations, corresponds to the beginning of the ground motion. The simulation is typically terminated at the time corresponding to 95 percent of the ground motion energy.

The duration that is actually run during simulation is, in a few cases, different from the duration presented in Table 5-14. Specifically, realizations 11 and 15 (see Table 5-20 in Section 5.3.1.2) are extended beyond the 95 percent time for the purpose of examining the damage-evolution trend as a function of time-history cutoff (BSC 2003 [DIRS 163425], Attachment II).

Table 5-14. Duration and Characteristic Times Corresponding to Ground Motions at 1×10^{-6} Annual Frequency of Occurrence

Ground Motion Number	5%-Time (s)	90%-Time (s)	95%-Time (s)	Starting Time (s)	Ending Time (s)	Duration of Simulation (s)	Realization Number
1	0.85	5.21	7.05	0	7.1	7.1	6
2	0.58	6.05	8.13	0	8.2	8.2	7
3	1.7	3.64	5.04	0	7.0	7.0	15
4	1.3	10.2	15.0	0	15.0	15.0	3
5	2.0	7.46	10.3	0	20.0	20.0	11
6	2.3	9.20	9.96	0	10.0	10.0	12
7	4.0	11.1	11.6	4.0	11.6	7.6	1
8	1.1	5.12	5.99	0	6.0	6.0	4
9	0.79	6.98	8.18	0	8.2	8.2	10
10	1.6	7.66	10.8	0	10.8	10.8	9
11	2.1	8.30	10.3	0	10.3	10.3	5
12	1.4	12.2	13.6	0	13.6	13.6	13
13	1.9	12.7	17.0	1.9	12.7	10.8	8
14	7.2	19.8	21.5	7.2	21.5	14.3	14
16	3.8	9.57	11.8	3.8	11.8	8.0	2

Source: BSC 2003 [DIRS 163425], Table 2.

In Table 5-15, the duration and characteristic times are listed for five 1×10^{-7} realizations performed in this study. The most pronounced difference between 1×10^{-6} and 1×10^{-7} realizations is that the latter are run only up to the time in which DS separation is unambiguously indicated.

The duration of simulations presented in the seventh column of Table 5-15 represents the termination time for the FE analyses reached prior to numerical instability. Continuation of the simulation beyond this time (i.e., extension of the duration of simulation) results in the numerical instability for all realizations presented in Table 5-15, with exception of realization 5. All other 1×10^{-7} realizations, not presented in Table 5-15, also failed due to the numerical instability but without the DS separation prior to failure (Section 5.3.3.2.3). Therefore, no DS damage conclusions can be based on these runs and they are not presented in this document. The kinematic analyses, conducted specifically to examine DS separation potential, do not result in numerical instabilities.

Table 5-15. Duration and Characteristic Times Corresponding to Ground Motions at 1×10^{-7} Annual Frequency of Occurrence

Ground Motion Number	5%-Time (s)	90%-Time (s)	95%-Time (s)	Starting Time (s)	Ending Time (s)	Duration of Simulation (s)	Realization Number
1	1.3	6.5	7.5	0	3.9	3.9	6
2	0.80	5.8	7.4	0	3.1	3.1	7
9	0.70	6.7	8.0	0	3.6	3.6	10
11	2.1	8.5	10.3	2.1	10.3	8.2	5
13	1.9	15.2	19.5	1.9	5.0	3.1	8

Source: BSC 2003 [DIRS 163425], Table 3.

5.2.5 Static and Dynamic Rockfall Loading Parameters

5.2.5.1 Quasi-Static Load of Caved Rock Rubble

Stability analysis of the DS for static pressure of the caved rock is carried out for the extreme conditions of complete collapse of the emplacement drift. The bounding estimate of the extent of the rock mass caving around the emplacement drifts is calculated by adjusting the rock mass cohesive strength to zero, thus forcing collapse. A description of this analysis of the degradation of the emplacement drift and the resulting static loads of the caved rock mass on the DS using a variety of different analytical and numerical methods can be found in Section 6.4.2.5 of *Drift Degradation Analysis* (BSC 2004 [DIRS 166107]). The analysis was done for the lithophysal rock mass only, because extensive drift collapse is not likely in the nonlithophysal rock mass. The summary of the average vertical pressure on the DS as a function of the average bulking factor (i.e., a measure of the volume increase of the rubblized rock mass after the collapse) in the caved rock mass is shown in Figure 5-30 for different cases analyzed (A description of different models and discussion of the results can be found in Section 6.4.2.5 of *Drift Degradation Analysis* (BSC 2004 [DIRS 166107]). The results are obtained using analytical (given by the continuous lines in Figure 5-30) and numerical methods, including both continuum and discontinuum[10] representations of the rock mass. The discontinuum numerical software code (UDEC, Itasca 2002 [DIRS 160331]) simulates the process of rock mass fracture, drift yield and deformation, and gravity-fall of rock particles in response to seismic or static (combined with time-dependent strength degradation) loading. This approach provides the most realistic representations (as opposed to analytical estimates) of the caving process and the subsequent load transfer through the collapsed rubble to the DS and drift invert. The calculation of the DS structural response to the static loads of the caved rock mass presented in *Structural Stability of a Drip Shield Under Quasi-Static Pressure* (BSC 2004 [DIRS 170791]), were performed using these discontinuum model predictions. An example of the UDEC emplacement drift model geometry after drift collapse is shown in Figure 5-31. The model represents the rock mass as an assembly of polygonal elastic blocks, which are created by a number of "incipient" fractures within the rock mass. As described in detail in *Drift Degradation Analysis* (BSC 2004 [DIRS 166107], Section 6.4.2.5), these fractures are bonded creating a synthetic material with the strength and stiffness properties of the rock mass. Thus, the fractures are "invisible" initially, and the rock mass behaves as an isotropic equivalent continuum material until the either the tensile or shear strength of the fractures is reached. Once the strength of the "incipient" fractures is reached, the fractures may break, propagating in any direction that the forces dictate. As the fractures propagate, blocks may form and fall by gravity to accumulate as rubble as on the drift invert and DS. The geometry of the blocks, which are used to represent the rock mass that can form upon fracture is random. The block size for quasi-static calculations is approximately 0.2 m, which is relatively small compared to the diameter of the emplacement drift, and thus the bock geometry does not have a large impact on the mode or extent of drift failure.

[10] As described in *Drift Degradation Analysis* (BSC 2004 [DIRS 166107]), the lithophysal rock mass was represented as a continuum material in which the yield response is given by a Mohr-Coulomb material model, and by a discontinuum mode in which the material is free to fracture into particles based on the stress conditions around the emplacement drifts. In the discontinuum method, the failure of the rock mass due to seismic or static (combined with time-dependent strength degradation) loading results in fracture and rubbilization of the tunnel periphery, leading to gravity fall of particles and filling of the drift.

Since the drift collapse mode and resulting pressures applied to the DS will vary somewhat as a function of the particular realization of block geometry, six simulations were carried out for different realizations of block geometry to provide a range of potential DS pressure distributions. The deformability of the DS will impact the predicted load distribution as deformation of the DS will allow a greater degree of stress to be carried by the rubble. To provide a realistic effect of load sharing between the rubble and DS, the two-dimensional representation of the DS is assumed to be linearly elastic. The representation is two-dimensional, but the geometry and elastic properties of the DS are calculated to have the correct stiffness, accounting for actual three-dimensional geometry of the structure (BSC 2004 [DIRS 166107], Appendix Y shows calibration of the UDEC DS model). The equilibrium rubble loads on the DS are calculated for 30 segments (i.e., 10 per each side and per top of the DS) shown in Figure 5-32. The distributions of the load on 30 segments of the DS for 6 realizations are summarized in Figure 5-33. The average pressures for these 6 cases are also shown in Figure 5-30, denoted in the legend as "Discontinuum 0.2 m block size, deformable DS". The predicted distribution of loading the rubble on the DS varies significantly due to the discrete nature of the caved rock mass and the resulting point loading. Although the average pressure on top of the DS of the six realizations, shown in Figure 5-33, varies between the 100 kN/m^2 and 200 kN/m^2, the localized pressures are in excess of 650 kN/m^2. Representation of the load of the caved rock mass on the DS as uniformly distributed would not be either realistic or conservative.

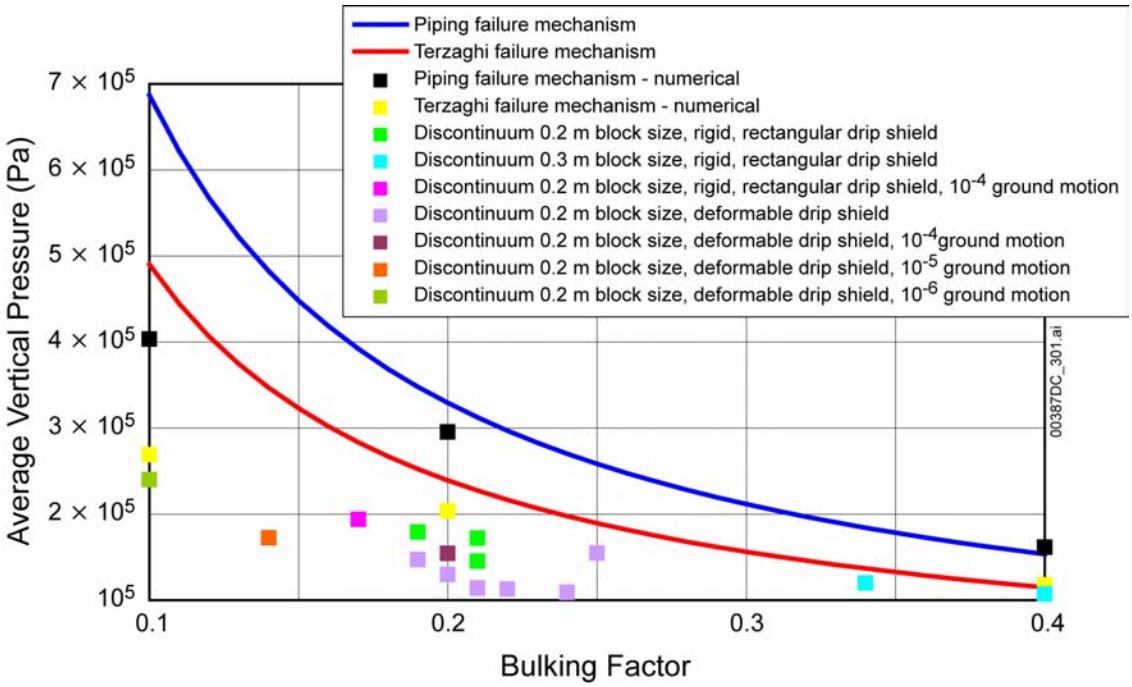

Source: BSC 2004 [DIRS 166107], Figure 6-179.

NOTE: Two different sizes of the randomly-shaped blocks used in the discontinuum analyses were used to produce a range of bulking factors.

Figure 5-30. Summary of Vertical Load on the Drip Shield as a Function of Bulking Factor

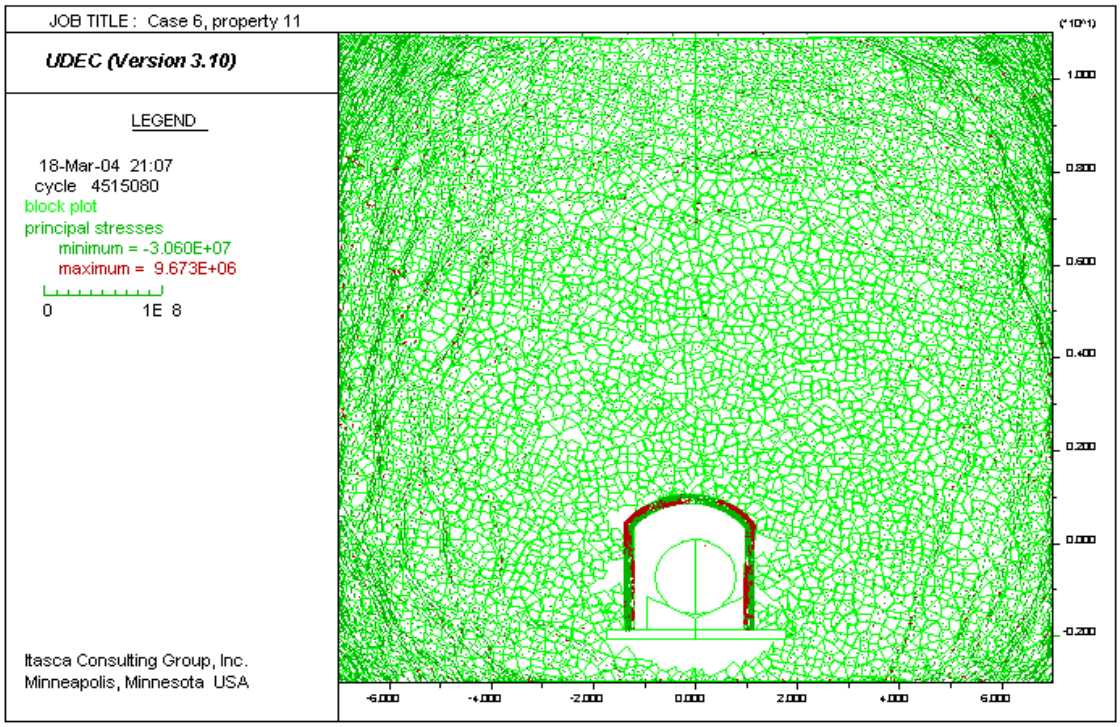

Source: BSC 2004 [DIRS 166107], Figure 6-173.

Figure 5-31. Configuration of the UDEC Model After Complete Drift Collapse (Realization 1)

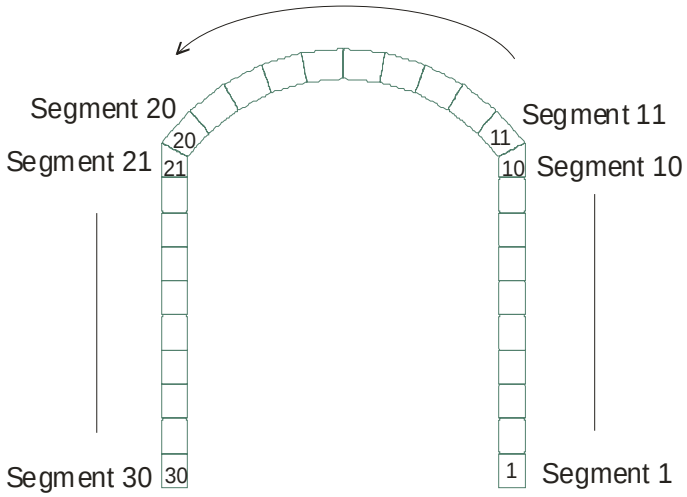

Figure 5-32. Numbering of the Segments on the Drip Shield

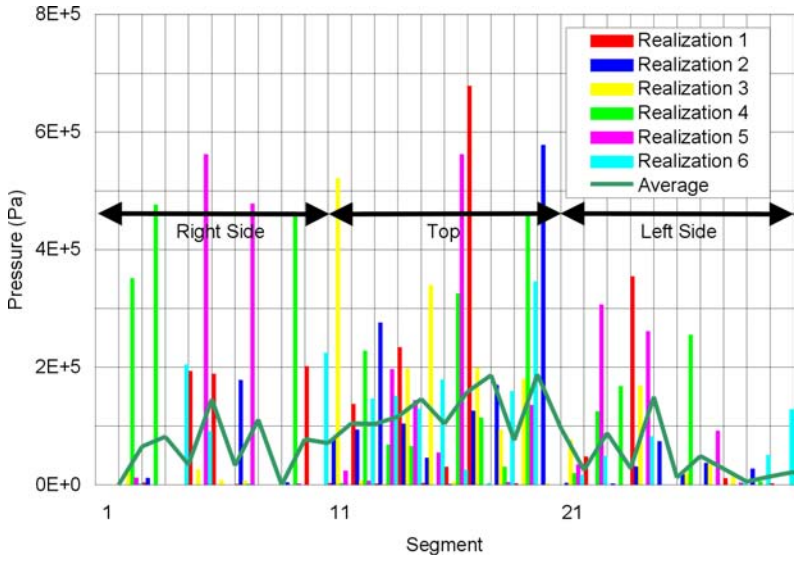

Source: DTN MO0407MWDDSLCR.000 [DIRS 170873].

Figure 5-33. Distribution of Drip Shield Loads for 6 Realizations of the UDEC Block Geometry

5.2.5.2 Dynamic Impact Load of Discrete Rock Blocks

Block impacts on the DS were calculated for rockfall in the nonlithophysal rock mass only since the predicted block masses are significantly larger than those expected in the lithophysal rock. Drift degradation in the nonlithophysal rock mass was analyzed using the 3DEC (Itasca 2002 [DIRS 160331]) three-dimensional discontinuum model to define the distribution of block masses and impact energies as a function of seismic loading (BSC 2004 [DIRS 168550], Section 6.3).

The rock mass surrounding an emplacement drift is subdivided into a large number of elastic blocks based on field-mapped distributions of natural rock fracturing. A large number of dynamic analyses of rockfall were conducted with this model for both preclosure and postclosure ground motions. From these analyses, a distribution of rockfall particle masses and impact energies that impact the DS were determined. Figure 5-34 shows an example state of the 3DEC model during the simulation of 1×10^{-6} annual frequency of occurrence, ground motion # 2, at t =6.6 s. The rockfall from 3 different probabilities of annual recurrence (discussed in Section 5.2.4) is calculated. Approximately 50 simulations are carried out for each level of probability of annual recurrence, combining different ground motions (when more that one ground motion is provided for particular probability of annual recurrence) with different realizations of natural fracturing of the rock mass. In the 3DEC model, the DS is represented simplistically as a rigid parallelepiped with dimensions approximately corresponding to dimensions of the DS (Figure 5-34).

The mass of the blocks impacting the DS, relative velocity between the block and the DS at the moment of impact, location, and energy are recorded for each impact to the DS during the 3DEC simulations. Histograms and relevant statistical parameters (e.g., mean and standard deviation) of those variables are generated for each level of probability of annual recurrence (BSC 2004 [DIRS 168550], Sections 6.3.1.2.3 and 6.3.1.2.4). The summary statistics for these analyses are presented in Tables 5-16 and 5-17 for 1×10^{-6} and 1×10^{-7} ground motions, respectively.) The

typical cases of impact for 1×10^{-6} and 1×10^{-7} ground motions are selected (Section 5.4.2.1) and used as input for analysis of structural integrity of the DS during the rockfall in the nonlithophysal rock mass.

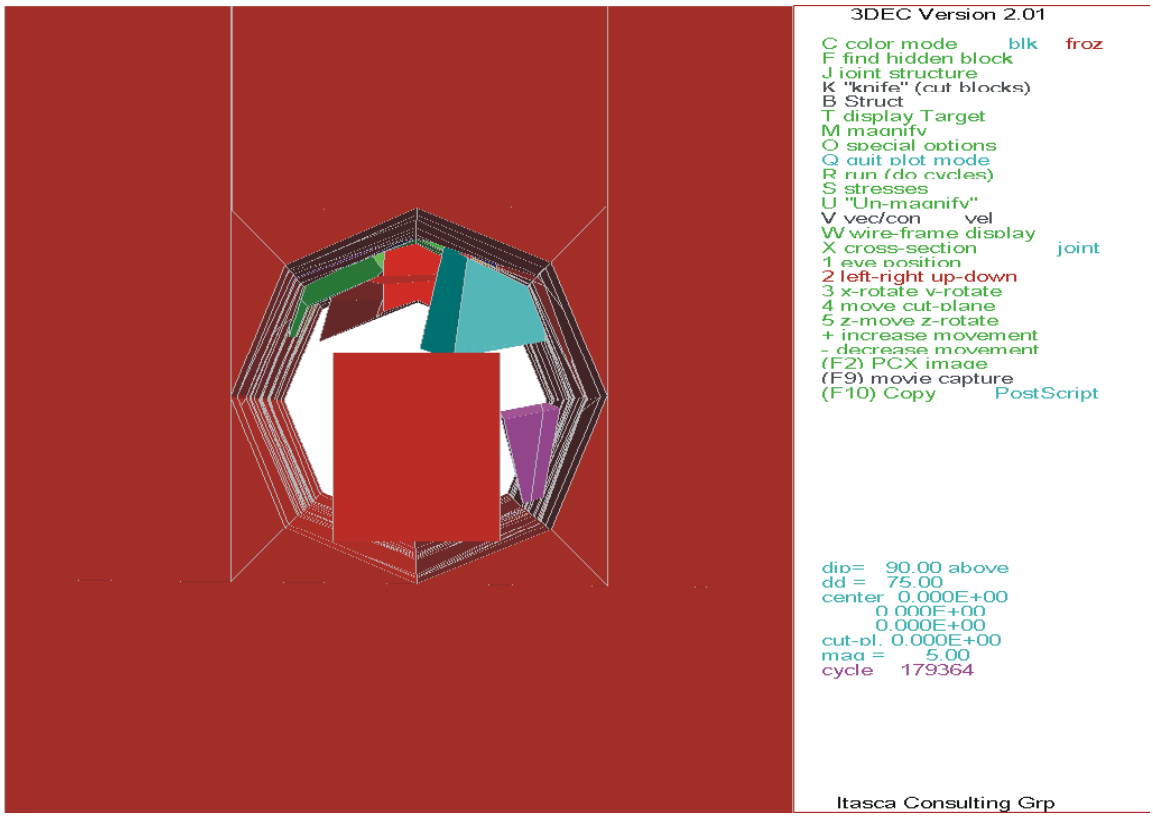

Source: BSC 2004 [DIRS 168550], Figure 44.

NOTE: 3DEC Simulation #55, 1×10^{-6} Ground Motion #12, at t = 6.6 seconds.

Figure 5-34. Illustration of the Simulation of Rockfall Impact to the Drip Shield

Table 5-16. Statistical Summary of the Rockfall Impact Parameters, 1×10^{-6} Annual Probability of Exceedance Hazard

	Block Mass (tons)	Relative Impact Velocity (m/s)	Impact Angle (degree)	Impact Momentum (kg*m/s)	Impact Energy (Joules)
Mean	0.87	3.39	132	2747	5267
Median	0.23	3.49	120	663	902
Standard Deviation	1.97	1.61	81	6209	12941
Skewness	6.04	0.04	1.12	6.23	7.52
Range	21.39	7.54	355	68836	163083
Minimum	0.02	0.02	5	4	0
Maximum	21.42	7.56	360	68840	163083
Sum	245.55	N/A	N/A	N/A	N/A

Source: BSC 2004 [DIRS 168550], Table 14.

NOTE: The impact angle is measured from the horizontal. N/A = Not Applicable.

Table 5-17. Statistical Summary of the Rockfall Impact Parameters, $1x10^{-7}$ Annual Probability of Exceedance Hazard

	Block Mass (tons)	Relative Impact Velocity (m/s)	Impact Angle (degree)	Impact Momentum (kg*m/s)	Impact Energy (Joules)
Mean	0.96	5.03	139	4169	11459
Median	0.23	4.63	127	980	2440
Standard Deviation	2.04	2.78	87	8489	27461
Skewness	5.01	1.00	1.06	4.64	6.73
Range	21.39	17.67	356	89485	348170
Minimum	0.02	0.07	1	18	4
Maximum	21.42	17.74	357	89502	348174
Sum	364.58	N/A	N/A	N/A	N/A

Source: BSC 2004 [DIRS 168550], Table 16.

NOTE: The impact angle is measured from the horizontal. N/A = Not Applicable.

5.2.6 System Damping for FE Analyses

In the calculation of the rockfall impact to the DS, no structural damping was used. This approach was conservative, and acceptable considering relatively short duration of impact (particularly compared to duration of seismic ground motions).

In order to obtain steady-state results after the simulation of vibratory motion or to conduct the quasi-static analysis, it is necessary to apply system damping. The mass-proportional system damping is applied globally.

As discussed in (Hallquist 1998 [DIRS 155373], Section 28.2), the most appropriate damping constant for the system is usually the critical damping constant. Therefore,

$$DC = 2 \cdot \omega_{\min} = 2 \cdot 58 = 116 \text{ rad/s}$$

where $\omega_{\min} = 2 \cdot \pi \cdot 9.3 \approx 58$ rad/s is the minimum circular non-zero frequency of the DS (BSC 2003 [DIRS 163425], Section 8, Table 5[11], for the minimum non-zero frequency of 9.3 Hz).

Because in the simulations of the vibratory motion the objects inside the emplacement drift (e.g., the DS and the waste package pallet) are unanchored, the damping constant is conservatively reduced to $DC = 50$ rad/s, to avoid over-damping of the system. This damping constant results in a slightly under-damped system, which is more appropriate since the numerical model will more accurately follow the dynamic response of the system without undue influence of damping on deformations and stress concentrations in the structure. The drawback of slight under-damping is that the numerical model may require longer time periods to reach quasi-static equilibrium.

[11]Table 5 refers to Attachment V, which are compact discs with input and output files from analyses. Damping parameters found in directory: *Modal Analysis*, file*: drip2MOD.out*, line #7792.

The damping constant DC = 100 rad/s is used in quasi-static calculations. The damping coefficient and the pressure ramp time of 0.1 s (i.e., the time over which the load is increased as a linear function of time from zero to the prescribed loading magnitude) are verified by inspection of the vertical deflection time history presented in Figure 5-35. The amplitude of the oscillations of the vertical deflection time history around the steady-state solution decays quickly for selected parameters. Note that the quasi-static solution by definition corresponds to the stationary value obtained at the end of the simulation. The evolution of the solution is, thus, purely numerical.

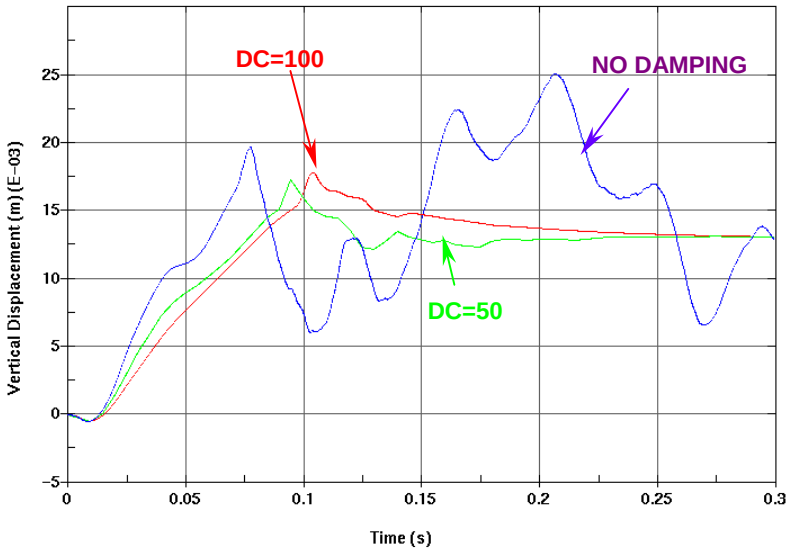

Source: BSC 2004 [DIRS 170791], Figure 6.

Figure 5-35. Vertical (Y-) Displacement Evolution of the Apex Drip Shield Node for Realization 5 for Various Damping Levels

5.3 ANALYSIS OF MECHANICAL EFFECTS OF VIBRATORY MOTION

5.3.1 Description of Calculations

The effects of vibratory ground motions on the DSs take place on different scales depending on the problem to be examined. These can be summarized as follows:

- **Examination of DS Separation During Vibratory Motion** - Rigid-body motion of the interlocked "chain" of the DSs and strains in the chain will affect connections between the DSs and the potential for their separation. To simulate this effect it is necessary to include a large number of the DSs in the numerical representation (i.e., to represent hundreds of meters of the emplacement drift). As a result of the large problem size, the numerical approach used must necessarily represent the DSs in a simple fashion in which the interaction of the DSs is approximately accounted for.

- **Examination of Damage from Localized Impact During Vibratory Motion** - Impacts to the DS during the vibratory ground motion and the resulting damage occur on the

length scale of decimeters or centimeters. To properly analyze the impact damage, it is necessary to use a sufficiently fine grid to represent details of the structural geometry of the DS components, but also to represent variation of the strain in the region of impact.

Dealing with such different length scales in these two types of problems (centimeters and hundred meters) in one numerical representation is a difficult and computationally demanding (if at all possible) task. Instead, the problem is addressed by using two numerical approaches. A kinematic calculation based on the DE code UDEC (BSC 2002 [DIRS 161949]) is used to analyze the response of the DSs change and potential for separation of a large number of interlocked DSs (e.g., 20 or 50) to vibratory ground motion. As discussed in Section 5.2.2.1.1, a two-dimensional numerical representation was used. The DS is represented as a rectangular body with mass and outline dimensions the same as the DS. For examination of the damage from vibratory motion and interaction of DSs, the detailed FE representation described in Section 5.2.2.1.2 is employed. The FE representation included three DSs with a sufficiently fine grid to define geometric details of the structural components. The middle DS of the three is deformable, allowing nonlinear material model representation using an elastic-plastic strain hardening constitutive mechanical behavior. A discussion is given in the following sections on the details of the problem approach to the kinematic and FE analyses, followed by a discussion of the results of the analyses in terms of potential for DS separation and damage.

5.3.1.1 Kinematic (DE) Calculations

5.3.1.1.1 Verification of the Approach

The kinematic calculation involves simplification of the geometry and mechanical behavior of the DS (Assumptions 3.20 and 3.21 and Section 5.2.2.1.1), and simplification of the mechanics of interaction between the DSs (Section 5.2.3.2.2.2). It is necessary to demonstrate that the simplifications used in the calculations are reasonable and do not affect the primary results of the calculation. The DS separation and overlap results obtained using the detailed FE calculations of three DSs for $1x10^{-6}$ and $1x10^{-7}$ ground motions (BSC 2003 [DIRS 163425], Sections 6.2 and 6.3) were used as a means for verification of the ability of the kinematic calculation to represent vibratory motion response of the DS.

Analysis of the structural response of the DS to vibratory ground motion is carried out using a detailed three-dimensional FE representation of the DS geometry that takes into account elastic and inelastic deformation of the structural components of the DS, and DS interaction with the waste package and the emplacement pallet (the FE representation is described in Section 5.2.2.1.2 and the results are discussed in Section 5.3.3.2.). Three interlocked DSs are included in the analysis with rigid longitudinal boundaries (moving synchronously with the far-field) on each end of the DS chain. The analyses have demonstrated that, for these conditions, the DSs do not separate for 1×10^{-6} ground motions (Section 5.3.3.2.2). However, for 1×10^{-7} ground motions, there is DS overlap and separation (Section 5.3.3.2.3) due to impact of the outer DSs with the rigid end boundaries.

The same problems have been analyzed using the simple kinematic model as a means of verification of the approach. The geometry of the numerical representation is shown in Figure 5-36. FE realization 6 from Table 5-20 was used for comparison to the kinematic

analysis. This case utilizes ground motion number 1 (from either $1x10^{-6}$ or $1x10^{-7}$ annual exceedance frequencies) and a uniform friction coefficient between the DS and the invert of 0.69; and uniform friction coefficient between the DSs of 0.27. Three simulated DSs were considered as in the equivalent FE calculation, and an initial gap between the DSs and the vertical end boundaries was 0.1 m. All other kinematic simulation parameters correspond to case 1 from Table 5-19. The final configurations of the DSs at the end of the dynamic simulations, are shown in Figures 5-37 and 5-38, for 1×10^{-6} and 1×10^{-7} ground motions, respectively. The results of the kinematic analyses are qualitatively in agreement with the predictions of the detailed LS-DYNA calculations (Section 5.3.3.2). The DSs remained interlocked at the end of the simulation for the 1×10^{-6} ground motion (Figure 5-37). The same result, as reported in Section 5.3.3.2.2, in terms of DS separation, is observed at the end of simulation for 1×10^{-6} ground motion using the detailed FE representation. In all FE cases simulated for 1×10^{-7} ground motion (discussed in Section 5.3.3.2.3), the DSs separate or overlap due to impact of the outer DSs with the rigid end boundary condition. Qualitatively, the same outcome is predicted in the kinematic calculations (shown in Figure 5-38). Although the details of the dominant mechanisms of DS separation taking place within the LS-DYNA simulations for 1×10^{-7} ground motions are not certain, the kinematic representation, illustrated in Figure 5-38, separates via chaotic motions induced by impact to the rigid end boundaries, resulting in breaking of the DS weld connections as the limiting axial force is exceeded. This verification shows that the simple kinematic model is able to qualitatively capture the basic separation and overlap response indicated by the detailed FE representation for a specific case of three DSs with fixed rigid boundary constraints.

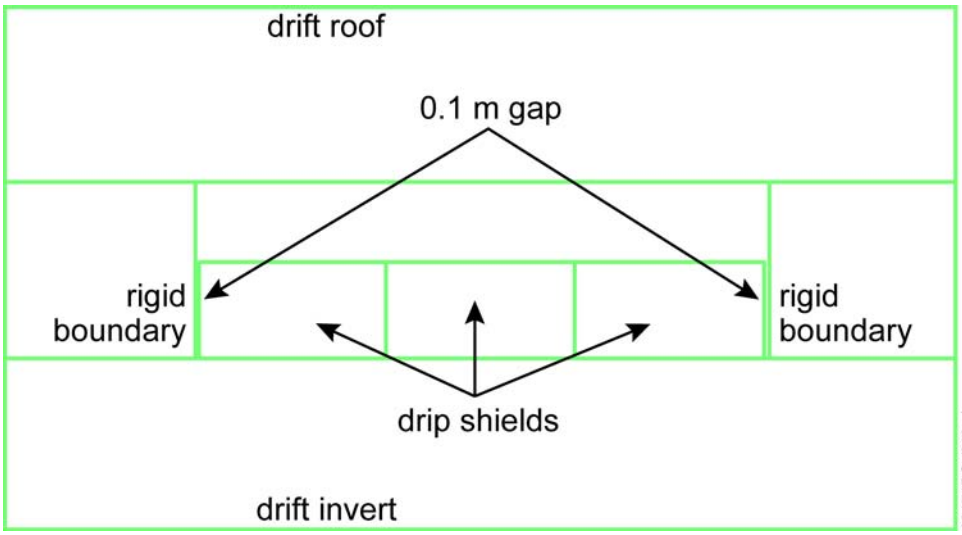

NOTE: Equivalent to the FE Representation Described in Section 5.2.2.1.2.

Figure 5-36. Geometry of Representation of 3 Drip Shields in the Kinematic Calculation

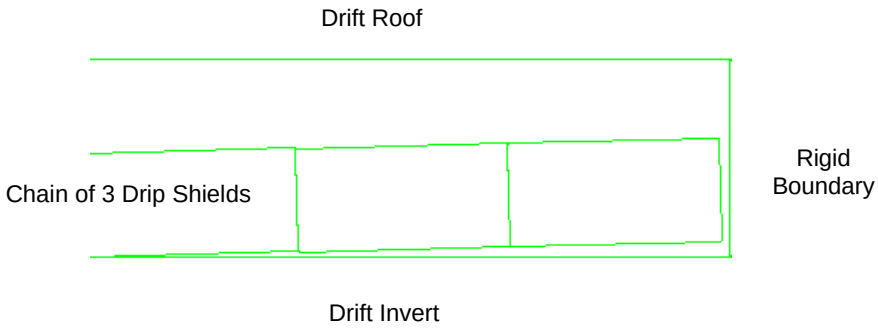

NOTE The presented state is at the end of dynamic simulation and the blocks are not in equilibrium. Further simulation until the blocks reach equilibrium will not cause their separation because the strong ground motion has already passed.

Figure 5-37. Configuration at the End of Simulation of 3 Drip Shields in the Kinematic Calculation for Application of $1x10^{-6}$ Ground Motion

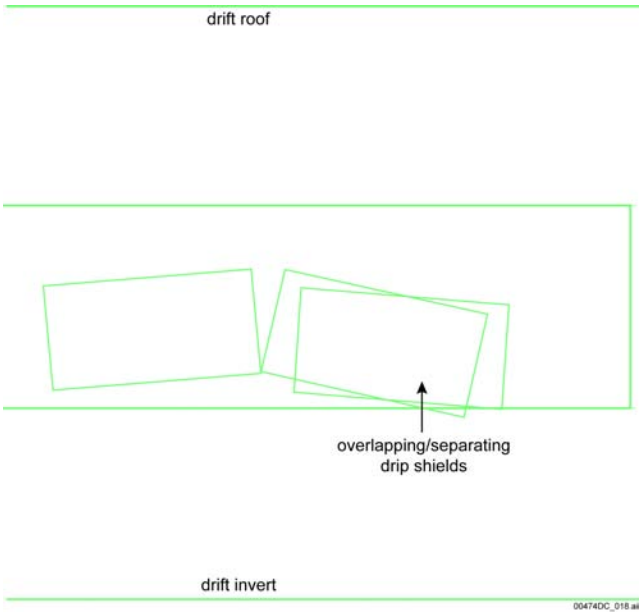

NOTE: The presented state is at the end of dynamic simulation and the model is not in equilibrium. The blocks that represent the DSs were allowed in the calculations to overlap freely after their connection was broken. The overlap is not prevented in the calculations (although the blocks are solid) because the DSs have the geometry that allows their overlap. For 1×10^{-7} ground motion equivalent to the calculation results are presented in Section 5.3.3.2.3.

Figure 5-38 Configuration at the End of Simulation of 3 Drip Shields in the Kinematic Calculation for Application of $1x10^{-7}$ Ground Motion

5.3.1.1.2 Description of the Kinematic Simulations

A sensitivity study was conducted to investigate the effects of various parameters on the potential for DS separation under vibratory motion. These parameters include:

- The number of DSs
- Friction coefficients
- Contact stiffnesses
- Ground motions
- Parameters that characterize interaction with the collapsed rock mass rubble.

A review of the parameters used in the sensitivity study is given in Table 5-19. Two ground motions, numbers 1 and 10, were considered from the ground motion sets for the 1×10^{-6} and 1×10^{-7} probabilities of annual occurrence. The PGVs and rankings of Arias Intensity for the sets number 1 and 10 among 15 ground motions of a given probability level are shown in Table 5-18. Ground motions 1 and 10 from the set of 1×10^{-6} have a PGV of approximately 2.44 m/s; ground motions 1 and 10 from the set of 1×10^{-7} have a PGV of approximately 5.35 m/s. These particular sets were chosen from among the 15 total sets of ground motions as they represent conditions among the highest amplitude ground motions (sets 1) and conditions of lowest amplitude ground motion (sets 10). The ground motions are bounded at a PGV of 5 m/s in the *Seismic Consequence Abstraction* (BSC 2004 [DIRS 169183], Section 6.4.4) as described in Section 5.3.2. Because set number 1 is a stronger ground motion (among highest level of Arias Intensity), most of the calculations were carried out for set number 1 to examine the conservative case of high energy intensity.

Table 5-18. Comparison of Ground Motion Parameters for Sets Number 1 and 10

Annual Hazard Level	Ground Motion Component	PGV Set #1 (cm/s)	Ranking of Arias Intensity Set #1	PGV Set #10 (cm/s)	Ranking of Arias Intensity Set #10
1×10^{-6} (revised)	H1	244.14	3	244.02	14
	H2	195.41		78.24	
	V	111.29		84.58	
1×10^{-7}	H1	535.26	4	535.24	13
	H2	428.42		171.62	
	V	298.44		226.79	

Source: BSC 2004 [DIRS 166107], Tables 6-5, 6-6 and X-3.

There are approximately 100 DSs in a typical 600-m long emplacement drift. A representative chain of 20 interlocked DSs is used in the analyses as a reasonable number to represent the vibratory response. Case 9, for 50 DSs (Table 5-19) was run to examine the effect of an increased number of DSs in the chain on potential for DS separation. The simulation has shown that the effect of increasing a number of the DSs to more than 20 is not significant, so the remaining simulations were conducted for 20 DSs. In all calculations, the friction coefficient between the DS and the invert is a random parameter from a uniform distribution between 0.2 and 0.8. The metal-to-metal, f_{m-m}, and rubble-to-metal, f_{r-m}, coefficients are varied between 0.2 and 0.8, as indicated in Table 5-19, but they are the same for all metal-to-metal or rubble-to-metal contacts in each calculation. A vertically-propagating incoming seismic wave

(i.e., $\alpha_{inc} = 0$ - see Figure 5-10) was considered in most calculations. In case 10, the effect of different angle of incidence ($\alpha_{inc} = 15^{\circ}$) was investigated. The effect of the wave inclination was not large, and remaining calculations were carried out for vertically propagating incoming waves only. Although rockfall is predicted to occur within seconds after strong ground motion begins, most calculations were carried out for conservative (regarding DS separation) conditions that the emplacement drift is completely open. The effect of rubble covering the DS is investigated in cases 11 through 14 and cases 22 through 24 (all for 1×10^{-7} ground motion). The effect of rubble filling the space between the DS and the drift walls (but not covering the top of the DS) is investigated in case 28, using a rubble-to-metal friction coefficient, f_{r-m}, equal to 0.5.

5.3.1.2 FE Calculations

In the FE calculations, the ground motion time histories and the friction coefficient values are independent stochastic parameters sampled for 15 realizations. The stochastic (uncertain) input parameters for the 15 simulations are the 15 sets of three-component ground motion time histories, the metal-to-metal friction coefficient, and the metal-to-rock friction coefficient. A Monte Carlo sampling scheme defines the appropriate combinations of ground motion and friction coefficients (BSC 2004 [DIRS 169999], Section 6.4) for each PGV level.

The stochastic (uncertain) input parameters provided for 15 realizations are listed in Table 5-20. The values of the friction coefficients presented in Table 5-20, for the purpose of this calculation, are presented (and used) with two significant digits. The ground motion (acceleration, velocity, and displacement) time histories are reviewed in *Drift Degradation Analysis* (BSC 2004 [DIRS 168550], Section 6.3.1.2.1). The time histories presented in these references are truncated for the purpose of this study. The time history cutoff and the simulation duration used in these calculations are discussed in detail in Section 5.2.4.2 (Tables 5-14 and 5-15).

Table 5-19. Summary of Kinematic Calculations

Case	No. of DS	Ground motion	Rock-fall on top	α_{inc}	f_{m-m}	E_r (MPa)	Rubble height (m)	ρ_r (kg/m^3)	Invert contact stiffness (MPa/m)	DS contact stiffness (MPa/m)	f_{r-m}
1	20	10^{-6} # 1	no	0	0.5	N/A	N/A	N/A	3	100	0
2	20	10^{-6} # 10	no	0	0.5	N/A	N/A	N/A	3	100	0
3	20	10^{-6} # 10	no	0	0.2	N/A	N/A	N/A	3	100	0
4	20	10^{-6} # 10	no	0	0.8	N/A	N/A	N/A	3	100	0
5	20	10^{-7} # 1	no	0	0.5	N/A	N/A	N/A	3	100	0
6	20	10^{-7} # 10	no	0	0.5	N/A	N/A	N/A	3	100	0
7	20	10^{-7} # 10	no	0	0.2	N/A	N/A	N/A	3	100	0
8	20	10^{-7} # 10	no	0	0.8	N/A	N/A	N/A	3	100	0
9	50	10^{-6} # 10	no	0	0.2	N/A	N/A	N/A	3	100	0
10	20	10^{-6} # 10	no	15	0.2	N/A	N/A	N/A	3	100	0
11	20	10^{-7} # 1	yes	0	0.5	100	5.5	2000	10	100	0
12	20	10^{-7} # 1	yes	0	0.5	100	5.5	200	10	100	0
13	20	10^{-7} # 1	yes	0	0.5	36	2.0	2000	10	100	0

Table 5-19. Summary of Kinematic Calculations (Continued)

Case	No. of DS	Ground motion	Rock-fall on top	α_{inc}	f_{m-m}	E_r (MPa)	Rubble height (m)	ρ_r (kg/m^3)	Invert contact stiffness (MPa/m)	DS contact stiffness (MPa/m)	f_{r-m}
14	20	10^{-7} # 1	yes	0	0.5	36	10	200	10	100	0
15	20	10^{-7} # 1	no	0	0.2	N/A	N/A	N/A	3	100	0
16	20	10^{-7} # 1	no	0	0.8	N/A	N/A	N/A	3	100	0
17	20	10^{-7} # 1	no	0	0.5	N/A	N/A	N/A	10	100	0
18	20	10^{-7} # 1	no	0	0.5	N/A	N/A	N/A	3	1000	0
19	20	10^{-7} # 1	no	0	0.5	N/A	N/A	N/A	20	100	0
20	20	10^{-6} # 1	no	0	0.5	N/A	N/A	N/A	3	1000	0
21	20	10^{-6} # 1	no	0	0.5	N/A	N/A	N/A	30	100	0
22	20	10^{-7} # 1	yes	0	0.2	10	5.5	2000	10	100	0
23	20	10^{-7} # 1	yes	0	0.5	10	5.5	200	10	100	0
24	20	10^{-7} # 1	yes	0	0.5	1	5.5	20	10	100	0
25	20	10^{-6} # 1	no	0	0.5	N/A	N/A	N/A	3	100	0
26[a]	20	10^{-6} # 1	no	0	0.5	N/A	N/A	N/A	3	100	0
27[a]	20	10^{-7} # 1	no	0	0.5	N/A	N/A	N/A	3	100	0
28	20	10^{-7} # 1	no	0	0.2	N/A	N/A	N/A	3	100	0.5

[a] All calculations except cases 26 and 27 were conducted using a "rounding length" of 0.4 m. The rounding length is the radius of curvature at the corners of the blocks in UDEC, which, instead of being sharp, are rounded. Rounding reduces the stochastic nature of the UDEC results. The physical justification for rounding is the fact that, in real materials with finite material strength, the corners are rounded as a result of material damage in regions of high stress concentrations or penetrate into other softer bodies, effectively behaving as if they are rounded. In cases 26 and 27, the rounding length was reduced to 0.05 m, compared to the otherwise equivalent cases 1 and 5, for which the rounding length was 0.4 m.

Table 5-20. Combinations of Ground Motion Numbers and Friction Coefficients Obtained by Random Sampling

Realization Number	Ground Motion Number	Friction Coefficient (-)	
		Metal to metal	Metal to rock
1	7	0.80	0.34
2	16	0.33	0.49
3	4	0.50	0.62
4	8	0.60	0.22
5	11	0.20	0.24
6	1	0.27	0.69
7	2	0.71	0.60
8	13	0.56	0.54
9	10	0.55	0.36
10	9	0.36	0.41
11	5	0.42	0.67
12	6	0.65	0.73
13	12	0.75	0.31
14	14	0.29	0.45
15	3	0.46	0.78

Source: DTN MO0301SPASIP27.004 [DIRS 161869], Table I-4.

The results described in Section 5.3.3.2 were obtained for open drifts (i.e., no rockfall has occurred) and, except for the waste package pallet assembly, there is no other obstacle to motion of the DS inside the emplacement drift. This assumption is proper for 5×10^{-4} ground motion for which rockfall is not expected in most of the repository (BSC 2004 [DIRS 166107]). However, the results presented in *Drift Degradation Analysis* (BSC 2004 [DIRS 166107]) show for strong ground motions (i.e., 1×10^{-6} and 1×10^{-7}) that the drifts (both in the lithophysal and non-lithophysal rock mass) either collapse or partially collapse, resulting in a significant volume of rockfall within seconds after the strong ground motion begins. The caved rock mass fills the space between the DS and the emplacement drift walls for partial collapse (in the nonlithophysal rock) or covers the DS for complete collapse in the lithophysal rock, thus restraining the motion of the DS (Figure 5-31). Under such circumstances, the possibility for separation of the DSs is very much reduced, and the simulations conducted assuming open drifts yield extreme outcomes. The other important simplification (due to reduction of model size) in the FE calculations that affects the predictions of DS separation are the use of rigid longitudinal boundaries (on two ends of the string of 3 DSs), which move synchronously with free-field motion of the rock mass. When displacements of the DSs are sufficiently large (i.e., > 0.1 m axial displacement), high energy impacts of the DSs into the longitudinal rigid boundary can occur. This impact can then result in chaotic movement of the DSs, and apparent separation. Therefore, estimation of damage to the DSs from the FE calculations is limited to those cases of $1x10^{-6}$ or higher annual exceedance probability. Analysis of DS separation relies on the DE kinematic analyses and not on the FE analyses.

5.3.2 Discussion of Simplifications in FE Calculations

The complexities inherent to the problem of simulation of DS response to vibratory motion render a detailed FE representation of the DS as prohibitively time-consuming. Consequently, it is necessary to simplify the FE representation without adversely affecting the results. All simplifications introduced in the course of development of the FE representation are generally conservative from the perspective of the estimate of the damaged area.

The criterion used to define the damaged area (independently of the conservatism related to the choice of the residual stress threshold) is also conservative. Specifically, the method used to evaluate the damaged area neglects the residual stress distribution across the thickness of the DS plates (i.e., it does not account for the possibility of crack arrest once the crack is nucleated).

The structural calculations of the interlocking DS's exposed to the vibratory ground motion have many complexities inherent in the nature of the problem, including the following:

- The externally applied loads (i.e., the ground motion time histories) are extremely intense. This causes a variety of numerical issues at 1×10^{-6} level and particularly at 1×10^{-7} level[12].

- The phenomena are highly nonlinear. Momentum is transferred among the repository emplacement drift and unanchored repository components (DS and waste package pallet assembly) solely by friction and impact. Geometrical nonlinearity (large deformations) is coupled with nonlinear constitutive behavior of the materials (elastoplastic behavior with kinematic hardening).

- Capturing both the large-scale kinematics and the occasional small-scale deformations (i.e., localized impacts) imposes extremely difficult FE meshing requirements.

- The extraordinary meshing requirements are, together with the intensity of ground motion, responsible for the very small time step required for numerical stability (approximately a microsecond, depending on annual frequency of occurrence and particular ground-motion time history). The very small time step is, in turn, necessary for simulation of a long-duration event (~30-40 s).

These complexities impose extreme computational requirements. Consequently, it is necessary to simplify the representation, but retain important features of the problem. The two most important simplifications are: 1) use of shell elements for representation of not only the DS plates but also some of the support structure, and 2) representation of the waste package and pallet as a single entity (waste package pallet assembly). These are discussed in the following sections.

[12]It is noted that the ground motion time histories used in this calculation were determined from a Probabilistic Seismic Hazard Assessment (PSHA) expert elicitation in which the aleatory variability in ground motion was described using unbounded lognormal distributions. As the PSHA calculations are extended to lower and lower annual probabilities of exceedence, the mean ground motions increase without bound, eventually reaching levels that are not credible. These levels of ground motion are not credible in that they eventually result in seismic strains that would cause the rock mass (in absence of any excavation) to fail through formation of fractures, an effect that is not observed at Yucca Mountain. An analysis analysis, presented in *Peak Ground Velocities for Seismic Events at Yucca Mountain, Nevada* (BSC 2004 [DIRS 170137]) estimates an upper bound to the ground motions at the Yucca Mountain site based on the shear strain increments (relative to the in situ stress state) required to damage (fracture) the repository rock mass. Such seismic-induced fractures are not observed in excavations at the Yucca Mountain site in repository host rocks that were erupted and cooled some 12.8 million years ago (BSC 2004 [DIRS 170137]). The upper bound for horizontal PGV developed from this analysis is in the range of 4.51 to 5 m/s, which is less than the 5.35 m/s PGV used in the present calculations for the $1x10^{-7}$ annual exceedance probability seismic event. Even though bounding peak ground velocities have been estimated, they have not been used explicitly in the calculations of seismic damage performed in the supporting calculations and summarized in this document. In other words, damage has been assessed for time histories with PGVs in excess of the bounding values defined in *Peak Ground Velocities for Seismic Events at Yucca Mountain, Nevada* (BSC 2004 [DIRS 170137]. Instead, the damage to EBS components is bounded within the *Seismic Consequence Abstraction* – i.e., damage associated with PGVs in excess of 5 m/s is bounded at the 5 m/s level (BSC 2004 [DIRS 169183], Section 6.4.4).

5.3.2.1 Use of Shell Elements in FE Representation

As discussed in Section 5.2.2.1.2, the time-efficient shell elements are used in the FE representation of the DS not only to represent the DS plates but also some of their support structure (most notably the bulkheads and support beams). The representation of the DS plate support structure by shell elements is discussed below in more detail.

This representation underestimates bending stiffness of the support structure, which may result in somewhat exaggerated deformation of the DS plates and, consequently, in a conservative estimate of the DS damaged area.

The connections between the DS parts represented by shell elements (for example, bulkheads and DS plates) are established by sharing the nodes on the intersection lines (or planes). These common nodes between the connected DS parts somewhat exaggerate the role of the shell reference (middle) surface compared to the actual physical situation when the connection is established by way of the surfaces of the connected parts. In other words, the middle shell surface close to the connections may take over, in some degree, the role of the actual physical surface of the connected parts. The effect of this aspect of shell elements use is conservatively bounded as long as the shell reference (middle) surface is taken into account in the damaged area evaluation.

The connections between the DS plate support structure and the DS plates are discontinuities that serve as preferential sites for development of the damaged area (BSC 2004 [DIRS 168993], Figures II-6 and II-7 as an example). The underestimated bending stiffness of the DS support structure is not, in this case, necessarily conservative. It must be recognized, though, that this effect is not pronounced when the DS loading is more uniform (BSC 2004 [DIRS 168993], Figures II-6 and II-7, referring to the rockfall on DS, are examples of extremely localized type of deformation). For 1×10^{-6} ground motions, the DS kinematics are such that the distribution of the impact load from the DS-invert interaction is relatively uniform. In cases when the DS impacts the invert with some angle of inclination, the effect of more localized loading is captured by the DSC support beams and the support beam-connectors that are represented by solid elements. Similarly, in the case of the interaction between DS and waste package pallet assembly, if their kinematics is such as to cause the inclined (i.e., localized) impact, the impact location is necessarily close to the DS end, and the effect of discontinuity is again captured by the DSC support beams and the support beam-connectors.

It is important to recognize that this discussion applies to simulations at annual frequencies of occurrence of 5×10^{-4} and 1×10^{-6}. For 1×10^{-7} realizations, only the kinematics of the DSs is of interest, primarily for use as a method of verification of the kinematic analyses.

5.3.2.2 Representation of Waste Package and Pallet by Waste Package Pallet Assembly

As discussed in Section 5.2.2.1.2, the structures of the 21-PWR waste package and pallet are, for the purpose of these calculations, simplified by reducing their FE representation to a rigid thick-wall structure of uniform density (waste package pallet assembly). The main purpose of waste package pallet assemblies is to ensure boundary conditions for the DSs (most importantly

the middle DS) that are conservative (from the standpoint of the DS damaged area) and time-efficient.

In adopting this approach it is important to acknowledge the results presented in *Structural Calculations of Waste Package Exposed to Vibratory Ground Motion* (BSC 2004 [DIRS 167083]). These results indicate that there is no waste package-DS interaction at the annual frequency of occurrence of 5×10^{-4} (BSC 2004 [DIRS 167083], Section 6.3), and that this interaction at the annual frequency of occurrence of 1×10^{-6} occurs rarely and is characterized by relatively modest impact speeds (mostly between 1 m/s and 2 m/s) (BSC 2004 [DIRS 167083], Section 6.1.3). On the other hand, the interaction between the pallet and the DS takes place more frequently than the interaction between the waste package and the DS due to the much smaller clearance between the former two repository components compared to the one between the latter two components. The pallet is much lighter and more flexible than the waste package. When the waste package and the pallet are merged into the rigid waste package pallet assembly (that has total mass uniformly distributed over the outside surface), each waste package pallet-DS impact would occur with a larger energy than in reality. That is particularly the case for the impacts in the region of the pallet. The waste package pallet assembly can be envisioned as a distorted waste package. The major consequence of this idealization is conservatism in estimating the impact energy between the DS and pallet.

Thus, the representation of the waste package and the pallet as a single entity with mass equal the cumulative mass of both repository components is conservative from the standpoint of the damaged area resulting from the waste package-DS and pallet-DS interactions for simulations at annual frequencies of occurrence of 5×10^{-4} and 1×10^{-6}.

In the case of realizations at annual frequency of occurrence of 1×10^{-7}, the kinematics of unanchored repository components is more complex due to the more intense ground motion. Thus, the representation of the waste package and the pallet as a single structural entity (waste package pallet assembly) may not capture with sufficient accuracy the damaged area of the DS plates. It is noted that the waste package pallet assembly is a likely cause of the contact instabilities that cause termination of simulations for the 1×10^{-7} ground motions. As discussed previously, this assembly is represented as a thick-walled structure with total mass of the waste package and the pallet being uniformly distributed over all waste package pallet-assembly nodes. Since waste package pallet assembly is relatively coarsely meshed and it does not have any interior structure, each waste package pallet-assembly node has very large nodal mass. Consequently, in the case of a high-speed impact between the waste package pallet assembly and the DS, instability may occur as a result of the large momentum being transferred from the waste package assembly to a very small portion of the DS (the localized nature of the transfer is promoted by the fact that the waste package pallet assembly is represented as rigid.). As a result of the numerical instabilities, damage assessment of the DS surface plates are not determined for the $1x10^{-7}$ ground motions.

5.3.3 Results

5.3.3.1 Kinematic Analysis of Drip Shield Separation

The results of the kinematic calculations can be summarized as follows:

- The DSs do not separate in any of the analyzed cases (listed in Table 5-19), even assuming strong ground motion (i.e., $1x10^{-7}$ probability of annual recurrence), open emplacement-drifts, and small friction coefficients for the DS-invert contact.

- Some of the cases for $1x10^{-7}$ ground motions that include completely open drifts (e.g., 5, 16, 17, 18, and 20 in Table 5-19) result in one of the two contacts in the connections breaking as a result of exceeding the axial force limit of the connector weld. However, in all of those cases, the second contact remained intact preventing separation of the DSs.

- Adding the effect of the rubble, either on the top of the DS (cases 11 through 14) or as friction acting on the sides of the DS (case 28), results in stabilization of the DS chain, reducing the magnitudes of displacements and forces in the contacts between the DS. In all of these cases, there is no interlocking connector weld breakage and no DS separation occurs.

- In all of the cases considered, the safety margin with respect to unlocking of the DSs is large. The largest transient shear deformation in the connection, recorded during seismic shaking, is 53 cm (case 5), while it is necessary to lift one DS relative to another approximately 102 cm in order to interlock them.

- In all cases listed in Table 5-19, the DSs remain connected during the entire simulation. There are two contacts between each DS connection, as shown in Figure 5-21. Time histories of the contact shear displacement, normal displacement and axial force for the upper contacts of each DS are shown in Figures 5-39 through 5-41 for case 1. The contact shear displacement in case 1 (for 1×10^{-6} ground motion) is less than 0.16 m (Figure 5-39), significantly less than the ~102 cm required to emplace and lock the DSs in place. A similar trend is observed for the axial force time history (Figure 5-41). The maximum axial force in case 1 reaches the 1.42 MN, much less than the conservatively-estimated limit of 3.5 MN. The maximum normal deformation of the contacts is approximately one centimeter (Figure 5-40).

It is observed by inspection of the calculation results that the asymmetrical conditions at the end of the DS "chain" (connected on one side and free on the other) introduce a velocity and displacement perturbation in the otherwise synchronous motion of the DSs. This perturbation is larger than that introduced due to the variability of the friction coefficient between the DS and the invert. This perturbation decays considerably within a distance of approximately five DSs from the ends (an example is shown in Figure 5-42). Therefore, although the results of the analyses show no separations, any possible separation for larger perturbations beyond the scope of this calculation would be expected near the interlocked DSs ends of the chain.

The summary of the maximum absolute displacements (shear and normal) and the maximum absolute forces (shear and normal) in the contacts between the DSs is listed in Table 5-21 for all of the sensitivity analyses. The maximums were determined from all 19 upper DS contacts. The summary illustrates that the largest shear displacement in the contacts are observed in case 5 (the maximum shear displacement of 53 cm), case 7 (45.6 cm) and case 15 (39.2 cm). These three cases are for 1×10^{-7} ground motions of completely open drifts (i.e., no rubble on the sides or on the top of the DS). Cases 7 and 15 apply to a low metal-to-metal friction coefficient of 0.2. Case 5 is for the metal-to-metal friction coefficient of 0.5. The results of cases 5 and 15 appear contradictory because the case with larger friction coefficient (0.5 for case 5) results in a larger maximum shear displacement than the case with smaller friction coefficient (0.2 for case 15). The reason for this apparent discrepancy is that the realization of friction coefficients between the DSs and the invert in the two cases is not the same (although they are selected from the same distributions). In addition, the maximum shear displacement is representative of extreme deformation of one contact and does not necessarily represent the general trend.

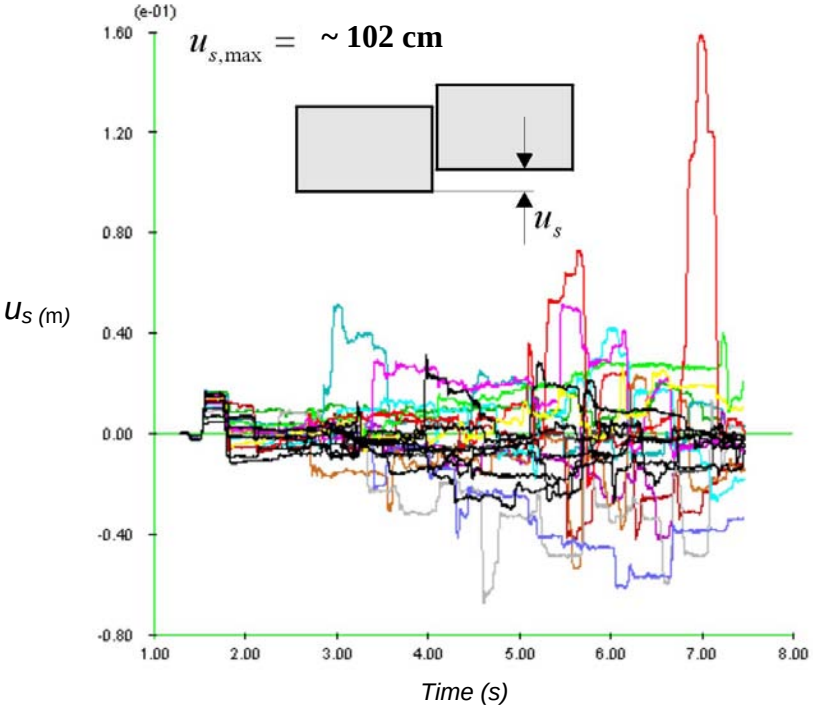

NOTE: The assumed maximum shear displacement when DSs separate is ~ 102 cm.

Figure 5-39 Case 1, $1x10^{-6}$ Ground Motion Shear Displacement (m) in DS Contacts as a Function of Time (s)

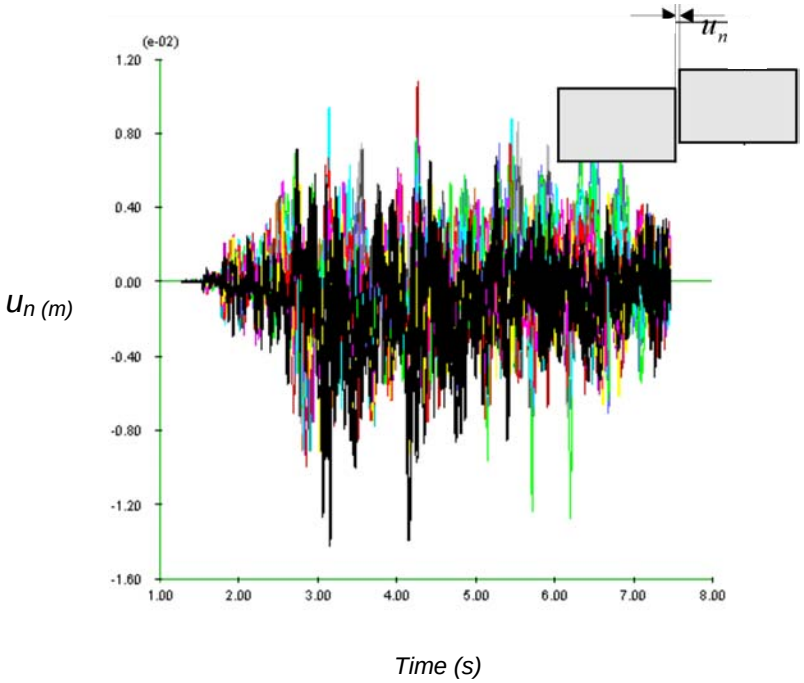

Figure 5-40. Case 1, 1x10^{-6} Normal Displacement (m) in DS Contacts as a Function of Time (s)

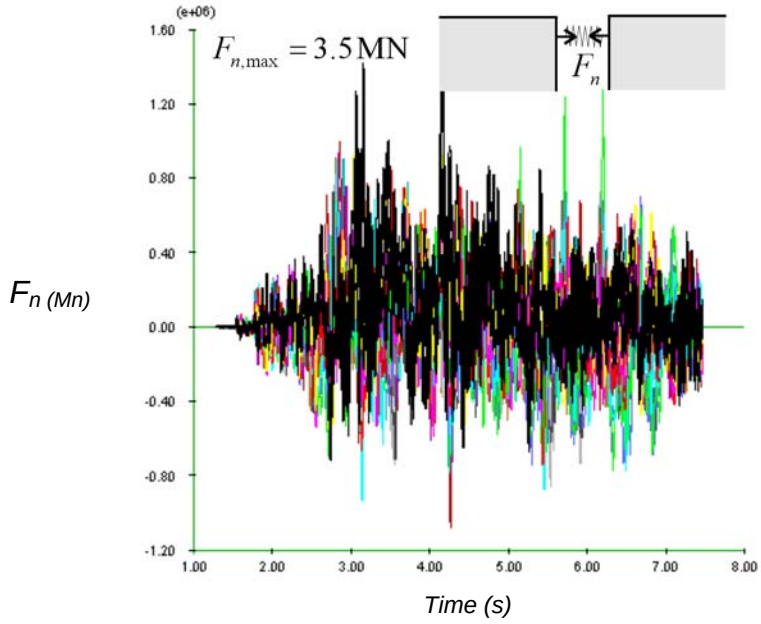

Figure 5-41. Case 1, 1x10^{-6} Ground Motion Normal Force (Mn) in DS Contacts as a Function of Time (s)

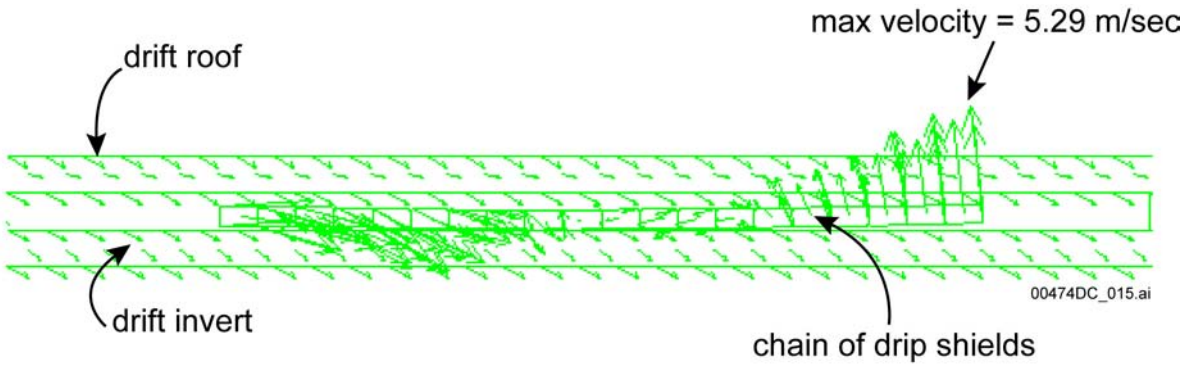

NOTE: Wave transmission down the "chain" of DSs can be seen in this figure. The amplification of the velocity at the face end of the DS chain is clearly visible.

Figure 5-42. Case 7, $1x10^{-7}$ Ground Motion Velocity (m/s) Vector Field at 4.47 s Showing Perturbation from Synchronous Motion Near the Ends of the Chain of Drip Shields

The maximum axial force in some cases (e.g., 5, 16, 17, 18, 20 and 23) reaches the limit of 3.5 MN, resulting in breakage of the upper contact (recall that 3.5 MN was conservatively chosen as 50 percent of the estimated strength). However, the forces shown are for the upper contacts only. The lower contact in those particular connections between DSs remained intact (as shown in Figure 5-43), preventing DS separation. The large normal displacements, as much as 104 cm in case 5, are transient and occurring during seismic ground motion. When the strong ground motions cease, the contacts return to their original position (before the vibratory motion) with the result that no separation occurs at simulation completion.

5.3.3.2 Results of FE Calculations

5.3.3.2.1 Results for Preclosure Ground Motion

Analysis of DS damage was conducted using the single $5x10^{-4}$ preclosure ground motion time history. The simulation was started at 3.0 s of the ground motion time history (corresponding to 5 percent of energy of ground motion), and the ending time was 15 s (corresponding to 65 percent of energy of ground motion) (BSC 2003 [DIRS 163425], Section 5.2.1). This duration covered the most intense strong motion period of ground motion time history. Further extension of the simulation is considered unnecessary due to the lack of damage observed in this analysis.

The ground motion with 5×10^{-4} annual frequency of occurrence is much less intense then 1×10^{-6} or 1×10^{-7} (as illustrated in Figure 5-29 and Table 5-14). Consequently, the extent of rigid-body motion during the 5×10^{-4} vibratory simulation is very limited and the maximum residual first principal stress is less than 3 MPa. The history of the first principal stress at a point on the DS plate during 5×10^{-4} vibratory simulation is shown in Figure 5-44.

The singular behavior at the onset of the simulation is nonphysical (unrelated to the nature of the problem). It is a consequence of a small initial gap between the DS and the invert in the FE representation, which is a side effect of the meshing technique. Specifically, it was necessary, in ANSYS V5.6.2, to create an artificial initial gap (0.2 mm) between the DS base and invert to prevent merging of neighboring nodes. Thus, the stress peak at the beginning of the simulation

results from the settling of the DS on the invert and should be disregarded (Note that, disregarded or not, this singular behavior at the onset of simulation does not affect the following conclusion.).

In summary, it can be concluded that the DS plates remain undamaged throughout the 5×10^{-4} event (i.e., the DS-plate area exceeding the established stress threshold is zero).

Table 5-21 Summary of Maximum Displacements and Forces at the Upper Kinematic DS Contact

Case	Maximum Shear Displacement (cm)	Maximum Normal Displacement (cm)	Maximum Shear Force (MN)	Maximum Normal Force (MN)
1	15.9	1.42	0.339	1.39
2	4.83	1.05	0.279	1.05
3	11.5	0.963	0.138	0.962
4	6.42	1.96	0.422	1.96
5	53.0	104.0[a]	1.04	>3.5[b]
6	6.80	2.32	0.486	2.33
7	45.6	2.22	0.261	2.22
8	6.32	2.28	0.583	2.28
9	18.5	1.28	0.229	1.28
10	27.1	1.83	0.322	1.84
11	3.11	1.84	0.573	1.84
12	1.72	0.495	0.153	0.495
13	1.39	0.518	0.205	0.517
14	2.22	1.14	0.324	1.14
15	39.2	3.40	0.681	3.44
16	23.4	58.6[a]	1.01	>3.5[b]
17	19.6	30.2[a]	1.07	>3.5[b]
18	37.7	121[a]	1.15	>3.5[b]
19	18.1	3.14	0.985	3.01
20	11.0	21.6[a]	1.12	>3.5[b]
21	6.81	1.43	0.378	1.44
22	17.2	1.68	0.297	1.67
23	18.8	19.2[a]	1.39	>3.5[b]
24	13.1	3.29	1.24	3.26
25	7.56	2.45	0.478	2.45
26	7.90	2.98	0.685	2.97
27	19.65	2.28	0.713	2.28
28	13.7	0.271	~0	0.271

NOTE: The shear displacements at separation is assumed at 102 cm and the maximum axial force at a contact is assumed at 3.5 MN. These results are for the upper contact only.

[a] These cases show failure at the upper contact only as shown in Figure 5-43.
[b] Axial maximum force exceeded at upper drip shield contact only.

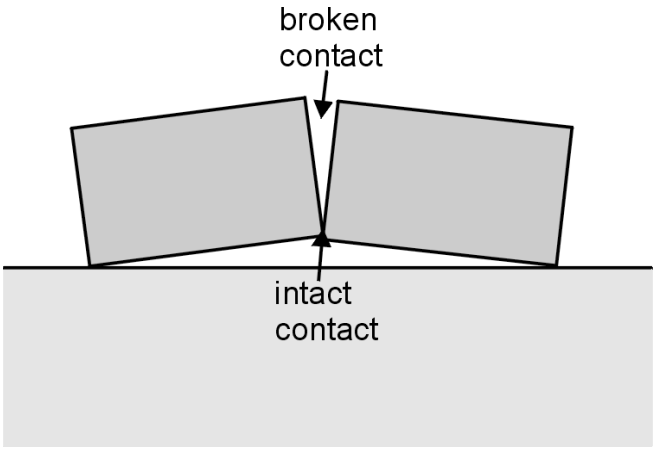

NOTE: Upper contact broken while lower contact remains intact.

Figure 5-43. Illustration of Partially Broken Connection

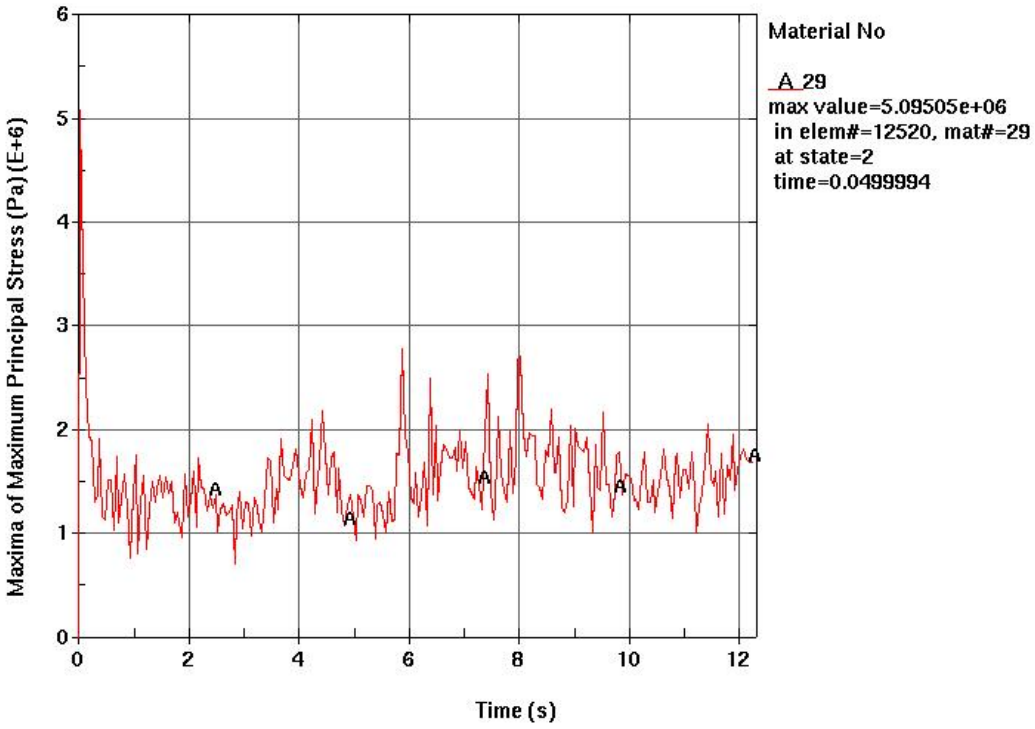

Source: BSC 2003 [DIRS 163425], Figure 4.

Figure 5-44. Maximum First Principal Stress Time History for DS Plates

5.3.3.2.2 Results for 1×10^{-6} Ground Motions

No DS separation was observed from the FE simulations of 1×10^{-6} ground motions with the exception of realization 6, which is discussed in greater detail below. According to the final configuration of DSs presented in Figure 5-45, one of the peripheral DSs is skewed with respect to the middle DS to the extent that there is an overlap on one side (of that end) that exceeds the ordinary overlap in the connector region. This effect may be partially a function of interactions with the end boundary and the waste package pallet assembly in which motion has occurred beneath the left hand side DS. It is reasonable to neglect this small DS overlap because: 1) the overlap is small and, thus, inconsequential from the standpoint of waste package protection (from direct seepage of water and rock impact); 2) the longitudinal wall does not give full credit to the DS connector assembly when it comes to the prevention of DS separation; and 3) the DS-separation effect is significantly amplified by the representation of the two outside DSs as rigid (recall only the center of the three DSs is deformable).

The damaged area (as defined in Assumption 3.18) is evaluated only in the DS plates of the middle DS. It is also presented as a fraction of the *total* area of the DS plates (the total area is equal to 38.2667 m^2, as calculated in *Drip Shield Structural Response to Rock Fall,* BSC 2004 [DIRS 168993], Section 5.6).

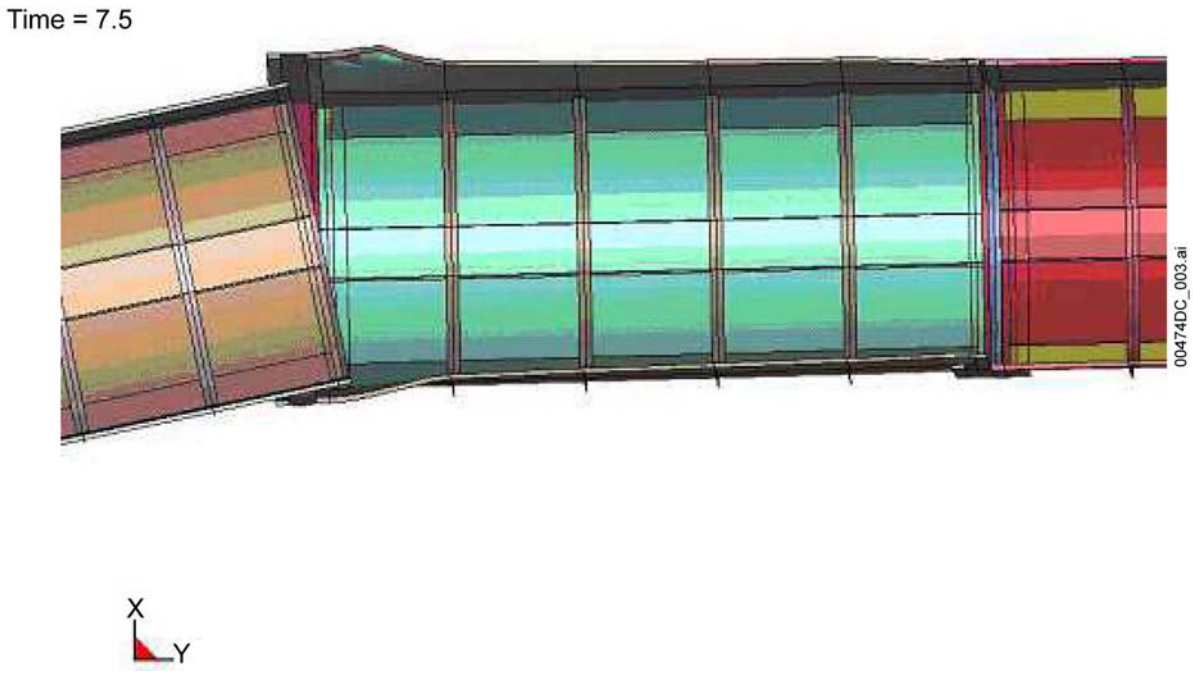

Source: BSC 2003 [DIRS 163425], Figure IV-8.

NOTE: Time is given in seconds.

Figure 5-45. Detail of Bottom View at Final Configuration in Realization 6 at 1×10^{-6} Annual Frequency Occurrence (t = 7.60 s)

Table 5-22 presents the damaged area resulting from 14 realizations at the 1×10^{-6} annual frequency of occurrence that were completed without any numerical problems. Realization 13 failed due to numerical instability. The damaged area is evaluated based on the residual first principal stress plot by using postprocessor LSPOST V2.

According to results presented in Table 5-22, the damaged area for 1×10^{-6} realizations vary within a wide range. The maximum and minimum damaged area correspond to 2.13 percent (realization 9) and 0.12 percent (realization 14) of the DS plates' total area, respectively. The average damaged area is 0.70 percent of the total area of the DS plates. Note that realization 9, characterized by the largest damaged area, is conspicuous not only for the large number of waste package-DS impacts but also for their intensity (BSC 2004 [DIRS 167083], Section 6.1.3).

Table 5-22 Damaged Area at Annual Frequency of Occurrence of $1x10^{-6}$

Realization Number	Ground Motion Number	Damaged Area (m^2; % of total area)
1	7	0.113; 0.30%
2	16	0.055; 0.14%
3	4	0.248; 0.65%
4	8	0.105; 0.27%
5	11	0.257; 0.67%
6	1	0.427; 1.12%
7	2	0.479; 1.25%
8	13	0.100; 0.26%
9	10	0.814; 2.13%
10	9	0.192; 0.50%
11	5	0.456; 1.19%
12	6	0.376; 0.98%
14	14	0.0456; 0.12%
15	3	0.0989; 0.26%

Source: BSC 2003 [DIRS 163425], Table 4.

5.3.3.2.3 Results of FE Calculation for 1×10^{-7} Ground Motions

The ground motions at 1×10^{-7} annual frequency of occurrence are much more intense than at 1×10^{-6} annual frequency of occurrence. As an example, the maximum peak ground acceleration reached in ground motion 9 is approximately $34\,g$ (where $g = 9.81\,\mathrm{m/s^2}$ is the acceleration of gravity), while the maximum peak ground velocity in ground motion 3 is approximately 16 m/s (BSC 2003 [DIRS 163425], Section 6.2.1). Hence, the kinematics of the unanchored repository components is characterized by a large rigid-body motion and numerous high-speed impacts. The impacts that have particular effect on DS separation and overlap involve impact of the DS to the rigid longitudinal boundaries, which are conservatively included in the calculation because of small model size. As a consequence of this high-intensity loading, only one 1×10^{-7} realization (number 5) terminated without numerical instability. The objective of 1×10^{-7} realizations is limited, therefore, only to reporting the separation of DS segments in the course of simulation before the numerical instability occurs, and for use in qualitative verification of the kinematic

model as presented in Section 5.3.1.1.1. The DS separation reported here is not used as input to the *Seismic Consequence Analysis* (BSC 2004 [DIRS 169183]).

All five 1×10^{-7} realizations indicate the DS separation, again, primarily resulting from impacts with the rigid end boundaries. None of these simulations, with exception of realization 5, reached 95 percent of the time history. Figure 5-46 shows a typical result from the $1x10^{-7}$ realizations, indicating overriding DSs resulting from chaotic motion due to impact of the DS with the rigid end boundary conditions. These results are used only for verification of the kinematic modeling as described in Section 5.3.1.1.1.

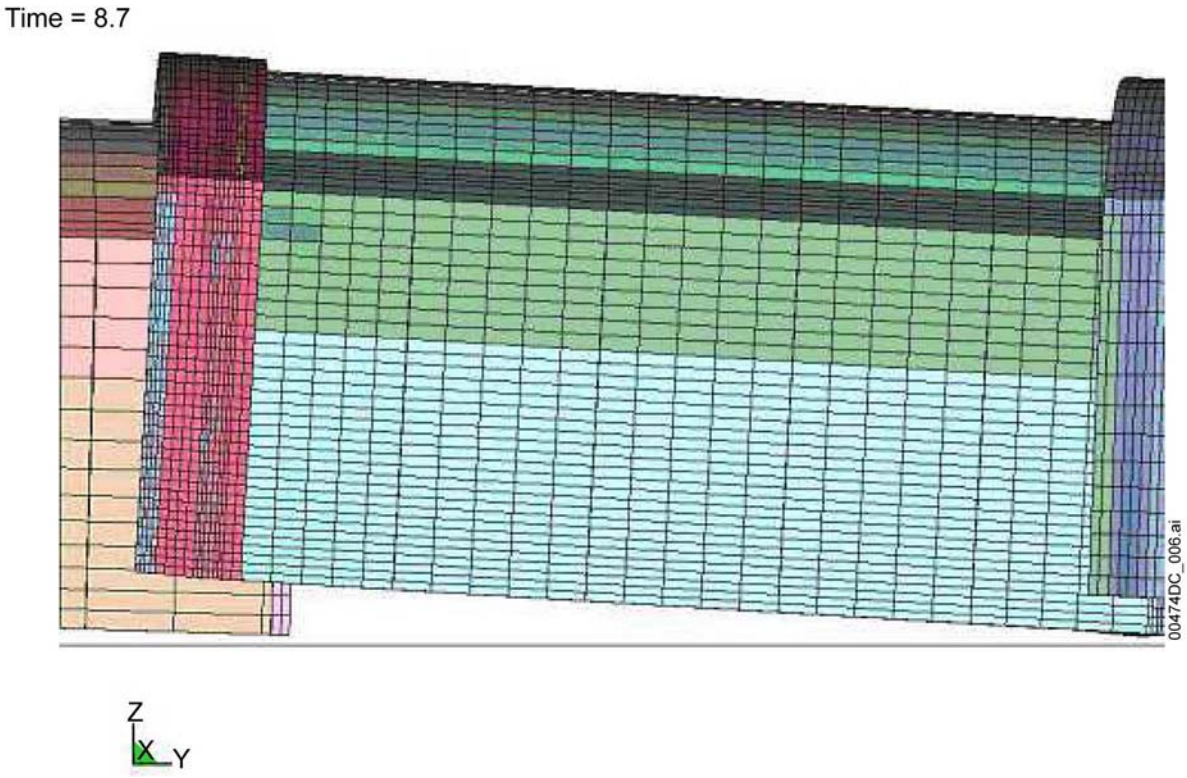

Source: BSC 2003 [DIRS 163425], Figure IV-3.

NOTE: Time in seconds.

Figure 5-46. Detail of Side View at Component Locations in Realization 5 at 1×10^{-7} Annual Frequency of Occurrence (t = 8.70 s)

5.4 ANALYSIS OF MECHANICAL EFFECTS OF ROCKFALL AND DRIFT DEGRADATION

5.4.1 Description of Calculations

Some level of drift degradation is expected during the regulatory period. Although the rockfall can occur under static loads (e.g., in situ and thermal stresses), the major factors that can cause instability of the drift walls and roof are strong ground motions (with small annual frequency of occurrence). The effect of the rockfall on DS functionality is investigated for two bounding conditions.

The impact of destabilized, flying blocks onto the DS, caused by seismic ground motions with 1×10^{-6} and 1×10^{-7} annual frequency of occurrence, was analyzed for rockfall in the nonlithophysal rock mass. These impact loads are bounding because: (a) the impact energy during the seismic ground motions is greater than during the rockfall that resulted from gradual drift deterioration due to time-dependent strength degradation; and (b) the block size in the nonlithophysal rock mass is greater than in the lithophysal rock mass, resulting in greater impact energy.

The loose, caved rock mass will accumulate at the bottom of the emplacement drift, initially filling the space between the DS and the drift walls but eventually (depending on the magnitude of the rockfall) completely covering the DS. As described in Section 5.2.5.1, the static loads on the DS are calculated for the case of total collapse of the drift due to the extreme condition of complete loss of cohesive strength of the rock mass. The DS is analyzed for the static loads due to the weight of the broken rock covering the DS after collapse of the emplacement drift.

5.4.2 Drip Shield Impact by Large Blocks in Nonlithophysal Rock

The analyzed cases of rock impact on the DS were selected based on results of rockfall analysis in nonlithophysal rock mass presented in *Drift Degradation Analysis* (BSC 2004 [DIRS 168550]). These rockfall analyses were subsequently updated (BSC 2004 [DIRS 166107], Section 6.3) using revised estimates of rock mass fracture density and revised ground motions. This revised fracture density is greater, with the resultant effect that the median predicted rock block masses are smaller, but the maximum impact energy is approximately the same. Some statistical parameters (i.e., mean and maximum of block size and impact energy) that characterize block impact in the DS, as obtained in the original (BSC 2004 [DIRS 168550], Section 6.3) and revised (BSC 2004 [DIRS 166107]) rockfall models, are shown in Table 5-23. The mean block size and impact energy predicted by original simulations (BSC 2004 [DIRS 168550]) are at least two times greater than the updated predictions (BSC 2004 [DIRS 166107]). Predictions of the maximum impact energies are practically the same. The impact conditions selected based on prediction of the original model are conservative considering the predictions of the updated model. Therefore, the calculations of the impact of blocks in the DS in the nonlithophysal rock mass are not updated as a result of predictions of rockfall for new 1×10^{-6} ground motions and synthetic model of jointing in nonlithophysal rock mass.

Table 5-23. Statistical Characterization of Impacts for 1×10^{-6} Ground Motion in Nonlithophysal Rock Mass

	REV 02	REV 03
Mean Block Mass (MT)	0.87	0.43
Maximum Block Mass (MT)	21.42	28.22
Mean Impact Energy (J)	5267	2350
Maximum Impact Energy (J)	163,083	163,657

Source: BSC 2004 [DIRS 168550], Table 14 for REV 02; BSC 2004 [DIRS 166107], Table 6-14 for REV 03.

MT = metric tons, J = Joules; Obtained using different revisions of Drift Degradation Analysis.

5.4.2.1 Conditions of Impact

Impacts by five different rock blocks from 1×10^{-6} ground motion and one rock block from 1×10^{-7} ground motion data have been analyzed in these calculations. These cases cover the entire range of impact energies observed in the drift degradation analysis (BSC 2004 [DIRS 168550], Section 6.3). The impact cases are summarized in Table 5-24 (MO0305MWDNLRKF.001 [DIRS 163438], file: *1e-6 3DEC non-lith analysis summary.xls*, sheet: impact information for 1×10^{-6} ground motions; and MO0301MWD3DE27.003 [DIRS 161536], file: *post-closure 1e-7 gm analysis summary.xls*, sheet: block info for 1×10^{-7} ground motions).

Table 5-24. Rockfall Impact Data in Nonlithophysal Rock Mass

Ground Motion [1/yr]	Mass [MT]	Line # in source file and sheet	Kinetic Energy [J]	Vertical Velocity [m/s]	Lateral Velocity [m/s]
10^{-6}	14.5	196	163,083	4.74	0.656
10^{-6}	3.3	13	24,712	3.86	0.0824
10^{-6}	0.15	95	902	3.49	0.955
10^{-6}	0.11	272	42	0.86	0.383
10^{-6}	0.25	235	~0	0.02	0.0103
10^{-7}	11.5	298	348,174	7.77	0.295

Source: DTNs MO0305MWDNLRKF.001 file: *1e-6 3DEC non-lith analysis summary.xls*, sheet: impact information, MO0301MWD3DE27.003, file: *post-closure 1e-7 gm analysis summary.xls*, sheet: block info.

MT = metric tons; J = Joules.

For each of six blocks, the analysis was conducted for three different impact points and impact directions at angles of 40°, 60°, and 90°. The angles are measured counterclockwise about the intersection of the plane of symmetry and the top of the invert, and beginning with 0° for the top of the invert. The idealized configurations of impact are shown in Figure 5-47.

The rock blocks considered in the calculations to impact the DS have the shape of a rectangular prism (Assumption 3.14) as shown in Figure 5-48. The enveloping dimensions (indicated in Figure 5-48) are listed in Table 5-25.

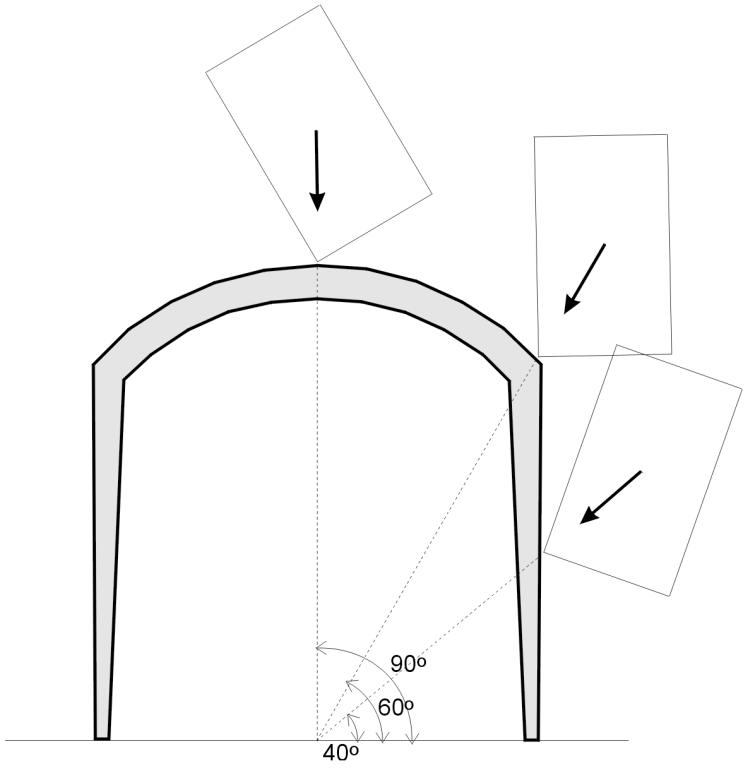

Figure 5-47. Schematic of Analyzed Configurations of Impact in Nonlithophysal Rock Mass

Table 5-25. Dimensions of Blocks Impacting the Drip Shield in Nonlithophysal Rock Mass

mass (MT)	a (m)	b (m)	c (m)
14.5	2.5	2.5	1.0
3.3	1.5	1.5	0.6
0.15	0.5	0.5	0.26
0.11	0.5	0.5	0.19
0.25	0.7	0.7	0.22

Source: BSC 2004 [DIRS 168993], Section 5.3.
MT = metric tons (1 MT = 1000 kg)

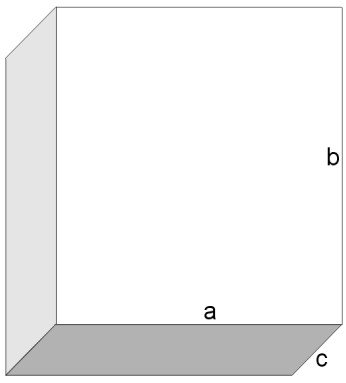

Figure 5-48. Idealized Geometry of Blocks in Nonlithophysal Rock Mass

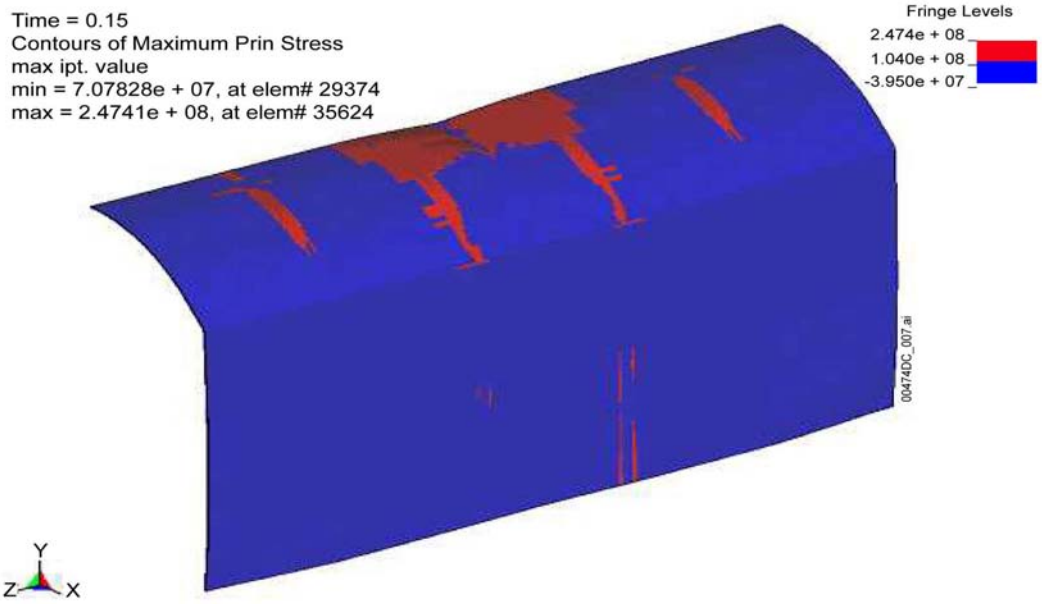

Source: BSC 2004 [DIRS 168993], Figure II-6.

NOTE: MT = metric tons.

Figure 5-49. Typical First Principal Residual Stress (Pa) Distribution on DS Plates (14.5 MT Vertical Rockfall)

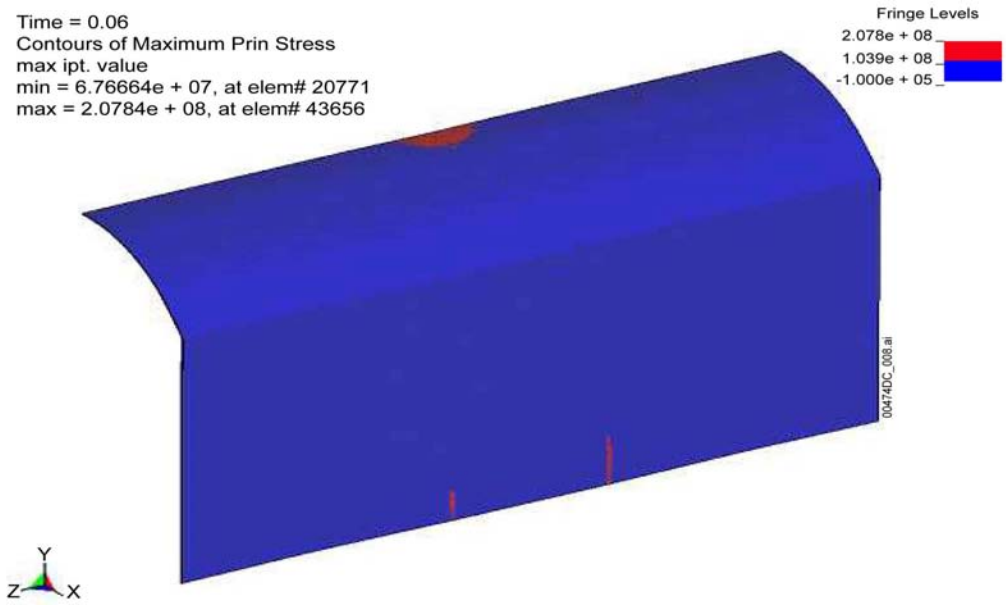

Source: BSC 2004 [DIRS 168993], Figure II-7.

NOTE: MT = metric tons.

Figure 5-50. Typical First Principal Residual Stress (Pa) Distribution on DS Plates (3.3 MT Vertical Rockfall)

5.4.2.2 Results

The objective of this calculation is to determine the areas of residual stress (damaged areas) that exceed 50 percent of the Ti-7 yield strength (Section 1). Distributions of the typical first principal stresses on the DS plates are shown in Figures 5-49 and 5-50. In the postprocessor, the first principal stress contours were used to select all-rectangular areas of the FE mesh that exceed the critical value.

Table 5-26 shows the results of LS-DYNA FE evaluations for the 1×10^{-6} ground motion rockfall on the DS. The damaged areas have been calculated using the regions of residual first principal stress, which exceed 50 percent of the Ti-7 yield strength at 150°C.

Table 5-27 shows the results of LS-DYNA FE evaluations for the 1×10^{-7} ground motion rockfall on DS. This additional look-up table can be used in conjunction with Table 5-26 to determine the structural response of the DS to rockfall in terms of the rock blocks (mass and velocity, i.e., kinetic energy) and the damaged areas.

All of the results indicate that increasing kinetic energy of the rock impact causes an increase in the damaged area, as expected. There is one notably large damaged area increase in the case of the 1×10^{-7} ground motion rockfall onto the DS corner (Table 5-27) relative to other cases. The reason for this is a localized deformation of the DS side-wall subjected to the substantially large vertical load from the rock block. This phenomenon is, however, observed mildly in the case of the 1×10^{-6} ground motion simulations (Table 5-26).

Table 5-26. LS-DYNA Finite Element Analysis Results for Seismic Rockfall on Drip Shield (10^{-6} Ground Motion)

Rock Mass and Kinetic Energy	Damaged Area (m^2) and Ratio of Damaged Area to Total DS Surface Area		
	Vertical Rockfall (90° from horizontal)	Rockfall onto DS Corner (60° from horizontal)	Rockfall onto DS Side-wall (40° from horizontal)
14.5 MT Rock (163083 J)	3.508 (9.17%)	0.612 (1.60%)	0.079 (0.21%)
3.3 MT Rock (24712 J)	0.548 (1.43%)	0.416 (1.09%)	0.0 (0.00%)
0.15 MT Rock (902 J)	0.0015 (0.00%)	0.0091 (0.02%)	0.0 (0.00%)
0.11 MT Rock (42 J)	0.0 (0.00%)	0.0 (0.00%)	0.0 (0.00%)
0.25 MT Rock (~0 J)	0.0 (0.00%)	0.0 (0.00%)	0.0 (0.00%)

Source: BSC 2004 [DIRS 168993], Table 6-2.

MT = metric tons (1 MT = 1000 kg); J = Joules

Table 5-27. LS-DYNA Finite Element Analysis Results for Seismic Rockfall on Drip Shield (10^{-7} Ground Motion)

Rock Mass and Kinetic Energy	Damaged Area (m^2) and Ratio of Damaged Area to Total DS Surface Area		
	Vertical Rockfall (90° from horizontal)	Rockfall onto DS Corner (60° from horizontal)	Rockfall onto DS Side-wall (40° from horizontal)
11.5 MT Rock (348,174 J)	4.304 (11.25%)	2.835 (7.41%)	1.126 (2.94%)

Source: BSC 2004 [DIRS 168993], Table 6-3.

MT = metric tons (1 MT = 1000 kg); J = Joules

The maximum vertical displacement in the DS components takes place in the longitudinal stiffener during the 11.5 MT vertical rockfall on DS. The reason for this result is because the kinetic energy of this rock block is the largest. Figure 5-51 shows that the maximum displacement is 25.4 cm.

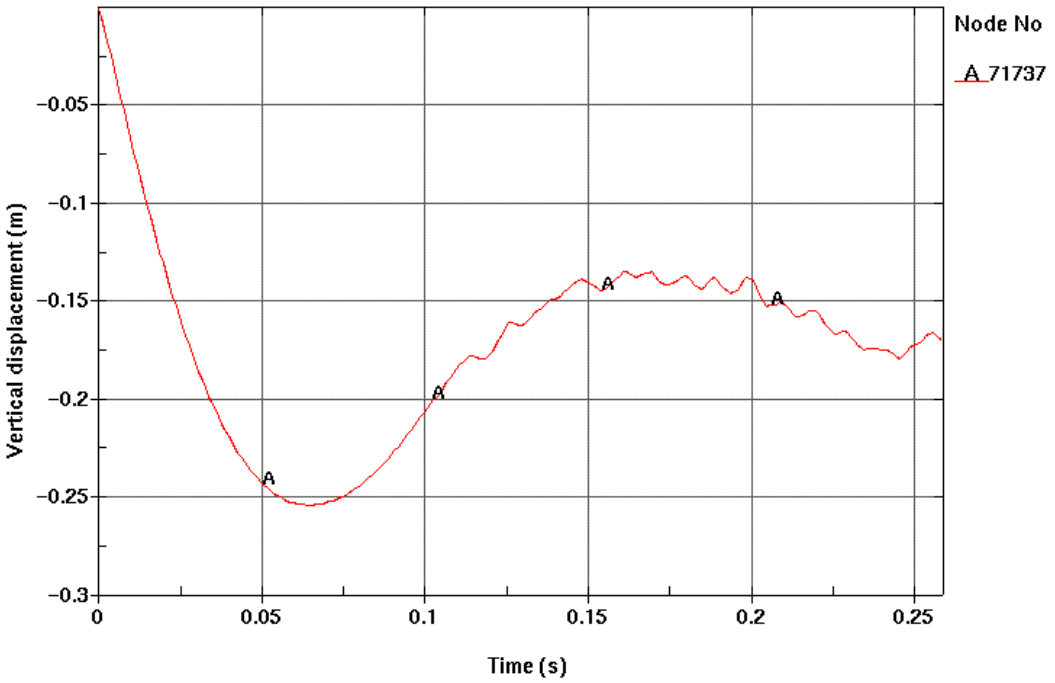

Source: BSC 2004 [DIRS 168993], Figure II-5.

NOTE: MT = metric tons (1 MT = 1000 kg).

Figure 5-51. Vertical Displacement for Element #71737 Maximum Peak Value in DS Longitudinal Stiffener 11.5 MT Vertical Rockfall for 1×10^{-7} Ground Motion

5.4.3 Static Load on Drip Shield

5.4.3.1 Loads From Caved Rubble

The rock block shapes in the lithophysal rock mass and the manner in which they fall and compact around the DS is a random process. The caved rock mass will consist of blocks of irregular shapes and size distribution with mean block size of approximately 0.2 m (BSC 2004 [DIRS 166107], Section 6.4). The static load of the caved rock mass will be transferred to the DS through Hertzian contacts among the rocks and between the rocks and the DS (a large number of localized contacts that are nearly point loads).

The distribution of the point loads in the cross-section and along the DS and their magnitude will vary significantly. This is illustrated by the distribution of the loads shown in Figure 5-33, obtained from 6 realizations calculated using a two-dimensional model. There is also almost 50 percent variability of the average pressures calculated for different realizations (Table 5-28). The pressure variability is due to the stochastic nature of the drift degradation (i.e., formation of the rock blocks of irregular shapes and different sizes and their fall and compaction). The average pressures on the top and the sides of the DS for 6 realizations are listed in Table 5-28. Although obtained from a two-dimensional model, pressure distribution for each realization is representative of the load on the DS for a finite length along the DS. The exact correlation between results of the two-dimensional model and actual three-dimensional load distribution cannot be established. However, it is reasonable to apply the pressure distribution from a particular realization over a drip shield axial length approximately equal to the average block size (i.e., 0.2 m). Considering the entire length of one DS (5.81 m), or even spacing of the bulkheads and support beams (1.07 m), compared to the length over which loads of one realization are representative (~0.2 m), the average load (represented as a continuous line load in Figure 5-33) of a number of different realizations controls the overall stability of each structural frame and the DS.

Table 5-28. Average Pressure Values on the Drip Shield for Quasi-Static Drift Degradation (0.2 m Rock Size)

Realization	Pressure (kPa)		
	Left	Top	Right
1	41.54	108.92	58.76
2	19.15	147.07	19.33
3	31.35	154.80	6.69
4	57.23	129.76	128.82
5	69.69	112.73	105.43
6	32.97	113.87	52.19
Average	41.99	127.86	61.87

Source: DTN MO0407MWDDSLCR.000 [DIRS 170873].

To account in a conservative way for variability in the loads (in one cross-section and between different cross-sections) the DS stability analysis was conducted for all six realizations in which the pressure in a particular segment (Figure 5-32) is obtained from a two-dimensional model and acts along entire length of the DS that is analyzed in the three-dimensional model. If stability of the DS is demonstrated for all 6 realizations using this conservative line-loading application, then it is also certain that the DS would be stable for the combined or average load resulting from those 6 realizations.

The factor-of-safety of the DS for static load of the caved rock mass is determined by increasing the load on the structure until the structure collapses. In this case, the problem of the factor-of-safety is ambiguous because the loads by the caved rock mass acting on the DS are both active and passive. Therefore, it is not justified to simply increase all loads (for 6 realizations or for the average pressure distribution) and apply them on the DS. The horizontal loads, which are predominantly passive loads, should increase during consideration of increased loading factor but not in the same proportion as the active loads. Instead, the passive loads are result of interaction between the structure and the caved rock mass, and should be determined from the coupled rock particle-DS interaction calculation. The loads on the DS are calculated using the UDEC coupled model of the drift degradation and the DS (discussed in Section 5.2.5.1). To calculate the factor-of-safety of the DS to static load of the caved rock mass, the density of the rock blocks inside the region that has caved is gradually increased and for each density increase the distribution of load on the structure is calculated after the equilibrium state is achieved. All six discontinuum UDEC block realizations are simulated for each level of density increase. For example, the average pressures on the DS calculated for 2.5 times density increase are listed in Table 5-29. The increase in the actual vertical load is roughly proportional to (slightly less than) the increase in density. For example, for 2.5 times increase in the density (shown in Table 5-29), the increase in the average vertical pressure is approximately 2 (compare Tables 5-28 and 5-29). The reason for this difference is the arching of the additional weight inside the caved rock mass. For factor-of-safety calculations the average pressures of six realizations were considered only. The DS was analyzed for increasing loads using the finite increments. The largest load analyzed for which the structure does not collapse is used as an approximation of the limit load for the DS.

Table 5-29. Average Pressure Values on the Drip Shield for Quasi-Static Drift Degradation (0.2 m Rock Size) Assuming 2.5 Times Increased Density of the Caved Rock Mass

Realization	Pressure (kPa)		
	Left	Top	Right
1	93.12	232.78	91.11
2	42.46	305.34	34.49
3	49.33	319.89	16.91
4	82.09	264.88	147.11
5	103.10	221.82	128.54
6	49.06	237.68	67.74
Average	69.86	263.73	80.98

Source: DTN MO0407MWDDSLCR.000 [DIRS 170873].

For the purpose of this calculation, the pressure distribution along the DS surface is discretized over 30 segments of approximately equal length as indicated in Figures 5-32 and 5-52. Note that the even-number segments are omitted from Figure 5-52 to improve visibility. The pressure distribution does not vary in the longitudinal (z) direction in this calculation. In order to capture the quasi-static nature of the loading and minimize the oscillations of results, the applied loads (the pressure and gravitational acceleration) are ramped from 0 to 0.1 s and than held constant. Thus, the loads are applied in full intensity at 0.1 s.

The simulations are terminated either when the static equilibrium of the DS is reached (based on the kinetic energy decreasing to very small values), or when the loss of the DS structural stability occurs. Thus, the termination times are different for different realizations due to the stochastic nature of the pressure distribution.

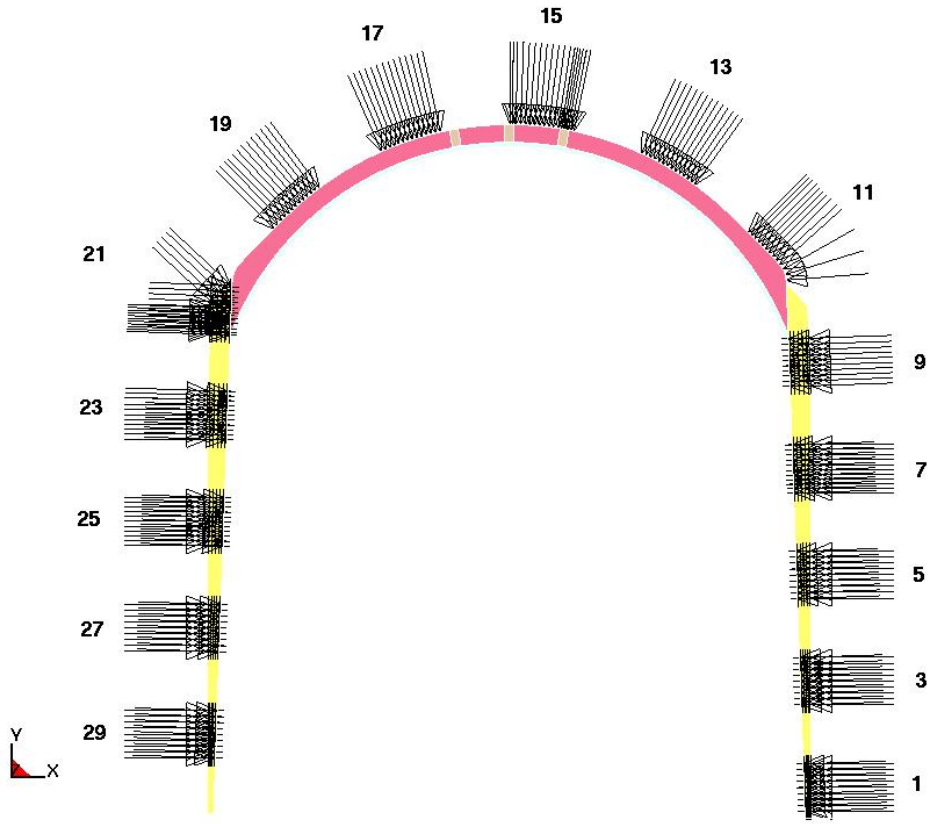

Source: BSC 2004 [DIRS 170791], Figure 5.

Figure 5-52. Application of the Static Pressure of Caved Rock Mass on the Drip Shield

5.4.3.2 Results

All six realizations indicate that the DS reaches static equilibrium without the loss of structural stability for the given non-uniform quasi-static pressure distributions. Figure 5-53a illustrates the final DS configuration for realization 3, which imposes the largest vertical load on the DS. The kinetic energy history plot presented in Figure 5-53b demonstrates that the final configuration corresponds to the DS static equilibrium.

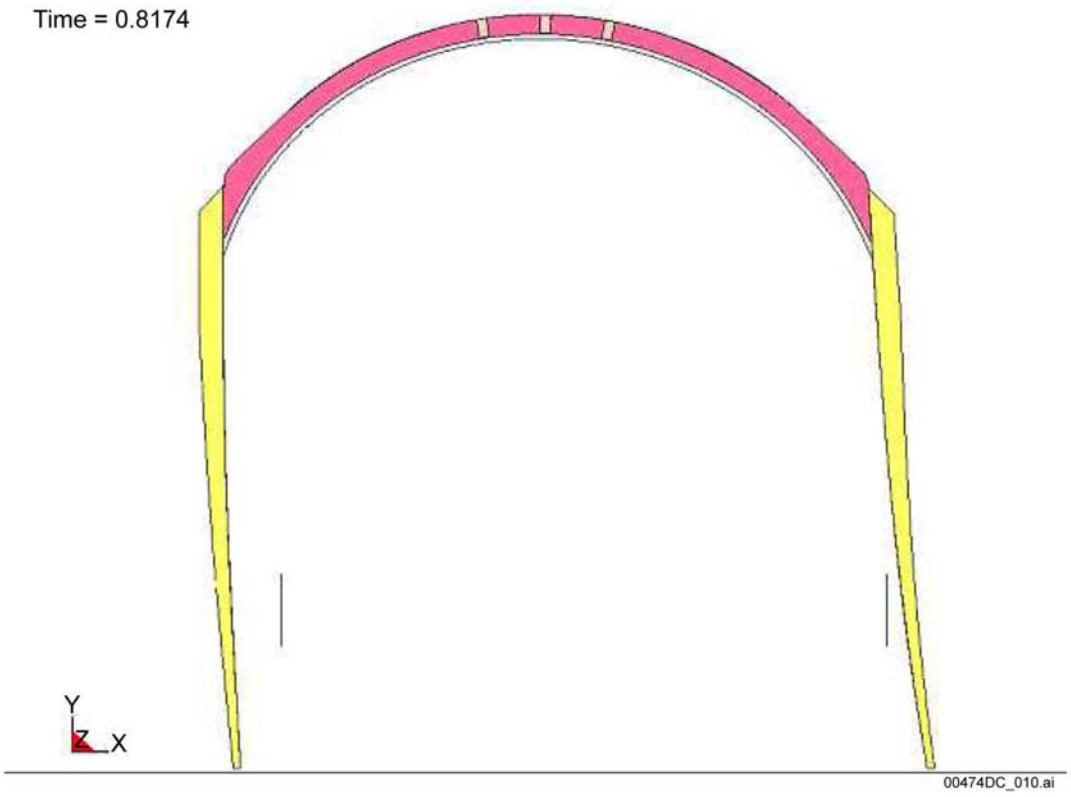

(a)

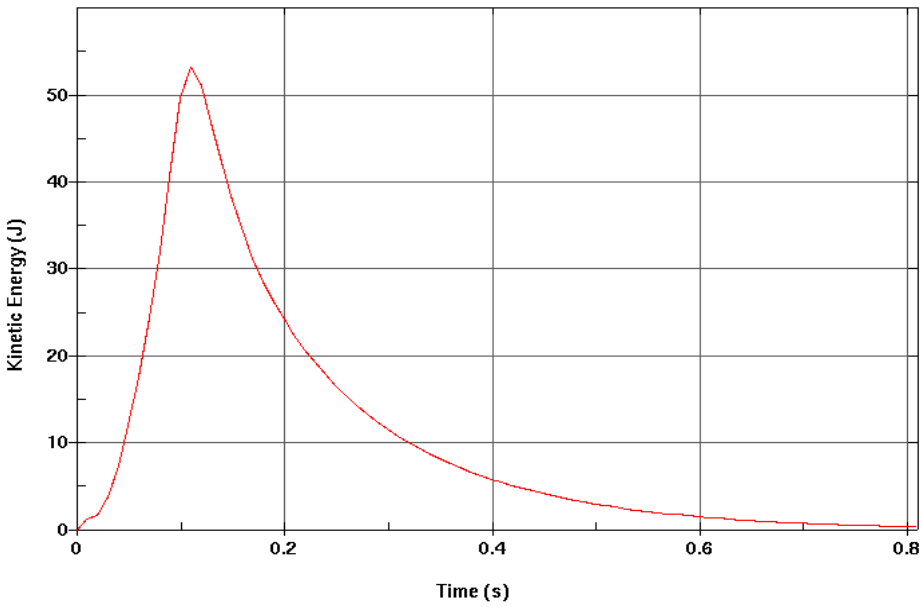

(b)

Source: BSC 2004 [DIRS 170791], Figure II-3.

NOTE: The constraints provided by the pallet are shown as vertical bars in (a) final drip shield configuration and (b) kinetic energy of the drip shield; J=Joules.

Figure 5-53. Typical Results for Realization 3

The vertical deflections of the DS top plate (DS plate 1), along the vertical symmetry plane are presented in Table 5-30. The deflections are recorded at the node located on the outside surface of the top plate above the bulkhead. Note that the positive value in Table 5-30 indicates the upward displacement.

As seen in Figure 5-54, the plot shows the damaged areas (i.e., where first principal stress exceeds 50 percent of the yield strength of Ti-7 as discussed in Section 5.2.3.1.4) in the Ti-7 plates for realization 1 of the load by caved rock. The red color in the figure indicates the damaged area. *Structural Stability of a Drip Shield Under Quasi-Static Pressure* (BSC 2004 [DIRS 170791], Attachment IV) contains the damage plots for all 6 realizations and the damaged areas are summarized in Table 5-31.

Table 5-30. Vertical Deflections of the Top Plate Along the Vertical Symmetry Plane

Realization	Vertical Displacement (10^{-3} m)
1	4.4
2	-9.3
3	-8.2
4	23.1
5	13.1
6	3.9

Source: BSC 2004 [DIRS 170791], Table 2.

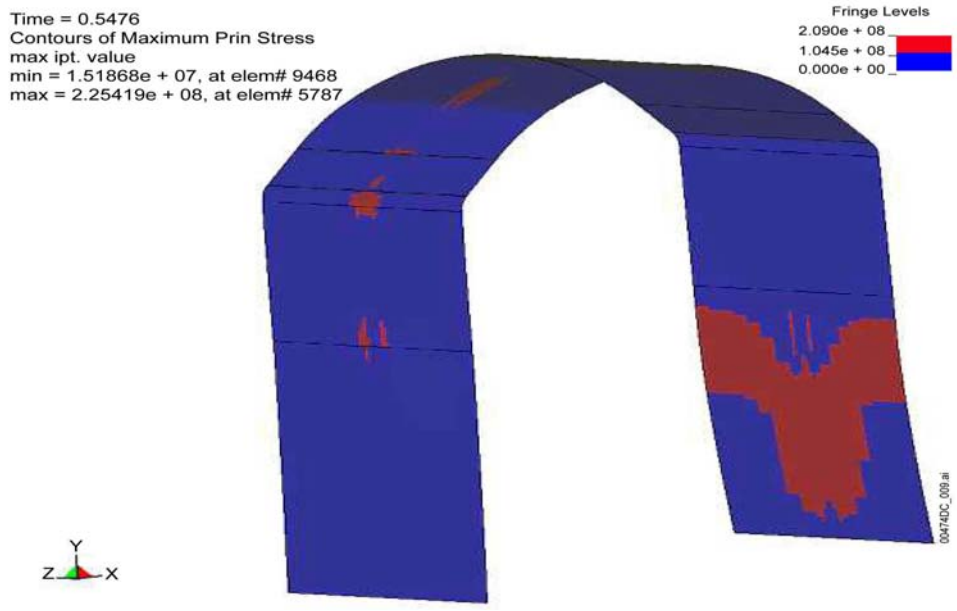

Source: BSC 2004 [DIRS 170791], Figure IV-1.

Figure 5-54. Damage Area of the Ti-7 Plates for Realization 1

Table 5-31. Damaged Area of the Drip Shield Top and Side Plates

Realization	Damaged Area (m2)	% of Total area
1	0.64	9%
2	0.90	12%
3	0.21	3%
4	2.42	32%
5	1.51	20%
6	1.10	15%

Source: BSC 2004 [DIRS 170791], Table 5.

Three additional simulations are performed for an average of all six realizations to examine the ultimate load-bearing capacity of the DS. As described previously, the loads for these simulations were derived from simulations in which the density of the caved rubble is increased to provide additional load application. Each segment of the quasi-static pressure distribution is averaged for the six realizations with the density of the surrounding rock multiplied by 2.5, 3.0, and 4.0. The pressure as a result of the density multiplication by 2.5 times does not result in the loss of the DS structural stability. On the other hand, the increase of the pressure values corresponding to the density multiplication by 4 times results in a severe deformation of the DS as illustrated by Figure 5-55. The average pressure on the top of the DS in the case of density multiplication by 4 times is 415.97 kPa (BSC 2004 [DIRS 170791], Table 3). Consequently, the average vertical load increased 3.25 times relative to the nominal case (i.e. the average pressure on the top of the drip shield of 127.86 kPa in Table 5-28). The shear stress contours (shown in Figure 5-56) and stress histories in 5 equally spaced points across the thickness of the section (shown in Figure 5-57) illustrate that most of the cross-section is deforming plastically (Ti-24 yields when the maximum shear stress exceeds $0.5\sigma_y$, which is 375 MPa), but there is still a portion of the cross-section deforming elastically (The stress histories show that material in 4 points in the cross-section yield; only at the point on the inner surface the stress is still elastic.). Even in this case the plastic hinge is not formed in the critically loaded section of the structure.

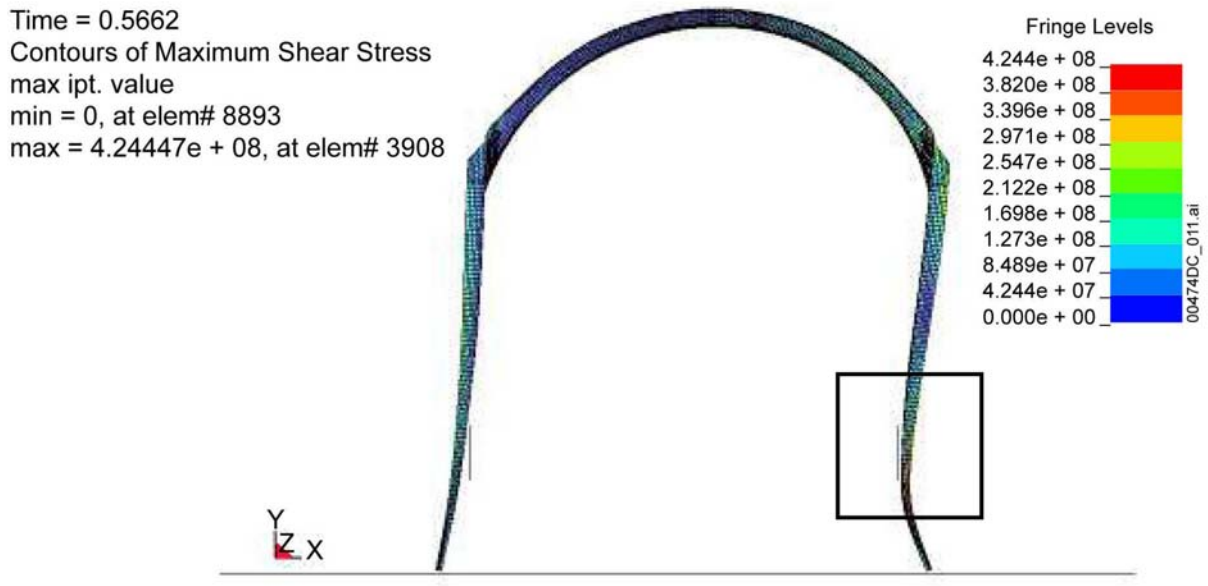

Source: BSC 2004 [DIRS 170791], Figure III-16.

NOTE: The indicated detail shown in Figure 5-37; Pa = Pascal.

Figure 5-55. Maximum Shear Stress Plot (Pa) for the Average of all Realizations with Density of Surrounding Rock Multiplied by 4.0

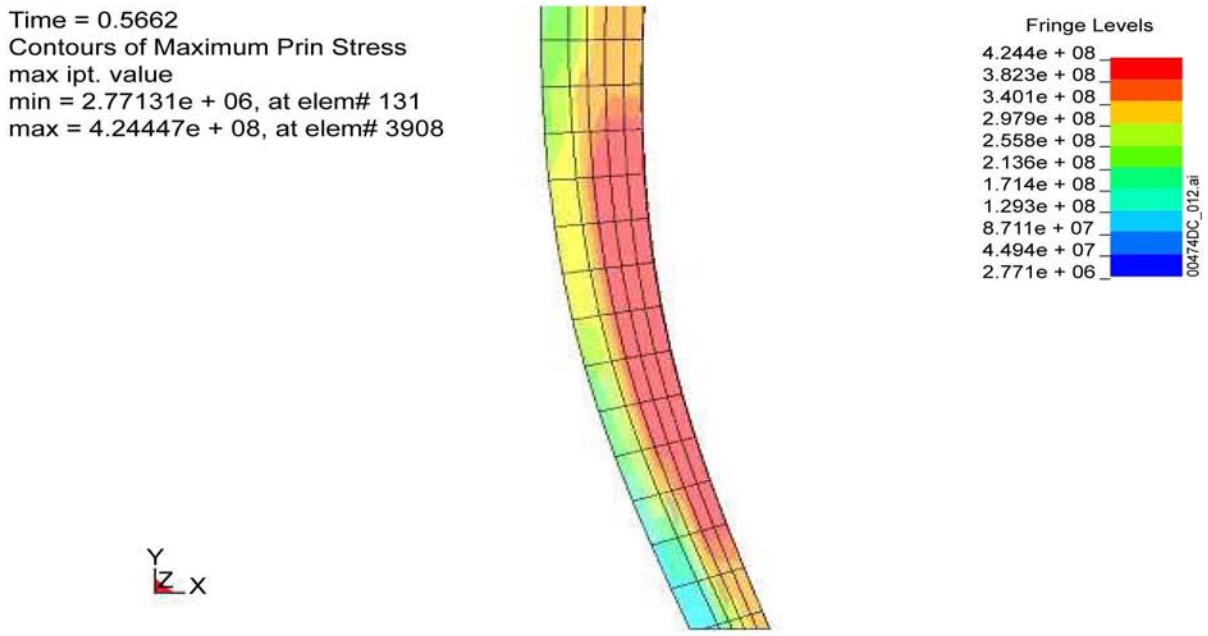

Source: BSC 2004 [DIRS 170791], Figure III-17.

NOTE: Pa = Pascal

Figure 5-56. Maximum Shear Stress Plot (Pa) of the Large Support Beam for the Average of All Realizations Density of Surrounding Rock Multiplied by 4.0

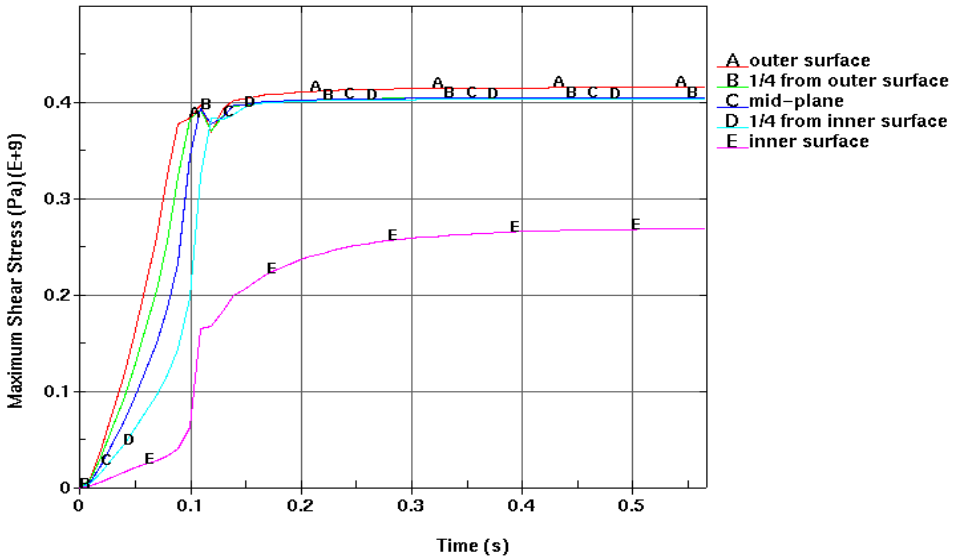

(a)

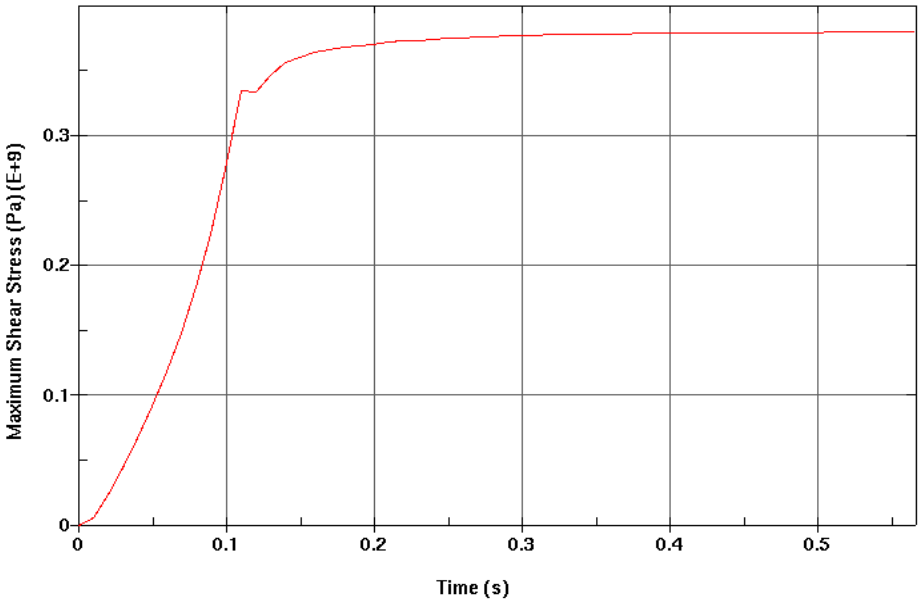

(b)

Source: BSC 2004 [DIRS 170791], Figure III-18.

NOTE: (a) Maximum shear stress at points through the cross-section and (b) average of the shear stress through the cross-section; Pa = Pascal

Figure 5-57. Maximum Shear Stress History Plots of the Large Support Beam for the Average of All Realizations with Density of Surrounding Rock Multiplied by 4.0

5.4.4 Use of Drip Shield Structural Analysis in the Seismic Scenario

5.4.4.1 Feeds of Drip Shield Structural Analysis to the Seismic Consequence Abstraction

The results of the DS calculations, in terms of damage from rockfall and vibratory motion, are used as direct input or corroborating data to the *Seismic Consequence Abstraction* (BSC 2004 [DIRS 169183]). The damage values, in terms of surface area of DS plates for a given value of PGV are supplied via the interface exchange drawing format used to communicate data from the Design and Engineering group to other functions. All DS damage data is presented in *D&E / PA/C IED Interlocking Drip Shield and Emplacement Pallet* (BSC 2004 [DIRS 169220]). The *Seismic Consequence Abstraction* provides the algorithms necessary for calculation of the mean dose consequence for the seismic scenario class of TSPA-LA. The primary output data supplied from the DS structural and damage analysis for direct and indirect input to the *Seismic Consequence Abstraction* is given in Table 5-32.

Table 5-32. References to Data for Structural Response of Drip Shield Used in Seismic Consequence

Input Information	Source
Damage to the Drip Shield from Vibratory Ground Motion:	
Damage to the drip shield due to impact by single rock blocks from the 2.44 m/s (10^{-6} per year) PGV level	BSC 2004 [DIRS 169220], Table 2
Damage to the drip shield due to impact by maximum rock block from the 5.35 m/s (10^{-7} per year) PGV level	BSC 2004 [DIRS 169220], Table 3
Damage to the drip shield for the single vibratory ground motion at the 0.190 m/s PGV level, corresponding to an annual exceedance frequency of 5×10^{-4} per year	BSC 2004 [DIRS 169220], Calculation Results I
Damage statistics for the area of the drip shield exceeding the residual stress threshold at 10^{-6} per year	BSC 2004 [DIRS 169220], Table 4
Damage statistics for the drip shield, based on a sampling of vibratory ground motions at the 5.35 m/s PGV level, corresponding to the 10^{-7} per year exceedance frequency	BSC 2004 [DIRS 169220], Calculation Results III

5.4.4.2 Review of Seismic Consequence Abstraction Feeds to TSPA-LA

The following discussion provides a summary of the ultimate feeds of DS damage from the *Seismic Consequence Abstraction* report (BSC 2004 [DIRS 169183]) to the TSPA-LA.

Damage from Rockfall Impact - In general, rockfall-related damage to the DS is considered to result in a network of stress corrosion cracks in those areas where the residual tensile stress exceeds the stress threshold for Titanium Grade 7. However, the resulting network of stress corrosion cracks are not considered to be a pathway for advective flow due to; a) infilling of narrow apertures with corrosion products, b) high surface tension when a narrow aperture is bridged by a single droplet, c) minimal head gradient or pressure gradient driving flow through narrow apertures with high tortuosity and surface roughness, and d) cracks on the DS are predicted to plug from evaporation-induced precipitation of calcite and other minerals over a few hundred years. In this situation, the DS remains intact as a long-term flow barrier after rockfall related damage. Rockfall related damage to the DS is therefore not included in the abstractions for the TSPA-LA in the seismic scenario class.

Stability from Static Load - Consideration is also given to potential DS failure due to buckling and collapse under static loads from rockfall induced by ground motion or time-dependent degradation of the emplacement drift. Structural response calculations provided in this document have demonstrated that the DS does not buckle or collapse under impact from the largest rock blocks and under the static rock load after catastrophic drift collapse. In this situation, damage to the DS from rockfall is again not included in the abstractions for the TSPA-LA.

Drip Shield Separation - Drip shield separation is excluded from TSPA-LA based on the results of the kinematic analysis presented in Section 5.3.3.1 of this document. To summarize:

- Analyses indicate that DS separation is highly unlikely, even in the case of an open drift subjected to low probability (1x10-6 and 1x10-7) ground motions and reasonable assumptions of DS to DS and DS to invert friction coefficients.

- Ground motion amplitudes that are sufficient to cause drip shield separation are also large enough to partially or completely collapse drifts in the repository.

- Rockfall occurs within the first second or two of the arrival of these large amplitude ground motion. In this situation, rockfall provides restraints on the motion of the drip shields, preventing differential motion that could lead to separation.

Even though the analyses indicate DS separation is highly unlikely in an open drift, the occurrence of drift degradation ensures that separation does not occur. Ground motion amplitudes near and above the 2.44 m/s PGV level are large enough to cause rockfall in both the lithophysal and nonlithophysal zones. In the lithophysal zones, drift collapse is observed at and above the 2 m/s PGV level (BSC 2004 [DIRS 166107], Section 6.4.2.2.2), and significant, but partial collapse occurs in nonlithophysal units (BSC 2004 [DIRS 166107], Section 6.3.1.6.4).

The collapse in the lithophysal rock is coincident with the arrival of the first strong ground motion – i.e., collapse occurs within seconds of the arrival of the first pulse of the accelerogram (BSC 2004 [DIRS 166107], Section 6.4.2.2.2). Large blocks also start to fall from the drift walls in the nonlithophysal zones shortly after the arrival of the ground motion (BSC 2004 [DIRS 166107], Section 6.3.1.6.1).

In either the lithophysal or nonlithophysal zones, rockfall occurs at PGV levels substantially lower than the 5.35 m/s PGV level characteristic of the $1x10^{-7}$ annual exceedance frequency. It follows that the drip shield is partly surrounded by rockfall whenever separation could potentially occur, and this rockfall can occur near the start of the ground motion. The larger rock blocks or the smaller rock fragments provide normal and shear confinement to the sidewalls and possibly the crown of the drip shield. The horizontal acceleration imparted to the drip shield by the ground motion will be resisted by the frictional forces between the rock and the drip shield plates and between the footings and the invert. Thus, the presence of rockfall around the drip shields will restrict the relative displacements that are required to separate adjacent drip shields, making separation very unlikely even for extreme ground motions.

It is important to note that smaller, more frequent seismic events will also provide rockfall around the drip shield. Smaller events are much more probable during a 10,000 year period. For a Poisson process, smaller seismic events with a rate of 10^{-5} per year are about 100 times more probable than extreme events with a rate of 10^{-7} per year. These smaller events can contribute to the buildup of rockfall around the drip shield before an extreme event occurs. For example, ground motions at the 1.5 m/s PGV level (near a 10^{-5} per year annual exceedance frequency) generate rockfall from partial collapse of the drifts in the lithophysal zones (BSC 2004 [DIRS 166107], Section 6.4.2.2.2). Since higher probability (e.g., 10^{-5}) events are much more likely than lower probability (e.g., 10^{-7}) events, it is reasonable to expect that significant rubble would exist in the drift and provide some confinement for the drip shield prior to the high amplitude, low probability ground motion that could result in drip shield separation.

5.5 CONCLUSIONS

The DS is a structure constructed of titanium designed to be placed over the waste package and the pallet when the repository is closed. The purpose of the DS is to protect the waste packages from: (a) water dripping directly from the drift crown and walls, and (b) direct impacts of loose, falling rock blocks. The adjacent DS's will partially overlap each other to provide continuous shielding of the waste packages. The functionality of the DS can be affected adversely if:

- The relative rigid body motion of the DS's creates a gap between them, exposing the waste package to direct water seepage or impacts from loose blocks.
- The DS loses structural integrity as a result of mechanical collapse or buckling.
- Impact damages the DS plates and provides necessary conditions for stress corrosion (the "damaged area" was defined conservatively in Section 5.2.3.1.4, as the area of the DS plate where the residual stress induced by impact exceeds 50 percent of the yield stress).

The mechanical loadings expected during the regulatory period that can affect the functionality of the DS are (a) seismic ground motion and (b) dynamic and static loads of loose blocks dislodged from the roof and walls of the emplacement drift. The causes for rockfall in the emplacement drifts can be both strong seismic ground motion and quasi-static stresses (due to in situ and thermal loads) combined with time-dependent strength degradation.

This report summarizes the results of calculations on the effects of these different loads on DS functionality as reported in *Structural Calculations of Drip Shield Exposed to Vibratory Ground Motion* (BSC 2003 [DIRS 163425]); *Drip Shield Structural Response to Rock Fall* (BSC 2004 [DIRS 168993]); and *Structural Stability of a Drip Shield Under Quasi-Static Pressure* (BSC 2004 [DIRS 170791]), and the results of the kinematic calculations which are reported in this document. The following bounding loading conditions were analyzed:

- Effect of vibratory ground motion (5×10^{-4}, 1×10^{-6} and 1×10^{-7} annual frequency of occurrence) on rigid body motion and damage of the DS, assuming that the emplacement drifts are open or filled with caved rock blocks inside the drifts (Section 5.3).

- Impact of the rock blocks shaken down in the nonlithophysal rock mass by seismic ground motions with 1×10^{-6} and 1×10^{-7} annual frequency of occurrence (Section 5.4.2).

- Static load on the DS by the rubble created by complete collapse of the emplacement drift (Section 5.4.3).

The results of the calculations indicate the following:

- The DS does not lose structural integrity or stability for any of the considered loads.

- The estimated factor-of-safety for DS under quasi-static load by the caved rock mass is approximately 3.2 (Section 5.4.3.2).

- Separation of the DS does not occur even for the strongest considered ground motion (1×10^{-7} annual frequency of occurrence) and for the conservative assumption that the drifts are not filled with caved rock blocks that act as obstacles to motion of the DSs (Section 5.3.3.1). The addition of the weight of caved rock resting on the DS or the frictional forces from caved rock in contact with the sides of the DS further resist separation during vibratory motion. All analyzed loads, except vibratory ground motion with 5×10^{-4} annual frequency of occurrence (Section 5.3.3.1), cause some degree of DS plates damage. Damage in the sense used here refers to denting of the surface and increased potential for development of regions of stress corrosion cracking. Tearing or piercing of the DS plates is not indicated. The maximum damaged area for vibratory ground motions with 1×10^{-6} annual frequency is 2.13 percent of the area of the DS plate for realization 9 (Table 5-22)[13]. The *Seismic Consequence Abstraction*, as discussed in Section 5.4.4.2, assumes that the DS damage occurs as stress corrosion cracks, which are not considered a pathway for advective flow and are thus screened out for consideration in the TSPA-LA.

- The maximum damaged area for the impact by loose rock blocks is 11.25 percent of the DS plate area for impact by an 11.5 MT block (the block with the greatest impact energy in Table 5-27).

- The maximum damaged area for the static load of the rock rubble is 32 percent of the DS plate area for realization 4 (Table 5-31).

The results are reasonable compared to the inputs and are suitable for the intended use.

[13]The damaged area is not reported for ground motions with 1×10^{-7} annual frequency of occurrence because only one of the numerical analyses converged without numerical instability.

5.6 YUCCA MOUNTAIN REVIEW PLAN ACCEPTANCE CRITERIA

The work described in this calculation addresses the *Yucca Mountain Review Plan* (NRC 2003 [DIRS 163274], Section 2.2.1.3.2) – Mechanical Disruption of Engineered Barriers. The following Acceptance Criteria were addressed:

Acceptance Criteria 1 – System Description and Model Integration

Subparts (1, 2, 3, 4 and 5) – The analyses incorporate important physical phenomena and couplings, including the effects of vibratory motion, rockfall and drift collapse on damage and structural stability of the drip shields. Environmental conditions including thermal and humidity effects are included in the analyses. The potential temperature impacts of rock rubble from drift collapse on drip shield material properties are included. The potential corrosion effects of drift humidity and the thinning of the drip shield structural components is accounted for in the analyses. Boundary and initial conditions to these analyses are consistent with the design of repository engineered barrier components and applied ground motion time histories. The input data and assumptions used in these analyses are consistent with other models and calculations. The assumptions and source documents are described in Section 3 – Assumptions as well as Section 5 - Calculation.

Acceptance Criteria 2 – Data are Sufficient for Model Justification

Subparts (1, 2, 3 and 4) – Input data and data assumptions are described in Section 3 – Assumptions. Justification of material properties of drip shield components and geologic data such as rockfall masses and rock rubble density are provided in Section 3. Failure models and material properties of the drip shield are described in 5.2.3 of this document.

Acceptance Criteria 3 – Data Uncertainty is Characterized and Propagated Through the Model Abstraction

Subparts (1, 2 and 3) – Data uncertainty is taken into account in these analyses in the following manner:

1) Input data in terms of ground motion time histories and contact friction angles are defined stochastically (Section 5.2.3 and 5.2.4)

2) Rockfall dynamic loading parameters have been defined from three-dimensional discontinuum analyses in which rock mass fracture geometries are stochastically-defined (Sections 5.2.5.2 and 5.4.2)

3) Rockfall static rubble loading is defined from a series of stochastic drift degradation models as described in Section 5.2.5.1 and 5.4.3.

Acceptance Criteria 4 – Model Uncertainty is Characterized and Propagated Through the Model Abstraction

Subparts (1, 2 and 3) – The analyses of drip shield structural response are consistent with available data and scientific understanding and limitations of the analyses are stated within

the document. Appropriate alternative models are used for analyses, including the use of discontinuum, kinematic approach as well as more sophisticated three-dimensional finite element analysis are used for examination of vibratory motion. Model uncertainties are propagated through damage estimates and structural stability calculations that provide input to the *Seismic Consequence Abstraction* (BSC 2004 [DIRS 169183]), which eventually provides input to the TSPA-LA.

INTENTIONALLY LEFT BLANK

6. REFERENCES

The following is a list of the references cited in this document. Column 2 represents the unique six digit numerical identifier (the Document Input Reference System number), which is placed in the text following the reference callout. The purpose of these numbers is to assist in locating a specific reference. Within the reference list, multiple sources by the same author are sorted alphabetically by title.

6.1 DOCUMENTS CITED

Avallone, E.A. and Baumeister, T., III, eds. 1987. *Marks' Standard Handbook for Mechanical Engineers.* 9th Edition. New York, New York: McGraw-Hill. TIC: 206891. 103508

Beer, F.P. and Johnston, E.R., Jr. 1977. *Vector Mechanics for Engineers, Statics.* 3rd Edition. New York, New York: McGraw-Hill Book Company. TIC: 247391. 145138

Belytschko, T.; Liu, W.K.; and Moran, B. 2000. *Nonlinear Finite Elements for Continua and Structures.* New York, New York: John Wiley & Sons. TIC: 248840. 153664

BSC (Bechtel SAIC Company) 2001. *Repository Multiple Waste Package Thermal Calculation.* CAL-WIS-TH-000010 REV 00. Las Vegas, Nevada: Bechtel SAIC Company. ACC: MOL.20010814.0330. 156276

BSC 2003. *Drop of Waste Package on Emplacement Pallet - A Mesh Study.* 000-00C-DSU0-02200-000-00A. Las Vegas, Nevada: Bechtel SAIC Company. ACC: ENG.20030915.0001. 165497

BSC 2003. *Emplacement Pallet.* 000-MW0-TEP0-00101-000-00A, and -00102-000-00A. 2 Sheets. Las Vegas, Nevada: Bechtel SAIC Company. ACC: ENG.20030205.0007; ENG.20030205.0008. 161520

BSC 2003. *Longevity of Emplacement Drift Ground Support Materials for LA.* 800-K0C-TEG0-01200-000-00A. Las Vegas, Nevada: Bechtel SAIC Company. ACC: ENG.20030922.0004. 165425

BSC 2003. *Structural Calculations of Drip Shield Exposed to Vibratory Ground Motion.* 000-00C-PEC0-00100-000-00A. Las Vegas, Nevada: Bechtel SAIC Company. ACC: ENG.20030618.0009. 163425

BSC 2003. *Repository Design, Drip Shield Envelope Dimensions.* 000-M00-PEC0-00102-000-00A. Las Vegas, Nevada: Bechtel SAIC Company. ACC: ENG.20030618.0002. 165038

BSC 2003. *Design and Engineering, Interlocking Drip Shield Configuration.* 000-M00-SSE0-00103-000-00A. Las Vegas, Nevada: Bechtel SAIC Company. ACC: ENG.20031028.0004. 166897

BSC 2004. *Aqueous Corrosion Rates for Waste Package Materials.* ANL-DSD-MD-000001 REV 01. Las Vegas, Nevada: Bechtel SAIC Company. ACC: DOC.20041012.0003. 169982

BSC 2004. *D&E / PA/C IED Interlocking Drip Shield and Emplacement Pallet.* 800-IED-WIS0-00401-000-00D. Las Vegas, Nevada: Bechtel SAIC Company. ACC: ENG.20040503.0018. 169220

BSC 2004. *Data Qualification and Data Summary Report: Intact Rock Properties Data on Poisson's Ratio and Young's Modulus.* TDR-MGR-GE-000004 REV 01 Errata 1. Las Vegas, Nevada: Bechtel SAIC Company. ACC: DOC.20040225.0001; DOC.20040419.0001. 170583

BSC 2004. *D&E/PA/C IED Typical Waste Package Components Assembly.* 800-IED-WIS0-00202-000-00C. Las Vegas, Nevada: Bechtel SAIC Company. ACC: ENG.20040517.0008. 169472

BSC 2004. *Design and Engineering, Interlocking Drip Shield Configuration.* 000-M00-SSE0-00101-000-00B. Las Vegas, Nevada: Bechtel SAIC Company. ACC: ENG.20040305.0020. 168275

BSC 2004. *Drift Cross Section Showing Emplaced Waste Package and Drip Shield.* 800-M00-WIS0-00101-000-00A. Las Vegas, Nevada: Bechtel SAIC Company. ACC: ENG.20040420.0013. 170074

BSC 2004. *Drift Degradation Analysis.* ANL-EBS-MD-000027 REV 02 with Errata 1. Las Vegas, Nevada: Bechtel SAIC Company. ACC: DOC.20040325.0002; DOC.20030709.0003. 168550

BSC 2004. *Drift Degradation Analysis.* ANL-EBS-MD-000027 REV 03. Las Vegas, Nevada: Bechtel SAIC Company. ACC: DOC.20040915.0010. 166107

BSC 2004. *Drip Shield Structural Response to Rock Fall.* 000-00C-SSE0-00300-000-00A. Las Vegas, Nevada: Bechtel SAIC Company. ACC: ENG.20040405.0019. 168993

BSC 2004. *Features, Events, and Processes: Disruptive Events.* ANL-WIS-MD-000005, Rev. 02. Las Vegas, Nevada: Bechtel SAIC Company. TBV: 6542. 170017

BSC 2004. *General Corrosion and Localized Corrosion of the Drip Shield.* ANL-EBS-MD-000004 REV 02. Las Vegas, Nevada: Bechtel SAIC Company. ACC: DOC.20040921.0002. 169845

BSC 2004. *Multiscale Thermohydrologic Model.* ANL-EBS-MD-000049, Rev. 02. Las Vegas, Nevada: Bechtel SAIC Company. TBV: 6552 169565

BSC 2004. *Peak Ground Velocities for Seismic Events at Yucca Mountain, Nevada.* ANL-MGR-GS-000004 REV 000A. Las Vegas, Nevada: Bechtel SAIC Company. ACC: TBV: 6278. 170137

BSC 2004. *Q-List.* 000-30R-MGR0-00500-000-000 REV 00. Las Vegas, Nevada: Bechtel SAIC Company. ACC: ENG.20040721.0007. 168361

BSC 2004. *Repository Subsurface Emplacement Drifts Steel Invert Structure Sect. & Committed Materials.* 800-SS0-SSE0-00102-000-00B. Las Vegas, Nevada: Bechtel SAIC Company. ACC: ENG.20040520.0005. 169776

BSC 2004. *Sampling of Stochastic Input Parameters for Rockfall Calculations and for Structural Response Calculations Under Vibratory Ground Motion.* ANL-EBS-PA-000009 REV 01. Las Vegas, Nevada: Bechtel SAIC Company. ACC: DOC.20040901.0004. 169999

BSC 2004. *Seismic Consequence Abstraction.* MDL-WIS-PA-000003 REV 01. Las Vegas, Nevada: Bechtel SAIC Company. ACC: DOC.20041025.0004. 169183

BSC 2004. *Stress Corrosion Cracking of the Drip Shield, the Waste Package Outer Barrier, and the Stainless Steel Structural Material.* ANL-EBS-MD-000005 REV 01 ICN 01. Las Vegas, Nevada: Bechtel SAIC Company. ACC: DOC.20040318.0010. 169042

BSC 2004. *Technical Work Plan for: Regulatory Integration Modeling of Drift Degradation, Waste Package and Drip Shield Vibratory Motion and Seismic Consequences.* TWP-MGR-GS-000003 REV 00 ICN 01. Las Vegas, Nevada: Bechtel SAIC Company. ACC: DOC.20040810.0003. 171520

BSC 2004. *Structural Stability of a Drip Shield under Quasi-Static Pressure.* 000-00C-SSE0-00500-000-00Aa. Las Vegas, Nevada: Bechtel SAIC Company. ACC: ENG.20040830.0032. 170791

Chen, W.F. 1982. Plasticity in Reinforced Concrete. New York, New York: McGraw-Hill Book Company. TIC: 240453. 159153

Cikanek, E.M.; Grant, T.A.; and Blakely, R.J. 2004. Data Qualification and Data Summary Report: Intact Rock Properties Data on Uniaxial Compressive Strength, Triaxial Compressive Strength, Friction Angle, and Cohesion, with Errata. TDR-MGR-GE-000003 REV 00 Errata 4. Las Vegas, Nevada: Bechtel SAIC Company. ACC: DOC.20030214.0007; DOC.20031007.0004; DOC.20031105.0007; DOC.20040506.0003; DOC.20040514.0003. 169642

DeGrassi, G. 1992. *Review of the Technical Basis and Verification of Current Analysis Methods Used to Predict Seismic Response of Spent Nuclear Fuel Racks.* NUREG/CR-5912. Washington, DC: U.S. Nuclear Regulatory Commission. TIC: 253724. 161539

Dieter, G.E. 1976. *Mechanical Metallurgy.* 2nd Edition. Materials Science and Engineering Series. New York, New York: McGraw-Hill Book Company. TIC: 247879. 118647

Fruchtbaum, J. 1988. "Handling Special Materials." *Bulk Materials Handling Handbook.* Pages 327-375. New York, New York: Van Nostrand Reinhold. TIC: 253872. 161774

Jaeger, J.C. and Cook, N.G.W. 1979. Fundamentals of Rock Mechanics. 3rd Edition. New York, New York: Chapman and Hall. TIC: 218325. 106219

Kramer, S.L. 1996. Geotechnical Earthquake Engineering. Prentice-Hall International Series in Civil Engineering and Engineering Mechanics. Hall, W.J., ed. Upper Saddle River, New Jersey: Prentice-Hall. TIC: 243891 103337

Marachi, N.D., C.K. Chan and H.B. Seed (1972) "*Evaluation of properties of rockfill materials*", *Journal of the Soil Mechanics and Foundations Division, Proceedings of the American Society of Civil Engineers*, 98, (SM1), 95-114. New York, New York: American Society of Civil Engineers. TIC: 252235. 157883

Mecham, D.C., ed. 2004. *Waste Package Component Design Methodology Report.* 000-30R-WIS0-00100-000-002. Las Vegas, Nevada: Bechtel SAIC Company. ACC: ENG.20040713.0003. 170673

Nicholas, T. 1980. *Dynamic Tensile Testing of Structural Materials Using A Split Hopkinson Bar Apparatus.* AFWAL-TR-80-4053. Wright-Patterson Air Force Base, Ohio: Air Force Wright Aeronautical Laboratories. TIC: 249469. 154072

Sowers, G.F. 1979. Introductory Soil Mechanics and Foundations: Geotechnical Engineering. Fourth Edition. MacMillan: New York. TIC: 245527. 107479

TIMET. 1993. First in Titanium Worldwide, Quality Products and Services. Denver, Colorado: [Titanium Metals Corporation]. TIC: 242692. 157726

TIMET. 2000. "Timetal 6-4, 6-4 ELI, 6-4-.1Ru Medium to High Strength General-Purpose Alloys." Denver, Colorado: Titanium Metals Corporation. Accessed August 26, 2002. TIC: 253102. http://www.timet.com/pdfs/6-4.pdf 160688

Williams, N.H. 2002. "Thermal Inputs for Evaluations Supporting TSPA-LA." Interoffice memorandum from N.H. Williams (BSC) to Distribution, September 16, 2002, 0911024159, with enclosures. ACC: MOL.20021008.0141. 159916

6.2 CODES, STANDARDS, REGULATIONS, AND PROCEDURES

ASM (American Society for Metals) 1980. *Properties and Selection: Stainless Steels, Tool Materials and Special-Purpose Metals.* Volume 3 of *Metals Handbook.* 9th Edition. Benjamin, D., ed. Metals Park, Ohio: ASMs. TIC: 2 09801. 104317

ASM International. 1990. *Properties and Selection: Nonferrous Alloys and Special-Purpose Materials.* Volume 2 of *ASM Handbook.* Formerly Tenth Edition, Metals Handbook. 5th Printing 1998. Materials Park, Ohio: ASM International. TIC: 241059. 141615

ASME (American Society of Mechanical Engineers) 2001. *2001 ASME Boiler and Pressure Vessel Code (includes 2002 addenda).* New York, New York: American Society of Mechanical Engineers. TIC: 251425. 158115

DOE (U.S. Department of Energy) 2004. *Quality Assurance Requirements and Description.* DOE/RW-0333P, Rev. 16. Washington, D.C.: U.S. Department of Energy, Office of Civilian Radioactive Waste Management. ACC: DOC.20040907.0002. 171539

NRC (U.S. Nuclear Regulatory Commission) 2003. *Yucca Mountain Review Plan, Final Report.* NUREG-1804, Rev. 2. Washington, D.C.: U.S. Nuclear Regulatory Commission, Office of Nuclear Material Safety and Safeguards. TIC: 254568. 163274

AP-3.12Q, Rev. 2, ICN 2. *Design Calculations and Analyses*. Washington, D.C.: U.S. Department of Energy, Office of Civilian Radioactive Waste Management. ACC: DOC.20040318.0002.

LP-SI.11Q-BSC, Rev. 0 ICN1. *Software Management*. Washington, D.C.: U.S. Department of Energy, Office of Civilian Radioactive Waste Management. ACC: DOC.20041005.0008.

6.3 SOURCE DATA, LISTED BY DATA TRACKING NUMBER

MO0003RIB00073.000. Physical and Chemical Characteristics of TI Grades 7 and 16. Submittal date: 03/13/2000. 152926

MO0301MWD3DE27.003. Results from 3DEC Nonlithophysal Rockfall Analyses with 10^{-7} Ground Motion Level. Submittal date: 01/23/2003. 161536

MO0301SPASIP27.004. Sampling of Stochastic Input Parameters for Rockfall Calculations and for Structural Response Calculations Under Vibratory Ground Motions. Submittal date: 01/15/2003. 161869

MO0303SPARESST.000. Residual Stress Failure Criteria for Seismic Damage Models of the Drip Shield and Waste Package. Submittal date: 03/04/2003. 162030

MO0305MWDNLRKF.001. Results from 3DEC Nonlithophysal Rockfall Analyses with 10-6 Ground Motion Level. Submittal date: 05/27/2003. 163438

MO0311RCKPRPCS.003. Intact Rock Properties Data on Uniaxial and Triaxial Compressive Strength. Submittal date: 11/04/2003. 166073

MO402DQRIRPPR.003. Intact Rock Properties Data on Poisson's Ratio and Young's Modulus. Submittal date: 02/19/2004. 168901

MO0407MWDDDDSLCR.000. Drip Shield Load in Collapsed Lithophysal Rock. Submittal date: 07/21/2004. 170873

MO0408MWDGLCDS.002. General Corrosion and Localized Corrosion of the Drip Shield for LA. Submittal date: 08/27/2004. 171486

SNL02030193001.027. Summary of Bulk Property Measurements Including Saturated Bulk Density for NRG-2, NRG-2A, NRG-2B, NRG-3, NRG-4, NRG-5, NRG-6, NRG-7/7A, SD-9, and SD12. Submittal date: 08/14/1996. 108410

6.4 SOFTWARE CODES

BSC 2002. *Software Code: ANSYS.* V5.6.2. HP-UX 11.00. 10364-5.6.2-01. 159357

BSC 2002. *Software Code: LS-DYNA.* V960.1106. HP9000. 10300-960.1106-00. 158898

BSC 2002. *Software Code: UDEC.* V3.1. PC WINDOWS 2000/NT 4.0. 10173-3.1-00. 161949

BSC 2002. *Software Definition Report for UDEC V3.1.* Document Number: 10173-SDR-3.1-00. Las Vegas, Nevada: Bechtel SAIC Company. ACC: MOL.20021105.0244. 171617

BSC 2002. *LS-DYNA Version 960.1106 Validation Test Report.* Software Baseline Documentation Number: 10300-VTR-960.1106-00. Las Vegas, Nevada: Bechtel SAIC Company. ACC: MOL.20020515.1915. 168545

BSC 2003. *Software Code: LS-DYNA.* V.970.3858 D MPP. HP Itanium2, HP-UX 11.22. 10300-970.3858 D MPP-00. 166918

DOE (U.S. Department of Energy) 2003. *Validation Test Report for LS-DYNA Version 970.3858 D MPP*. 10300-VTR-970.3858 D MPP-00. Las Vegas, Nevada: U.S. Department of Energy, Office of Repository Development. ACC: MOL.20031218.0337. 168558

Hallquist, J.O. 1998. *LS-DYNA, Theoretical Manual.* Livermore, California: Livermore Software Technology Corporation. TIC: 238997. 155373

Itasca Consulting Group. 2002. *Itasca Software–Cutting Edge Tools for Computational Mechanics.* Minneapolis, Minnesota: Itasca Consulting Group. TIC: 252592. 160331

Livermore Software Technology Corporation. 2001. *LS-DYNA Keyword User's Manual.* Version 960. Two volumes. Livermore, California: Livermore Software Technology Corporation. TIC: 252119. 159166

Livermore Software Technology Corporation. 2003. *LS-DYNA Keyword User's Manual.* Version 970. Livermore, California: Livermore Software Technology Corporation. TIC: 254203. 166841

INTENTIONALLY LEFT BLANK

7. DESCRIPTION OF ATTACHMENT A

The following Attachment A consists of 1 compact disc of UDEC V3.1 electronic files of the kinematic analyses summarized in Table 5-19. The naming convention used for the files is given in Section 4. Table 7-1 provides a list of the files submitted on the compact disc as the Attachment.

Table 7-1. List of Electronic Files in Attachment

Name	Date	Time	Size (Byte)
Folder Case 1-4			
1e-6h1_10.vel	2/16/2004	09:45a	34,000
1e-6h1_11.vel	2/16/2004	09:45a	140,080
1e-6h1_1.vel	2/16/2004	09:45a	140,080
1e-6h1_12.vel	2/16/2004	09:45a	68,000
1e-6h1_13.vel	2/16/2004	09:45a	271,692
1e-6h1_14.vel	2/16/2004	09:46a	272,000
1e-6h1_16.vel	2/16/2004	09:46a	108,800
1e-6h1_2.vel	2/16/2004	09:46a	140,080
1e-6h1_3.vel	2/16/2004	09:46a	68,000
1e-6h1_4.vel	2/16/2004	09:46a	88,808
1e-6h1_5.vel	2/16/2004	09:46a	68,000
1e-6h1_6.vel	2/16/2004	09:46a	68,000
1e-6h1_7.vel	2/16/2004	09:46a	110,602
1e-6h1_8.vel	2/16/2004	09:46a	140,080
1e-6h1_9.vel	2/16/2004	09:46a	203,864
1e-6h2_1.vel	2/16/2004	09:46a	140,080
1e-6h2_10.vel	2/16/2004	09:46a	34,000
1e-6h2_11.vel	2/16/2004	09:46a	140,080
1e-6h2_12.vel	2/16/2004	09:46a	68,000
1e-6h2_13.vel	2/16/2004	09:46a	271,692
1e-6h2_14.vel	2/16/2004	09:46a	272,000
1e-6h2_16.vel	2/16/2004	09:46a	108,800
1e-6h2_2.vel	2/16/2004	09:47a	140,080
1e-6h2_3.vel	2/16/2004	09:47a	68,000
1e-6h2_4.vel	2/16/2004	09:47a	88,812
1e-6h2_5.vel	2/16/2004	09:47a	68,000
1e-6h2_6.vel	2/16/2004	09:47a	68,000
1e-6h2_7.vel	2/16/2004	09:47a	110,602
1e-6h2_8.vel	2/16/2004	09:47a	140,080
1e-6h2_9.vel	2/16/2004	09:47a	203,862
1e-6up_1.vel	2/16/2004	09:47a	140,080
1e-6up_10.vel	2/16/2004	09:47a	34,000
1e-6up_11.vel	2/16/2004	09:47a	140,080
1e-6up_12.vel	2/16/2004	09:47a	68,000

Table 7-1 List of Electronic Files in Attachment (Continued)

Name	Date	Time	Size (Byte)
1e-6up_13.vel	2/16/2004	09:47a	271,694
1e-6up_14.vel	2/16/2004	09:47a	272,000
1e-6up_16.vel	2/16/2004	09:47a	108,800
1e-6up_2.vel	2/16/2004	09:47a	140,080
1e-6up_3.vel	2/16/2004	09:47a	68,000
1e-6up_4.vel	2/16/2004	09:47a	88,806
1e-6up_5.vel	2/16/2004	09:47a	68,000
1e-6up_6.vel	2/16/2004	09:47a	68,000
1e-6up_7.vel	2/16/2004	09:48a	110,602
1e-6up_8.vel	2/16/2004	09:48a	140,080
1e-6up_9.vel	2/16/2004	09:48a	203,862
Bb.fin	10/11/1996	09:50a	2,142
Block.fin	1/24/2000	08:59a	5,768
Boucnr.fin	11/3/1999	06:01a	2,292
Cable.fin	11/3/1999	05:54a	2,323
Case1property1motion1step7.sav	8/30/2004	01:16p	15,318,919
Case2property1motion10step8.sav	8/30/2004	04:18p	19,355,043
Case3property1motion10step8.sav	8/31/2004	12:20a	19,355,043
Case4property1motion10step8.sav	8/31/2004	03:21a	19,355,823
Contact.fin	11/23/1999	05:27a	3,622
Domain.fin	11/23/1999	05:28a	1,756
geom.sav	10/5/2004	06:55a	389,555
hist1.pcx	10/5/2004	06:50a	47,301
hist2.pcx	10/5/2004	06:50a	56,427
hist3.pcx	10/5/2004	06:50a	52,448
hist4.pcx	10/5/2004	06:50a	56,940
Jmat.fin	11/3/1999	06:22a	4,334
matnumb.pcx	9/2/2004	08:56a	22,821
model.dat	8/30/2004	10:36a	5,555
model1.dat	9/2/2004	08:51a	5,560
plot.dat	9/2/2004	12:39p	437
Reinf.fin	11/3/1999	05:58a	1,612
setup.fis	8/30/2004	10:34a	10,870
Str.fin	1/24/2000	09:08a	4,290
Support.fin	11/23/1999	05:29a	1,674
test.dat	8/9/2004	02:07p	330
times.fis	2/16/2004	09:48a	1,053
udec.lnk	8/30/2004	10:35a	411
Zmat.fin	11/3/1999	06:12a	3,971
Folder Case 11-14			
1e-7h1_10.vel	11/7/2002	03:44p	33,000
1e-7h1_1.vel	11/7/2002	03:44p	135,960
1e-7h1_11.vel	11/7/2002	03:44p	135,960
1e-7h1_12.vel	11/7/2002	03:44p	66,000

Table 7-1 List of Electronic Files in Attachment (Continued)

Name	Date	Time	Size (Byte)
1e-7h1_13.vel	11/7/2002	03:44p	263,703
1e-7h1_14.vel	11/7/2002	03:44p	264,000
1e-7h1_15.vel	11/7/2002	03:44p	198,033
1e-7h1_16.vel	11/7/2002	03:44p	105,600
1e-7h1_17.vel	11/7/2002	03:44p	198,000
1e-7h1_2.vel	11/7/2002	03:44p	135,960
1e-7h1_3.vel	11/7/2002	03:44p	66,000
1e-7h1_4.vel	11/7/2002	03:44p	86,196
1e-7h1_5.vel	11/7/2002	03:44p	66,000
1e-7h1_6.vel	11/7/2002	03:44p	66,000
1e-7h1_7.vel	11/7/2002	03:44p	107,349
1e-7h1_8.vel	11/7/2002	03:44p	135,960
1e-7h1_9.vel	11/7/2002	03:44p	197,868
1e-7h2_1.vel	11/7/2002	03:50p	135,960
1e-7h2_10.vel	11/7/2002	03:50p	33,000
1e-7h2_11.vel	11/7/2002	03:50p	135,960
1e-7h2_12.vel	11/7/2002	03:50p	66,000
1e-7h2_13.vel	11/7/2002	03:50p	263,703
1e-7h2_14.vel	11/7/2002	03:50p	264,000
1e-7h2_15.vel	11/7/2002	03:50p	198,033
1e-7h2_16.vel	11/7/2002	03:50p	105,600
1e-7h2_17.vel	11/7/2002	03:50p	198,000
1e-7h2_2.vel	11/7/2002	03:50p	135,960
1e-7h2_3.vel	11/7/2002	03:50p	66,000
1e-7h2_4.vel	11/7/2002	03:50p	86,196
1e-7h2_5.vel	3/25/2004	01:34p	68,000
1e-7h2_6.vel	11/7/2002	03:50p	66,000
1e-7h2_7.vel	11/7/2002	03:50p	107,349
1e-7h2_8.vel	11/7/2002	03:50p	135,960
1e-7h2_9.vel	11/7/2002	03:50p	197,868
1e-7up_1.vel	11/7/2002	03:50p	135,960
1e-7up_10.vel	11/7/2002	03:50p	33,000
1e-7up_11.vel	11/7/2002	03:50p	135,960
1e-7up_12.vel	11/7/2002	03:50p	66,000
1e-7up_13.vel	11/7/2002	03:50p	263,703
1e-7up_14.vel	11/7/2002	03:50p	264,000
1e-7up_15.vel	11/7/2002	03:50p	198,033
1e-7up_16.vel	11/7/2002	03:50p	105,600
1e-7up_17.vel	11/7/2002	03:50p	198,000
1e-7up_2.vel	11/7/2002	03:50p	135,960
1e-7up_3.vel	11/7/2002	03:50p	66,000
1e-7up_4.vel	11/7/2002	03:50p	86,196
1e-7up_5.vel	11/7/2002	03:50p	66,000
1e-7up_6.vel	11/7/2002	03:50p	66,000

Table 7-1 List of Electronic Files in Attachment (Continued)

Name	Date	Time	Size (Byte)
1e-7up_7.vel	11/7/2002	03:50p	107,349
1e-7up_8.vel	11/7/2002	03:50p	135,960
1e-7up_9.vel	11/7/2002	03:50p	197,868
Bb.fin	10/11/1996	09:50a	2,142
Block.fin	1/24/2000	08:59a	5,768
Boucnr.fin	11/3/1999	06:01a	2,292
Cable.fin	11/3/1999	05:54a	2,323
Case11property1motion10step8.sav	8/30/2004	02:10p	19,350,915
Case12property1motion10step8.sav	8/30/2004	12:22p	19,349,347
Case13property1motion10step8.sav	8/30/2004	03:29p	19,347,299
Case14property1motion10step8.sav	8/30/2004	11:53p	19,360,175
Contact.fin	11/23/1999	05:27a	3,622
Domain.fin	11/23/1999	05:28a	1,756
geom.sav	10/5/2004	07:28a	271,979
Jmat.fin	11/3/1999	06:22a	4,334
model.dat	8/20/2004	12:37p	6,810
plot.dat	9/2/2004	12:39p	437
Reinf.fin	11/3/1999	05:58a	1,612
setup.fis	8/30/2004	10:49a	11,507
Str.fin	1/24/2000	09:08a	4,290
Support.fin	11/23/1999	05:29a	1,674
times.fis	3/25/2004	01:46p	1,004
udec.lnk	8/30/2004	10:57a	615
Zmat.fin	11/3/1999	06:12a	3,971
Folder Case 15, 16, 18			
1e-7h1_10.vel	11/7/2002	03:44p	33,000
1e-7h1_1.vel	11/7/2002	03:44p	135,960
1e-7h1_11.vel	11/7/2002	03:44p	135,960
1e-7h1_12.vel	11/7/2002	03:44p	66,000
1e-7h1_13.vel	11/7/2002	03:44p	263,703
1e-7h1_14.vel	11/7/2002	03:44p	264,000
1e-7h1_15.vel	11/7/2002	03:44p	198,033
1e-7h1_16.vel	11/7/2002	03:44p	105,600
1e-7h1_17.vel	11/7/2002	03:44p	198,000
1e-7h1_2.vel	11/7/2002	03:44p	135,960
1e-7h1_3.vel	11/7/2002	03:44p	66,000
1e-7h1_4.vel	11/7/2002	03:44p	86,196
1e-7h1_5.vel	11/7/2002	03:44p	66,000
1e-7h1_6.vel	11/7/2002	03:44p	66,000
1e-7h1_7.vel	11/7/2002	03:44p	107,349
1e-7h1_8.vel	11/7/2002	03:44p	135,960
1e-7h1_9.vel	11/7/2002	03:44p	197,868
1e-7h2_1.vel	11/7/2002	03:50p	135,960
1e-7h2_10.vel	11/7/2002	03:50p	33,000

Table 7-1 List of Electronic Files in Attachment (Continued)

Name	Date	Time	Size (Byte)
1e-7h2_11.vel	11/7/2002	03:50p	135,960
1e-7h2_12.vel	11/7/2002	03:50p	66,000
1e-7h2_13.vel	11/7/2002	03:50p	263,703
1e-7h2_14.vel	11/7/2002	03:50p	264,000
1e-7h2_15.vel	11/7/2002	03:50p	198,033
1e-7h2_16.vel	11/7/2002	03:50p	105,600
1e-7h2_17.vel	11/7/2002	03:50p	198,000
1e-7h2_2.vel	11/7/2002	03:50p	135,960
1e-7h2_3.vel	11/7/2002	03:50p	66,000
1e-7h2_4.vel	11/7/2002	03:50p	86,196
1e-7h2_5.vel	3/25/2004	01:34p	68,000
1e-7h2_6.vel	11/7/2002	03:50p	66,000
1e-7h2_7.vel	11/7/2002	03:50p	107,349
1e-7h2_8.vel	11/7/2002	03:50p	135,960
1e-7h2_9.vel	11/7/2002	03:50p	197,868
1e-7up_1.vel	11/7/2002	03:50p	135,960
1e-7up_10.vel	11/7/2002	03:50p	33,000
1e-7up_11.vel	11/7/2002	03:50p	135,960
1e-7up_12.vel	11/7/2002	03:50p	66,000
1e-7up_13.vel	11/7/2002	03:50p	263,703
1e-7up_14.vel	11/7/2002	03:50p	264,000
1e-7up_15.vel	11/7/2002	03:50p	198,033
1e-7up_16.vel	11/7/2002	03:50p	105,600
1e-7up_17.vel	11/7/2002	03:50p	198,000
1e-7up_2.vel	11/7/2002	03:50p	135,960
1e-7up_3.vel	11/7/2002	03:50p	66,000
1e-7up_4.vel	11/7/2002	03:50p	86,196
1e-7up_5.vel	11/7/2002	03:50p	66,000
1e-7up_6.vel	11/7/2002	03:50p	66,000
1e-7up_7.vel	11/7/2002	03:50p	107,349
1e-7up_8.vel	11/7/2002	03:50p	135,960
1e-7up_9.vel	11/7/2002	03:50p	197,868
Bb.fin	10/11/1996	09:50a	2,142
Block.fin	1/24/2000	08:59a	5,768
Boucnr.fin	11/3/1999	06:01a	2,292
Cable.fin	11/3/1999	05:54a	2,323
Case15property1motion1step7.sav	8/30/2004	04:00p	15,321,071
Case16property1motion1step7.sav	8/31/2004	07:16a	15,320,183
Case18property1motion1step7.sav	9/1/2004	04:48a	16,986,219
Contact.fin	11/23/1999	05:27a	3,622
Domain.fin	11/23/1999	05:28a	1,756
Jmat.fin	11/3/1999	06:22a	4,334
model.dat	10/5/2004	07:33a	4,169
model1.dat	10/5/2004	07:26a	6,815

Table 7-1 List of Electronic Files in Attachment (Continued)

Name	Date	Time	Size (Byte)
plot.dat	9/2/2004	12:39p	437
Reinf.fin	11/3/1999	05:58a	1,612
setup.fis	8/30/2004	10:24a	10,872
Str.fin	1/24/2000	09:08a	4,290
Support.fin	11/23/1999	05:29a	1,674
test.dat	8/9/2004	02:07p	330
times.fis	3/25/2004	01:46p	1,004
udec.lnk	9/2/2004	12:25p	711
Zmat.fin	11/3/1999	06:12a	3,971
Folder Case 17			
1e-7h1_10.vel	11/7/2002	03:44p	33,000
1e-7h1_1.vel	11/7/2002	03:44p	135,960
1e-7h1_11.vel	11/7/2002	03:44p	135,960
1e-7h1_12.vel	11/7/2002	03:44p	66,000
1e-7h1_13.vel	11/7/2002	03:44p	263,703
1e-7h1_14.vel	11/7/2002	03:44p	264,000
1e-7h1_15.vel	11/7/2002	03:44p	198,033
1e-7h1_16.vel	11/7/2002	03:44p	105,600
1e-7h1_17.vel	11/7/2002	03:44p	198,000
1e-7h1_2.vel	11/7/2002	03:44p	135,960
1e-7h1_3.vel	11/7/2002	03:44p	66,000
1e-7h1_4.vel	11/7/2002	03:44p	86,196
1e-7h1_5.vel	11/7/2002	03:44p	66,000
1e-7h1_6.vel	11/7/2002	03:44p	66,000
1e-7h1_7.vel	11/7/2002	03:44p	107,349
1e-7h1_8.vel	11/7/2002	03:44p	135,960
1e-7h1_9.vel	11/7/2002	03:44p	197,868
1e-7h2_1.vel	11/7/2002	03:50p	135,960
1e-7h2_10.vel	11/7/2002	03:50p	33,000
1e-7h2_11.vel	11/7/2002	03:50p	135,960
1e-7h2_12.vel	11/7/2002	03:50p	66,000
1e-7h2_13.vel	11/7/2002	03:50p	263,703
1e-7h2_14.vel	11/7/2002	03:50p	264,000
1e-7h2_15.vel	11/7/2002	03:50p	198,033
1e-7h2_16.vel	11/7/2002	03:50p	105,600
1e-7h2_17.vel	11/7/2002	03:50p	198,000
1e-7h2_2.vel	11/7/2002	03:50p	135,960
1e-7h2_3.vel	11/7/2002	03:50p	66,000
1e-7h2_4.vel	11/7/2002	03:50p	86,196
1e-7h2_5.vel	3/25/2004	01:34p	68,000
1e-7h2_6.vel	11/7/2002	03:50p	66,000
1e-7h2_7.vel	11/7/2002	03:50p	107,349
1e-7h2_8.vel	11/7/2002	03:50p	135,960
1e-7h2_9.vel	11/7/2002	03:50p	197,868

Table 7-1 List of Electronic Files in Attachment (Continued)

Name	Date	Time	Size (Byte)
1e-7up_1.vel	11/7/2002	03:50p	135,960
1e-7up_10.vel	11/7/2002	03:50p	33,000
1e-7up_11.vel	11/7/2002	03:50p	135,960
1e-7up_12.vel	11/7/2002	03:50p	66,000
1e-7up_13.vel	11/7/2002	03:50p	263,703
1e-7up_14.vel	11/7/2002	03:50p	264,000
1e-7up_15.vel	11/7/2002	03:50p	198,033
1e-7up_16.vel	11/7/2002	03:50p	105,600
1e-7up_17.vel	11/7/2002	03:50p	198,000
1e-7up_2.vel	11/7/2002	03:50p	135,960
1e-7up_3.vel	11/7/2002	03:50p	66,000
1e-7up_4.vel	11/7/2002	03:50p	86,196
1e-7up_5.vel	11/7/2002	03:50p	66,000
1e-7up_6.vel	11/7/2002	03:50p	66,000
1e-7up_7.vel	11/7/2002	03:50p	107,349
1e-7up_8.vel	11/7/2002	03:50p	135,960
1e-7up_9.vel	11/7/2002	03:50p	197,868
Bb.fin	10/11/1996	09:50a	2,142
Block.fin	1/24/2000	08:59a	5,768
Boucnr.fin	11/3/1999	06:01a	2,292
Cable.fin	11/3/1999	05:54a	2,323
Case17property1motion1step7.sav	9/10/2004	01:32p	15,323,823
Contact.fin	11/23/1999	05:27a	3,622
Domain.fin	11/23/1999	05:28a	1,756
Jmat.fin	11/3/1999	06:22a	4,334
model.dat	10/5/2004	07:37a	2,788
plot.dat	9/2/2004	12:39p	437
Reinf.fin	11/3/1999	05:58a	1,612
setup.fis	8/30/2004	10:24a	10,872
Str.fin	1/24/2000	09:08a	4,290
Support.fin	11/23/1999	05:29a	1,674
test.dat	8/9/2004	02:07p	330
times.fis	3/25/2004	01:46p	1,004
udec.lnk	9/2/2004	12:25p	711
Zmat.fin	11/3/1999	06:12a	3,971
Folder Case 19			
1e-7h1_10.vel	11/7/2002	03:44p	33,000
1e-7h1_1.vel	11/7/2002	03:44p	135,960
1e-7h1_11.vel	11/7/2002	03:44p	135,960
1e-7h1_12.vel	11/7/2002	03:44p	66,000
1e-7h1_13.vel	11/7/2002	03:44p	263,703
1e-7h1_14.vel	11/7/2002	03:44p	264,000
1e-7h1_15.vel	11/7/2002	03:44p	198,033
1e-7h1_16.vel	11/7/2002	03:44p	105,600

Table 7-1 List of Electronic Files in Attachment (Continued)

Name	Date	Time	Size (Byte)
1e-7h1_17.vel	11/7/2002	03:44p	198,000
1e-7h1_2.vel	11/7/2002	03:44p	135,960
1e-7h1_3.vel	11/7/2002	03:44p	66,000
1e-7h1_4.vel	11/7/2002	03:44p	86,196
1e-7h1_5.vel	11/7/2002	03:44p	66,000
1e-7h1_6.vel	11/7/2002	03:44p	66,000
1e-7h1_7.vel	11/7/2002	03:44p	107,349
1e-7h1_8.vel	11/7/2002	03:44p	135,960
1e-7h1_9.vel	11/7/2002	03:44p	197,868
1e-7h2_1.vel	11/7/2002	03:50p	135,960
1e-7h2_10.vel	11/7/2002	03:50p	33,000
1e-7h2_11.vel	11/7/2002	03:50p	135,960
1e-7h2_12.vel	11/7/2002	03:50p	66,000
1e-7h2_13.vel	11/7/2002	03:50p	263,703
1e-7h2_14.vel	11/7/2002	03:50p	264,000
1e-7h2_15.vel	11/7/2002	03:50p	198,033
1e-7h2_16.vel	11/7/2002	03:50p	105,600
1e-7h2_17.vel	11/7/2002	03:50p	198,000
1e-7h2_2.vel	11/7/2002	03:50p	135,960
1e-7h2_3.vel	11/7/2002	03:50p	66,000
1e-7h2_4.vel	11/7/2002	03:50p	86,196
1e-7h2_5.vel	3/25/2004	01:34p	68,000
1e-7h2_6.vel	11/7/2002	03:50p	66,000
1e-7h2_7.vel	11/7/2002	03:50p	107,349
1e-7h2_8.vel	11/7/2002	03:50p	135,960
1e-7h2_9.vel	11/7/2002	03:50p	197,868
1e-7up_1.vel	11/7/2002	03:50p	135,960
1e-7up_10.vel	11/7/2002	03:50p	33,000
1e-7up_11.vel	11/7/2002	03:50p	135,960
1e-7up_12.vel	11/7/2002	03:50p	66,000
1e-7up_13.vel	11/7/2002	03:50p	263,703
1e-7up_14.vel	11/7/2002	03:50p	264,000
1e-7up_15.vel	11/7/2002	03:50p	198,033
1e-7up_16.vel	11/7/2002	03:50p	105,600
1e-7up_17.vel	11/7/2002	03:50p	198,000
1e-7up_2.vel	11/7/2002	03:50p	135,960
1e-7up_3.vel	11/7/2002	03:50p	66,000
1e-7up_4.vel	11/7/2002	03:50p	86,196
1e-7up_5.vel	11/7/2002	03:50p	66,000
1e-7up_6.vel	11/7/2002	03:50p	66,000
1e-7up_7.vel	11/7/2002	03:50p	107,349
1e-7up_8.vel	11/7/2002	03:50p	135,960
1e-7up_9.vel	11/7/2002	03:50p	197,868
Bb.fin	10/11/1996	09:50a	2,142

Table 7-1 List of Electronic Files in Attachment (Continued)

Name	Date	Time	Size (Byte)
Block.fin	1/24/2000	08:59a	5,768
Boucnr.fin	11/3/1999	06:01a	2,292
Cable.fin	11/3/1999	05:54a	2,323
Case19property1motion1step7.sav	9/10/2004	02:05p	15,324,347
Contact.fin	11/23/1999	05:27a	3,622
Domain.fin	11/23/1999	05:28a	1,756
Jmat.fin	11/3/1999	06:22a	4,334
model.dat	10/5/2004	07:46a	1,395
plot.dat	9/2/2004	12:39p	437
Reinf.fin	11/3/1999	05:58a	1,612
setup.fis	8/30/2004	10:24a	10,872
Str.fin	1/24/2000	09:08a	4,290
Support.fin	11/23/1999	05:29a	1,674
test.dat	8/9/2004	02:07p	330
times.fis	3/25/2004	01:46p	1,004
udec.lnk	9/10/2004	05:47a	711
Zmat.fin	11/3/1999	06:12a	3,971
Folder Case 20-22			
1e-6h1_10.vel	2/16/2004	09:45a	34,000
1e-6h1_11.vel	2/16/2004	09:45a	140,080
1e-6h1_12.vel	2/16/2004	09:45a	68,000
1e-6h1_13.vel	2/16/2004	09:45a	271,692
1e-6h1_14.vel	2/16/2004	09:46a	272,000
1e-6h1_1.vel	2/16/2004	09:45a	140,080
1e-6h1_16.vel	2/16/2004	09:46a	108,800
1e-6h1_2.vel	2/16/2004	09:46a	140,080
1e-6h1_3.vel	2/16/2004	09:46a	68,000
1e-6h1_4.vel	2/16/2004	09:46a	88,808
1e-6h1_5.vel	2/16/2004	09:46a	68,000
1e-6h1_6.vel	2/16/2004	09:46a	68,000
1e-6h1_7.vel	2/16/2004	09:46a	110,602
1e-6h1_8.vel	2/16/2004	09:46a	140,080
1e-6h1_9.vel	2/16/2004	09:46a	203,864
1e-6h2_1.vel	2/16/2004	09:46a	140,080
1e-6h2_10.vel	2/16/2004	09:46a	34,000
1e-6h2_11.vel	2/16/2004	09:46a	140,080
1e-6h2_12.vel	2/16/2004	09:46a	68,000
1e-6h2_13.vel	2/16/2004	09:46a	271,692
1e-6h2_14.vel	2/16/2004	09:46a	272,000
1e-6h2_16.vel	2/16/2004	09:46a	108,800
1e-6h2_2.vel	2/16/2004	09:47a	140,080
1e-6h2_3.vel	2/16/2004	09:47a	68,000
1e-6h2_4.vel	2/16/2004	09:47a	88,812
1e-6h2_5.vel	2/16/2004	09:47a	68,000

Table 7-1 List of Electronic Files in Attachment (Continued)

Name	Date	Time	Size (Byte)
1e-6h2_6.vel	2/16/2004	09:47a	68,000
1e-6h2_7.vel	2/16/2004	09:47a	110,602
1e-6h2_8.vel	2/16/2004	09:47a	140,080
1e-6h2_9.vel	2/16/2004	09:47a	203,862
1e-6up_1.vel	2/16/2004	09:47a	140,080
1e-6up_10.vel	2/16/2004	09:47a	34,000
1e-6up_11.vel	2/16/2004	09:47a	140,080
1e-6up_12.vel	2/16/2004	09:47a	68,000
1e-6up_13.vel	2/16/2004	09:47a	271,694
1e-6up_14.vel	2/16/2004	09:47a	272,000
1e-6up_16.vel	2/16/2004	09:47a	108,800
1e-6up_2.vel	2/16/2004	09:47a	140,080
1e-6up_3.vel	2/16/2004	09:47a	68,000
1e-6up_4.vel	2/16/2004	09:47a	88,806
1e-6up_5.vel	2/16/2004	09:47a	68,000
1e-6up_6.vel	2/16/2004	09:47a	68,000
1e-6up_7.vel	2/16/2004	09:48a	110,602
1e-6up_8.vel	2/16/2004	09:48a	140,080
1e-6up_9.vel	2/16/2004	09:48a	203,862
Bb.fin	10/11/1996	09:50a	2,142
Block.fin	1/24/2000	08:59a	5,768
Boucnr.fin	11/3/1999	06:01a	2,292
Cable.fin	11/3/1999	05:54a	2,323
Case20property1motion1step7.sav	8/30/2004	10:26p	16,982,535
Case21property1motion1step7.sav	8/31/2004	08:44a	15,321,191
Case22property1motion1step7.sav	8/31/2004	02:02p	15,321,191
Contact.fin	11/23/1999	05:27a	3,622
Domain.fin	11/23/1999	05:28a	1,756
Jmat.fin	11/3/1999	06:22a	4,334
model.dat	8/30/2004	10:35a	4,176
plot.dat	9/2/2004	12:39p	437
Reinf.fin	11/3/1999	05:58a	1,612
setup.fis	8/30/2004	10:37a	10,870
Str.fin	1/24/2000	09:08a	4,290
Support.fin	11/23/1999	05:29a	1,674
test.dat	8/9/2004	02:07p	330
times.fis	2/16/2004	09:48a	1,053
udec.lnk	9/8/2004	12:10p	411
Zmat.fin	11/3/1999	06:12a	3,971
Folder Case 23-25			
1e-7h1_10.vel	11/7/2002	03:44p	33,000
1e-7h1_1.vel	11/7/2002	03:44p	135,960
1e-7h1_11.vel	11/7/2002	03:44p	135,960
1e-7h1_12.vel	11/7/2002	03:44p	66,000

Table 7-1 List of Electronic Files in Attachment (Continued)

Name	Date	Time	Size (Byte)
1e-7h1_13.vel	11/7/2002	03:44p	263,703
1e-7h1_14.vel	11/7/2002	03:44p	264,000
1e-7h1_15.vel	11/7/2002	03:44p	198,033
1e-7h1_16.vel	11/7/2002	03:44p	105,600
1e-7h1_17.vel	11/7/2002	03:44p	198,000
1e-7h1_2.vel	11/7/2002	03:44p	135,960
1e-7h1_3.vel	11/7/2002	03:44p	66,000
1e-7h1_4.vel	11/7/2002	03:44p	86,196
1e-7h1_5.vel	11/7/2002	03:44p	66,000
1e-7h1_6.vel	11/7/2002	03:44p	66,000
1e-7h1_7.vel	11/7/2002	03:44p	107,349
1e-7h1_8.vel	11/7/2002	03:44p	135,960
1e-7h1_9.vel	11/7/2002	03:44p	197,868
1e-7h2_1.vel	11/7/2002	03:50p	135,960
1e-7h2_10.vel	11/7/2002	03:50p	33,000
1e-7h2_11.vel	11/7/2002	03:50p	135,960
1e-7h2_12.vel	11/7/2002	03:50p	66,000
1e-7h2_13.vel	11/7/2002	03:50p	263,703
1e-7h2_14.vel	11/7/2002	03:50p	264,000
1e-7h2_15.vel	11/7/2002	03:50p	198,033
1e-7h2_16.vel	11/7/2002	03:50p	105,600
1e-7h2_17.vel	11/7/2002	03:50p	198,000
1e-7h2_2.vel	11/7/2002	03:50p	135,960
1e-7h2_3.vel	11/7/2002	03:50p	66,000
1e-7h2_4.vel	11/7/2002	03:50p	86,196
1e-7h2_5.vel	3/25/2004	01:34p	68,000
1e-7h2_6.vel	11/7/2002	03:50p	66,000
1e-7h2_7.vel	11/7/2002	03:50p	107,349
1e-7h2_8.vel	11/7/2002	03:50p	135,960
1e-7h2_9.vel	11/7/2002	03:50p	197,868
1e-7up_1.vel	11/7/2002	03:50p	135,960
1e-7up_10.vel	11/7/2002	03:50p	33,000
1e-7up_11.vel	11/7/2002	03:50p	135,960
1e-7up_12.vel	11/7/2002	03:50p	66,000
1e-7up_13.vel	11/7/2002	03:50p	263,703
1e-7up_14.vel	11/7/2002	03:50p	264,000
1e-7up_15.vel	11/7/2002	03:50p	198,033
1e-7up_16.vel	11/7/2002	03:50p	105,600
1e-7up_17.vel	11/7/2002	03:50p	198,000
1e-7up_2.vel	11/7/2002	03:50p	135,960
1e-7up_3.vel	11/7/2002	03:50p	66,000
1e-7up_4.vel	11/7/2002	03:50p	86,196
1e-7up_5.vel	11/7/2002	03:50p	66,000
1e-7up_6.vel	11/7/2002	03:50p	66,000

Table 7-1 List of Electronic Files in Attachment (Continued)

Name	Date	Time	Size (Byte)
1e-7up_7.vel	11/7/2002	03:50p	107,349
1e-7up_8.vel	11/7/2002	03:50p	135,960
1e-7up_9.vel	11/7/2002	03:50p	197,868
Bb.fin	10/11/1996	09:50a	2,142
Block.fin	1/24/2000	08:59a	5,768
Boucnr.fin	11/3/1999	06:01a	2,292
Cable.fin	11/3/1999	05:54a	2,323
Case23property1motion1step7.sav	8/30/2004	02:03p	15,324,951
Case24property1motion1step7.sav	8/31/2004	03:05a	15,321,707
Case25property1motion1step7.sav	8/31/2004	11:08a	15,321,763
Contact.fin	11/23/1999	05:27a	3,622
Domain.fin	11/23/1999	05:28a	1,756
Jmat.fin	11/3/1999	06:22a	4,334
model.dat	8/20/2004	02:32p	5,106
plot.dat	9/2/2004	12:39p	437
Reinf.fin	11/3/1999	05:58a	1,612
setup.fis	8/30/2004	10:49a	11,507
Str.fin	1/24/2000	09:08a	4,290
Support.fin	11/23/1999	05:29a	1,674
times.fis	3/25/2004	01:46p	1,004
udec.lnk	9/8/2004	11:06a	615
Zmat.fin	11/3/1999	06:12a	3,971
Folder Case 26			
1e-6h1_10.vel	2/16/2004	09:45a	34,000
1e-6h1_11.vel	2/16/2004	09:45a	140,080
1e-6h1_12.vel	2/16/2004	09:45a	68,000
1e-6h1_13.vel	2/16/2004	09:45a	271,692
1e-6h1_14.vel	2/16/2004	09:46a	272,000
1e-6h1_1.vel	2/16/2004	09:45a	140,080
1e-6h1_16.vel	2/16/2004	09:46a	108,800
1e-6h1_2.vel	2/16/2004	09:46a	140,080
1e-6h1_3.vel	2/16/2004	09:46a	68,000
1e-6h1_4.vel	2/16/2004	09:46a	88,808
1e-6h1_5.vel	2/16/2004	09:46a	68,000
1e-6h1_6.vel	2/16/2004	09:46a	68,000
1e-6h1_7.vel	2/16/2004	09:46a	110,602
1e-6h1_8.vel	2/16/2004	09:46a	140,080
1e-6h1_9.vel	2/16/2004	09:46a	203,864
1e-6h2_1.vel	2/16/2004	09:46a	140,080
1e-6h2_10.vel	2/16/2004	09:46a	34,000
1e-6h2_11.vel	2/16/2004	09:46a	140,080
1e-6h2_12.vel	2/16/2004	09:46a	68,000
1e-6h2_13.vel	2/16/2004	09:46a	271,692
1e-6h2_14.vel	2/16/2004	09:46a	272,000

Table 7-1 List of Electronic Files in Attachment (Continued)

Name	Date	Time	Size (Byte)
1e-6h2_16.vel	2/16/2004	09:46a	108,800
1e-6h2_2.vel	2/16/2004	09:47a	140,080
1e-6h2_3.vel	2/16/2004	09:47a	68,000
1e-6h2_4.vel	2/16/2004	09:47a	88,812
1e-6h2_5.vel	2/16/2004	09:47a	68,000
1e-6h2_6.vel	2/16/2004	09:47a	68,000
1e-6h2_7.vel	2/16/2004	09:47a	110,602
1e-6h2_8.vel	2/16/2004	09:47a	140,080
1e-6h2_9.vel	2/16/2004	09:47a	203,862
1e-6up_1.vel	2/16/2004	09:47a	140,080
1e-6up_10.vel	2/16/2004	09:47a	34,000
1e-6up_11.vel	2/16/2004	09:47a	140,080
1e-6up_12.vel	2/16/2004	09:47a	68,000
1e-6up_13.vel	2/16/2004	09:47a	271,694
1e-6up_14.vel	2/16/2004	09:47a	272,000
1e-6up_16.vel	2/16/2004	09:47a	108,800
1e-6up_2.vel	2/16/2004	09:47a	140,080
1e-6up_3.vel	2/16/2004	09:47a	68,000
1e-6up_4.vel	2/16/2004	09:47a	88,806
1e-6up_5.vel	2/16/2004	09:47a	68,000
1e-6up_6.vel	2/16/2004	09:47a	68,000
1e-6up_7.vel	2/16/2004	09:48a	110,602
1e-6up_8.vel	2/16/2004	09:48a	140,080
1e-6up_9.vel	2/16/2004	09:48a	203,862
Bb.fin	10/11/1996	09:50a	2,142
Block.fin	1/24/2000	08:59a	5,768
Boucnr.fin	11/3/1999	06:01a	2,292
Cable.fin	11/3/1999	05:54a	2,323
Case26property1motion1step7.sav	8/31/2004	03:40p	15,322,087
Contact.fin	11/23/1999	05:27a	3,622
Domain.fin	11/23/1999	05:28a	1,756
Jmat.fin	11/3/1999	06:22a	4,334
model.dat	8/31/2004	08:00a	1,401
plot.dat	9/2/2004	12:39p	437
Reinf.fin	11/3/1999	05:58a	1,612
setup.fis	8/30/2004	10:34a	10,870
Str.fin	1/24/2000	09:08a	4,290
Support.fin	11/23/1999	05:29a	1,674
test.dat	8/9/2004	02:07p	330
times.fis	2/16/2004	09:48a	1,053
udec.lnk	8/30/2004	10:35a	411
Zmat.fin	11/3/1999	06:12a	3,971
Folder Case 27			

Table 7-1 List of Electronic Files in Attachment (Continued)

Name	Date	Time	Size (Byte)
1e-7h1_10.vel	11/7/2002	03:44p	33,000
1e-7h1_1.vel	11/7/2002	03:44p	135,960
1e-7h1_11.vel	11/7/2002	03:44p	135,960
1e-7h1_12.vel	11/7/2002	03:44p	66,000
1e-7h1_13.vel	11/7/2002	03:44p	263,703
1e-7h1_14.vel	11/7/2002	03:44p	264,000
1e-7h1_15.vel	11/7/2002	03:44p	198,033
1e-7h1_16.vel	11/7/2002	03:44p	105,600
1e-7h1_17.vel	11/7/2002	03:44p	198,000
1e-7h1_2.vel	11/7/2002	03:44p	135,960
1e-7h1_3.vel	11/7/2002	03:44p	66,000
1e-7h1_4.vel	11/7/2002	03:44p	86,196
1e-7h1_5.vel	11/7/2002	03:44p	66,000
1e-7h1_6.vel	11/7/2002	03:44p	66,000
1e-7h1_7.vel	11/7/2002	03:44p	107,349
1e-7h1_8.vel	11/7/2002	03:44p	135,960
1e-7h1_9.vel	11/7/2002	03:44p	197,868
1e-7h2_1.vel	11/7/2002	03:50p	135,960
1e-7h2_10.vel	11/7/2002	03:50p	33,000
1e-7h2_11.vel	11/7/2002	03:50p	135,960
1e-7h2_12.vel	11/7/2002	03:50p	66,000
1e-7h2_13.vel	11/7/2002	03:50p	263,703
1e-7h2_14.vel	11/7/2002	03:50p	264,000
1e-7h2_15.vel	11/7/2002	03:50p	198,033
1e-7h2_16.vel	11/7/2002	03:50p	105,600
1e-7h2_17.vel	11/7/2002	03:50p	198,000
1e-7h2_2.vel	11/7/2002	03:50p	135,960
1e-7h2_3.vel	11/7/2002	03:50p	66,000
1e-7h2_4.vel	11/7/2002	03:50p	86,196
1e-7h2_5.vel	3/25/2004	01:34p	68,000
1e-7h2_6.vel	11/7/2002	03:50p	66,000
1e-7h2_7.vel	11/7/2002	03:50p	107,349
1e-7h2_8.vel	11/7/2002	03:50p	135,960
1e-7h2_9.vel	11/7/2002	03:50p	197,868
1e-7up_1.vel	11/7/2002	03:50p	135,960
1e-7up_10.vel	11/7/2002	03:50p	33,000
1e-7up_11.vel	11/7/2002	03:50p	135,960
1e-7up_12.vel	11/7/2002	03:50p	66,000
1e-7up_13.vel	11/7/2002	03:50p	263,703
1e-7up_14.vel	11/7/2002	03:50p	264,000
1e-7up_15.vel	11/7/2002	03:50p	198,033
1e-7up_16.vel	11/7/2002	03:50p	105,600
1e-7up_17.vel	11/7/2002	03:50p	198,000
1e-7up_2.vel	11/7/2002	03:50p	135,960

Table 7-1 List of Electronic Files in Attachment (Continued)

Name	Date	Time	Size (Byte)
1e-7up_3.vel	11/7/2002	03:50p	66,000
1e-7up_4.vel	11/7/2002	03:50p	86,196
1e-7up_5.vel	11/7/2002	03:50p	66,000
1e-7up_6.vel	11/7/2002	03:50p	66,000
1e-7up_7.vel	11/7/2002	03:50p	107,349
1e-7up_8.vel	11/7/2002	03:50p	135,960
1e-7up_9.vel	11/7/2002	03:50p	197,868
Bb.fin	10/11/1996	09:50a	2,142
Block.fin	1/24/2000	08:59a	5,768
Boucnr.fin	11/3/1999	06:01a	2,292
Cable.fin	11/3/1999	05:54a	2,323
Case27property1motion1step7.sav	8/31/2004	03:30p	15,325,331
Contact.fin	11/23/1999	05:27a	3,622
Domain.fin	11/23/1999	05:28a	1,756
Jmat.fin	11/3/1999	06:22a	4,334
model.dat	10/5/2004	07:55a	1,394
plot.dat	9/2/2004	12:39p	437
Reinf.fin	11/3/1999	05:58a	1,612
setup.fis	8/30/2004	10:24a	10,872
Str.fin	1/24/2000	09:08a	4,290
Support.fin	11/23/1999	05:29a	1,674
test.dat	8/9/2004	02:07p	330
times.fis	3/25/2004	01:46p	1,004
udec.lnk	8/19/2004	01:58p	711
Zmat.fin	11/3/1999	06:12a	3,971
Folder Case 28			
1e-7h1_10.vel	11/7/2002	03:44p	33,000
1e-7h1_1.vel	11/7/2002	03:44p	135,960
1e-7h1_11.vel	11/7/2002	03:44p	135,960
1e-7h1_12.vel	11/7/2002	03:44p	66,000
1e-7h1_13.vel	11/7/2002	03:44p	263,703
1e-7h1_14.vel	11/7/2002	03:44p	264,000
1e-7h1_15.vel	11/7/2002	03:44p	198,033
1e-7h1_16.vel	11/7/2002	03:44p	105,600
1e-7h1_17.vel	11/7/2002	03:44p	198,000
1e-7h1_2.vel	11/7/2002	03:44p	135,960
1e-7h1_3.vel	11/7/2002	03:44p	66,000
1e-7h1_4.vel	11/7/2002	03:44p	86,196
1e-7h1_5.vel	11/7/2002	03:44p	66,000
1e-7h1_6.vel	11/7/2002	03:44p	66,000
1e-7h1_7.vel	11/7/2002	03:44p	107,349
1e-7h1_8.vel	11/7/2002	03:44p	135,960
1e-7h1_9.vel	11/7/2002	03:44p	197,868
1e-7h2_1.vel	11/7/2002	03:50p	135,960

Table 7-1 List of Electronic Files in Attachment (Continued)

Name	Date	Time	Size (Byte)
1e-7h2_10.vel	11/7/2002	03:50p	33,000
1e-7h2_11.vel	11/7/2002	03:50p	135,960
1e-7h2_12.vel	11/7/2002	03:50p	66,000
1e-7h2_13.vel	11/7/2002	03:50p	263,703
1e-7h2_14.vel	11/7/2002	03:50p	264,000
1e-7h2_15.vel	11/7/2002	03:50p	198,033
1e-7h2_16.vel	11/7/2002	03:50p	105,600
1e-7h2_17.vel	11/7/2002	03:50p	198,000
1e-7h2_2.vel	11/7/2002	03:50p	135,960
1e-7h2_3.vel	11/7/2002	03:50p	66,000
1e-7h2_4.vel	11/7/2002	03:50p	86,196
1e-7h2_5.vel	3/25/2004	01:34p	68,000
1e-7h2_6.vel	11/7/2002	03:50p	66,000
1e-7h2_7.vel	11/7/2002	03:50p	107,349
1e-7h2_8.vel	11/7/2002	03:50p	135,960
1e-7h2_9.vel	11/7/2002	03:50p	197,868
1e-7up_1.vel	11/7/2002	03:50p	135,960
1e-7up_10.vel	11/7/2002	03:50p	33,000
1e-7up_11.vel	11/7/2002	03:50p	135,960
1e-7up_12.vel	11/7/2002	03:50p	66,000
1e-7up_13.vel	11/7/2002	03:50p	263,703
1e-7up_14.vel	11/7/2002	03:50p	264,000
1e-7up_15.vel	11/7/2002	03:50p	198,033
1e-7up_16.vel	11/7/2002	03:50p	105,600
1e-7up_17.vel	11/7/2002	03:50p	198,000
1e-7up_2.vel	11/7/2002	03:50p	135,960
1e-7up_3.vel	11/7/2002	03:50p	66,000
1e-7up_4.vel	11/7/2002	03:50p	86,196
1e-7up_5.vel	11/7/2002	03:50p	66,000
1e-7up_6.vel	11/7/2002	03:50p	66,000
1e-7up_7.vel	11/7/2002	03:50p	107,349
1e-7up_8.vel	11/7/2002	03:50p	135,960
1e-7up_9.vel	11/7/2002	03:50p	197,868
Bb.fin	10/11/1996	09:50a	2,142
Block.fin	1/24/2000	08:59a	5,768
Boucnr.fin	11/3/1999	06:01a	2,292
Cable.fin	11/3/1999	05:54a	2,323
Case28property1motion1step7.sav	9/1/2004	03:51p	15,332,199
Contact.fin	11/23/1999	05:27a	3,622
Domain.fin	11/23/1999	05:28a	1,756
Jmat.fin	11/3/1999	06:22a	4,334
model.dat	9/1/2004	06:38a	4,541
plot.dat	9/2/2004	12:39p	437
Reinf.fin	11/3/1999	05:58a	1,612

Table 7-1 List of Electronic Files in Attachment (Continued)

Name	Date	Time	Size (Byte)
setup.fis	9/1/2004	06:14a	12,677
Str.fin	1/24/2000	09:08a	4,290
Support.fin	11/23/1999	05:29a	1,674
test.dat	8/9/2004	02:07p	330
times.fis	3/25/2004	01:46p	1,004
udec.lnk	8/31/2004	02:22p	711
Zmat.fin	11/3/1999	06:12a	3,971
Folder Case 5-8			
1e-7h1_10.vel	11/7/2002	03:44p	33,000
1e-7h1_11.vel	11/7/2002	03:44p	135,960
1e-7h1_12.vel	11/7/2002	03:44p	66,000
1e-7h1_13.vel	11/7/2002	03:44p	263,703
1e-7h1_1.vel	11/7/2002	03:44p	135,960
1e-7h1_14.vel	11/7/2002	03:44p	264,000
1e-7h1_15.vel	11/7/2002	03:44p	198,033
1e-7h1_16.vel	11/7/2002	03:44p	105,600
1e-7h1_17.vel	11/7/2002	03:44p	198,000
1e-7h1_2.vel	11/7/2002	03:44p	135,960
1e-7h1_3.vel	11/7/2002	03:44p	66,000
1e-7h1_4.vel	11/7/2002	03:44p	86,196
1e-7h1_5.vel	11/7/2002	03:44p	66,000
1e-7h1_6.vel	11/7/2002	03:44p	66,000
1e-7h1_7.vel	11/7/2002	03:44p	107,349
1e-7h1_8.vel	11/7/2002	03:44p	135,960
1e-7h1_9.vel	11/7/2002	03:44p	197,868
1e-7h2_1.vel	11/7/2002	03:50p	135,960
1e-7h2_10.vel	11/7/2002	03:50p	33,000
1e-7h2_11.vel	11/7/2002	03:50p	135,960
1e-7h2_12.vel	11/7/2002	03:50p	66,000
1e-7h2_13.vel	11/7/2002	03:50p	263,703
1e-7h2_14.vel	11/7/2002	03:50p	264,000
1e-7h2_15.vel	11/7/2002	03:50p	198,033
1e-7h2_16.vel	11/7/2002	03:50p	105,600
1e-7h2_17.vel	11/7/2002	03:50p	198,000
1e-7h2_2.vel	11/7/2002	03:50p	135,960
1e-7h2_3.vel	11/7/2002	03:50p	66,000
1e-7h2_4.vel	11/7/2002	03:50p	86,196
1e-7h2_5.vel	3/25/2004	01:34p	68,000
1e-7h2_6.vel	11/7/2002	03:50p	66,000
1e-7h2_7.vel	11/7/2002	03:50p	107,349
1e-7h2_8.vel	11/7/2002	03:50p	135,960
1e-7h2_9.vel	11/7/2002	03:50p	197,868
1e-7up_1.vel	11/7/2002	03:50p	135,960
1e-7up_10.vel	11/7/2002	03:50p	33,000

Table 7-1 List of Electronic Files in Attachment (Continued)

Name	Date	Time	Size (Byte)
1e-7up_11.vel	11/7/2002	03:50p	135,960
1e-7up_12.vel	11/7/2002	03:50p	66,000
1e-7up_13.vel	11/7/2002	03:50p	263,703
1e-7up_14.vel	11/7/2002	03:50p	264,000
1e-7up_15.vel	11/7/2002	03:50p	198,033
1e-7up_16.vel	11/7/2002	03:50p	105,600
1e-7up_17.vel	11/7/2002	03:50p	198,000
1e-7up_2.vel	11/7/2002	03:50p	135,960
1e-7up_3.vel	11/7/2002	03:50p	66,000
1e-7up_4.vel	11/7/2002	03:50p	86,196
1e-7up_5.vel	11/7/2002	03:50p	66,000
1e-7up_6.vel	11/7/2002	03:50p	66,000
1e-7up_7.vel	11/7/2002	03:50p	107,349
1e-7up_8.vel	11/7/2002	03:50p	135,960
1e-7up_9.vel	11/7/2002	03:50p	197,868
Bb.fin	10/11/1996	09:50a	2,142
Block.fin	1/24/2000	08:59a	5,768
Boucnr.fin	11/3/1999	06:01a	2,292
Cable.fin	11/3/1999	05:54a	2,323
Case5property1motion1step7.sav	8/30/2004	01:07p	15,323,267
Case6property1motion10step8.sav	8/30/2004	04:12p	19,355,927
Case7property1motion10step8.sav	8/31/2004	12:18a	19,356,027
Case8property1motion10step8.sav	8/31/2004	03:23a	19,355,879
Contact.fin	11/23/1999	05:27a	3,622
Domain.fin	11/23/1999	05:28a	1,756
Jmat.fin	11/3/1999	06:22a	4,334
model.dat	8/19/2004	01:55p	5,549
Case7property1motion10movie1_056.pcx	8/30/2004	10:16p	119,088
plot.dat	9/2/2004	12:39p	437
Reinf.fin	11/3/1999	05:58a	1,612
setup.fis	8/30/2004	10:24a	10,872
Str.fin	1/24/2000	09:08a	4,290
Support.fin	11/23/1999	05:29a	1,674
test.dat	8/9/2004	02:07p	330
times.fis	3/25/2004	01:46p	1,004
udec.lnk	8/19/2004	01:58p	711
Zmat.fin	11/3/1999	06:12a	3,971
Folder Case 9-10			
1e-6h1_10.vel	2/16/2004	09:45a	34,000
1e-6h1_11.vel	2/16/2004	09:45a	140,080
1e-6h1_12.vel	2/16/2004	09:45a	68,000
1e-6h1_13.vel	2/16/2004	09:45a	271,692
1e-6h1_14.vel	2/16/2004	09:46a	272,000
1e-6h1_1.vel	2/16/2004	09:45a	140,080

Table 7-1 List of Electronic Files in Attachment (Continued)

Name	Date	Time	Size (Byte)
1e-6h1_16.vel	2/16/2004	09:46a	108,800
1e-6h1_2.vel	2/16/2004	09:46a	140,080
1e-6h1_3.vel	2/16/2004	09:46a	68,000
1e-6h1_4.vel	2/16/2004	09:46a	88,808
1e-6h1_5.vel	2/16/2004	09:46a	68,000
1e-6h1_6.vel	2/16/2004	09:46a	68,000
1e-6h1_7.vel	2/16/2004	09:46a	110,602
1e-6h1_8.vel	2/16/2004	09:46a	140,080
1e-6h1_9.vel	2/16/2004	09:46a	203,864
1e-6h2_1.vel	2/16/2004	09:46a	140,080
1e-6h2_10.vel	2/16/2004	09:46a	34,000
1e-6h2_11.vel	2/16/2004	09:46a	140,080
1e-6h2_12.vel	2/16/2004	09:46a	68,000
1e-6h2_13.vel	2/16/2004	09:46a	271,692
1e-6h2_14.vel	2/16/2004	09:46a	272,000
1e-6h2_16.vel	2/16/2004	09:46a	108,800
1e-6h2_2.vel	2/16/2004	09:47a	140,080
1e-6h2_3.vel	2/16/2004	09:47a	68,000
1e-6h2_4.vel	2/16/2004	09:47a	88,812
1e-6h2_5.vel	2/16/2004	09:47a	68,000
1e-6h2_6.vel	2/16/2004	09:47a	68,000
1e-6h2_7.vel	2/16/2004	09:47a	110,602
1e-6h2_8.vel	2/16/2004	09:47a	140,080
1e-6h2_9.vel	2/16/2004	09:47a	203,862
1e-6up_1.vel	2/16/2004	09:47a	140,080
1e-6up_10.vel	2/16/2004	09:47a	34,000
1e-6up_11.vel	2/16/2004	09:47a	140,080
1e-6up_12.vel	2/16/2004	09:47a	68,000
1e-6up_13.vel	2/16/2004	09:47a	271,694
1e-6up_14.vel	2/16/2004	09:47a	272,000
1e-6up_16.vel	2/16/2004	09:47a	108,800
1e-6up_2.vel	2/16/2004	09:47a	140,080
1e-6up_3.vel	2/16/2004	09:47a	68,000
1e-6up_4.vel	2/16/2004	09:47a	88,806
1e-6up_5.vel	2/16/2004	09:47a	68,000
1e-6up_6.vel	2/16/2004	09:47a	68,000
1e-6up_7.vel	2/16/2004	09:48a	110,602
1e-6up_8.vel	2/16/2004	09:48a	140,080
1e-6up_9.vel	2/16/2004	09:48a	203,862
Bb.fin	10/11/1996	09:50a	2,142
Block.fin	1/24/2000	08:59a	5,768
Boucnr.fin	11/3/1999	06:01a	2,292
Cable.fin	11/3/1999	05:54a	2,323
Case10property1motion1step7.sav	8/31/2004	09:52a	15,321,191

Table 7-1 List of Electronic Files in Attachment (Continued)

Name	Date	Time	Size (Byte)
Case9property1motion1step7.sav	8/31/2004	01:34a	38,658,855
Contact.fin	11/23/1999	05:27a	3,622
Domain.fin	11/23/1999	05:28a	1,756
Jmat.fin	11/3/1999	06:22a	4,334
model.dat	8/19/2004	02:00p	2,805
plot.dat	9/2/2004	12:39p	437
Reinf.fin	11/3/1999	05:58a	1,612
setup.fis	8/30/2004	10:22a	10,869
Str.fin	1/24/2000	09:08a	4,290
Support.fin	11/23/1999	05:29a	1,674
test.dat	8/9/2004	02:07p	330
times.fis	2/16/2004	09:48a	1,053
udec.lnk	8/19/2004	01:57p	711
Zmat.fin	11/3/1999	06:12a	3,971
Folder three DS 1e-6			
1e-6h1_10.vel	2/16/2004	09:45a	34,000
1e-6h1_11.vel	2/16/2004	09:45a	140,080
1e-6h1_12.vel	2/16/2004	09:45a	68,000
1e-6h1_13.vel	2/16/2004	09:45a	271,692
1e-6h1_1.vel	2/16/2004	09:45a	140,080
1e-6h1_14.vel	2/16/2004	09:46a	272,000
1e-6h1_16.vel	2/16/2004	09:46a	108,800
1e-6h1_2.vel	2/16/2004	09:46a	140,080
1e-6h1_3.vel	2/16/2004	09:46a	68,000
1e-6h1_4.vel	2/16/2004	09:46a	88,808
1e-6h1_5.vel	2/16/2004	09:46a	68,000
1e-6h1_6.vel	2/16/2004	09:46a	68,000
1e-6h1_7.vel	2/16/2004	09:46a	110,602
1e-6h1_8.vel	2/16/2004	09:46a	140,080
1e-6h1_9.vel	2/16/2004	09:46a	203,864
1e-6h2_1.vel	2/16/2004	09:46a	140,080
1e-6h2_10.vel	2/16/2004	09:46a	34,000
1e-6h2_11.vel	2/16/2004	09:46a	140,080
1e-6h2_12.vel	2/16/2004	09:46a	68,000
1e-6h2_13.vel	2/16/2004	09:46a	271,692
1e-6h2_14.vel	2/16/2004	09:46a	272,000
1e-6h2_16.vel	2/16/2004	09:46a	108,800
1e-6h2_2.vel	2/16/2004	09:47a	140,080
1e-6h2_3.vel	2/16/2004	09:47a	68,000
1e-6h2_4.vel	2/16/2004	09:47a	88,812
1e-6h2_5.vel	2/16/2004	09:47a	68,000
1e-6h2_6.vel	2/16/2004	09:47a	68,000
1e-6h2_7.vel	2/16/2004	09:47a	110,602
1e-6h2_8.vel	2/16/2004	09:47a	140,080

Table 7-1 List of Electronic Files in Attachment (Continued)

Name	Date	Time	Size (Byte)
1e-6h2_9.vel	2/16/2004	09:47a	203,862
1e-6up_1.vel	2/16/2004	09:47a	140,080
1e-6up_10.vel	2/16/2004	09:47a	34,000
1e-6up_11.vel	2/16/2004	09:47a	140,080
1e-6up_12.vel	2/16/2004	09:47a	68,000
1e-6up_13.vel	2/16/2004	09:47a	271,694
1e-6up_14.vel	2/16/2004	09:47a	272,000
1e-6up_16.vel	2/16/2004	09:47a	108,800
1e-6up_2.vel	2/16/2004	09:47a	140,080
1e-6up_3.vel	2/16/2004	09:47a	68,000
1e-6up_4.vel	2/16/2004	09:47a	88,806
1e-6up_5.vel	2/16/2004	09:47a	68,000
1e-6up_6.vel	2/16/2004	09:47a	68,000
1e-6up_7.vel	2/16/2004	09:48a	110,602
1e-6up_8.vel	2/16/2004	09:48a	140,080
1e-6up_9.vel	2/16/2004	09:48a	203,862
1e-7h1_1.vel	11/7/2002	03:44p	135,960
1e-7h1_10.vel	11/7/2002	03:44p	33,000
1e-7h1_11.vel	11/7/2002	03:44p	135,960
1e-7h1_12.vel	11/7/2002	03:44p	66,000
1e-7h1_13.vel	11/7/2002	03:44p	263,703
1e-7h1_14.vel	11/7/2002	03:44p	264,000
1e-7h1_15.vel	11/7/2002	03:44p	198,033
1e-7h1_16.vel	11/7/2002	03:44p	105,600
1e-7h1_17.vel	11/7/2002	03:44p	198,000
1e-7h1_2.vel	11/7/2002	03:44p	135,960
1e-7h1_3.vel	11/7/2002	03:44p	66,000
1e-7h1_4.vel	11/7/2002	03:44p	86,196
1e-7h1_5.vel	11/7/2002	03:44p	66,000
1e-7h1_6.vel	11/7/2002	03:44p	66,000
1e-7h1_7.vel	11/7/2002	03:44p	107,349
1e-7h1_8.vel	11/7/2002	03:44p	135,960
1e-7h1_9.vel	11/7/2002	03:44p	197,868
1e-7h2_1.vel	11/7/2002	03:50p	135,960
1e-7h2_10.vel	11/7/2002	03:50p	33,000
1e-7h2_11.vel	11/7/2002	03:50p	135,960
1e-7h2_12.vel	11/7/2002	03:50p	66,000
1e-7h2_13.vel	11/7/2002	03:50p	263,703
1e-7h2_14.vel	11/7/2002	03:50p	264,000
1e-7h2_15.vel	11/7/2002	03:50p	198,033
1e-7h2_16.vel	11/7/2002	03:50p	105,600
1e-7h2_17.vel	11/7/2002	03:50p	198,000
1e-7h2_2.vel	11/7/2002	03:50p	135,960
1e-7h2_3.vel	11/7/2002	03:50p	66,000

Table 7-1 List of Electronic Files in Attachment (Continued)

Name	Date	Time	Size (Byte)
1e-7h2_4.vel	11/7/2002	03:50p	86,196
1e-7h2_5.vel	3/25/2004	01:34p	68,000
1e-7h2_6.vel	11/7/2002	03:50p	66,000
1e-7h2_7.vel	11/7/2002	03:50p	107,349
1e-7h2_8.vel	11/7/2002	03:50p	135,960
1e-7h2_9.vel	11/7/2002	03:50p	197,868
1e-7up_1.vel	11/7/2002	03:50p	135,960
1e-7up_10.vel	11/7/2002	03:50p	33,000
1e-7up_11.vel	11/7/2002	03:50p	135,960
1e-7up_12.vel	11/7/2002	03:50p	66,000
1e-7up_13.vel	11/7/2002	03:50p	263,703
1e-7up_14.vel	11/7/2002	03:50p	264,000
1e-7up_15.vel	11/7/2002	03:50p	198,033
1e-7up_16.vel	11/7/2002	03:50p	105,600
1e-7up_17.vel	11/7/2002	03:50p	198,000
1e-7up_2.vel	11/7/2002	03:50p	135,960
1e-7up_3.vel	11/7/2002	03:50p	66,000
1e-7up_4.vel	11/7/2002	03:50p	86,196
1e-7up_5.vel	11/7/2002	03:50p	66,000
1e-7up_6.vel	11/7/2002	03:50p	66,000
1e-7up_7.vel	11/7/2002	03:50p	107,349
1e-7up_8.vel	11/7/2002	03:50p	135,960
1e-7up_9.vel	11/7/2002	03:50p	197,868
Bb.fin	10/11/1996	09:50a	2,142
Block.fin	1/24/2000	08:59a	5,768
Boucnr.fin	11/3/1999	06:01a	2,292
Cable.fin	11/3/1999	05:54a	2,323
Case5property1motion1step7.sav	8/31/2004	09:18a	2,080,523
Contact.fin	11/23/1999	05:27a	3,622
Domain.fin	11/23/1999	05:28a	1,756
geom.sav	10/5/2004	08:03a	298,683
Jmat.fin	11/3/1999	06:22a	4,334
model.dat	8/31/2004	07:22a	1,580
model1.dat	10/5/2004	08:01a	1,585
plot.dat	8/29/2004	08:35a	318
Reinf.fin	11/3/1999	05:58a	1,612
setup.fis	8/30/2004	01:45p	11,276
Str.fin	1/24/2000	09:08a	4,290
Support.fin	11/23/1999	05:29a	1,674
test.dat	8/9/2004	02:07p	330
times.fis	2/16/2004	09:48a	1,053
udec.lnk	8/30/2004	10:35a	411
Zmat.fin	11/3/1999	06:12a	3,971

Table 7-1 List of Electronic Files in Attachment (Continued)

Name	Date	Time	Size (Byte)
Folder three DS 1e-7			
1e-7h1_10.vel	11/7/2002	02:44p	33,000
1e-7h1_1.vel	11/7/2002	02:44p	135,960
1e-7h1_11.vel	11/7/2002	02:44p	135,960
1e-7h1_12.vel	11/7/2002	02:44p	66,000
1e-7h1_13.vel	11/7/2002	02:44p	263,703
1e-7h1_14.vel	11/7/2002	02:44p	264,000
1e-7h1_15.vel	11/7/2002	02:44p	198,033
1e-7h1_16.vel	11/7/2002	02:44p	105,600
1e-7h1_17.vel	11/7/2002	02:44p	198,000
1e-7h1_2.vel	11/7/2002	02:44p	135,960
1e-7h1_3.vel	11/7/2002	02:44p	66,000
1e-7h1_4.vel	11/7/2002	02:44p	86,196
1e-7h1_5.vel	11/7/2002	02:44p	66,000
1e-7h1_6.vel	11/7/2002	02:44p	66,000
1e-7h1_7.vel	11/7/2002	02:44p	107,349
1e-7h1_8.vel	11/7/2002	02:44p	135,960
1e-7h1_9.vel	11/7/2002	02:44p	197,868
1e-7h2_1.vel	11/7/2002	02:50p	135,960
1e-7h2_10.vel	11/7/2002	02:50p	33,000
1e-7h2_11.vel	11/7/2002	02:50p	135,960
1e-7h2_12.vel	11/7/2002	02:50p	66,000
1e-7h2_13.vel	11/7/2002	02:50p	263,703
1e-7h2_14.vel	11/7/2002	02:50p	264,000
1e-7h2_15.vel	11/7/2002	02:50p	198,033
1e-7h2_16.vel	11/7/2002	02:50p	105,600
1e-7h2_17.vel	11/7/2002	02:50p	198,000
1e-7h2_2.vel	11/7/2002	02:50p	135,960
1e-7h2_3.vel	11/7/2002	02:50p	66,000
1e-7h2_4.vel	11/7/2002	02:50p	86,196
1e-7h2_5.vel	3/25/2004	12:34p	68,000
1e-7h2_6.vel	11/7/2002	02:50p	66,000
1e-7h2_7.vel	11/7/2002	02:50p	107,349
1e-7h2_8.vel	11/7/2002	02:50p	135,960
1e-7h2_9.vel	11/7/2002	02:50p	197,868
1e-7up_1.vel	11/7/2002	02:50p	135,960
1e-7up_10.vel	11/7/2002	02:50p	33,000
1e-7up_11.vel	11/7/2002	02:50p	135,960
1e-7up_12.vel	11/7/2002	02:50p	66,000
1e-7up_13.vel	11/7/2002	02:50p	263,703
1e-7up_14.vel	11/7/2002	02:50p	264,000
1e-7up_15.vel	11/7/2002	02:50p	198,033
1e-7up_16.vel	11/7/2002	02:50p	105,600
1e-7up_17.vel	11/7/2002	02:50p	198,000

Table 7-1 List of Electronic Files in Attachment (Continued)

Name	Date	Time	Size (Byte)
1e-7up_2.vel	11/7/2002	02:50p	135,960
1e-7up_3.vel	11/7/2002	02:50p	66,000
1e-7up_4.vel	11/7/2002	02:50p	86,196
1e-7up_5.vel	11/7/2002	02:50p	66,000
1e-7up_6.vel	11/7/2002	02:50p	66,000
1e-7up_7.vel	11/7/2002	02:50p	107,349
1e-7up_8.vel	11/7/2002	02:50p	135,960
1e-7up_9.vel	11/7/2002	02:50p	197,868
Bb.fin	10/11/1996	09:50a	2,142
Block.fin	1/24/2000	07:59a	5,768
Boucnr.fin	11/3/1999	05:01a	2,292
Cable.fin	11/3/1999	04:54a	2,323
Case5property1motion1step7.sav	8/31/2004	09:01a	2,083,023
Contact.fin	11/23/1999	04:27a	3,622
Domain.fin	11/23/1999	04:28a	1,756
Jmat.fin	11/3/1999	05:22a	4,334
model.dat	8/31/2004	07:12a	1,582
plot.dat	8/29/2004	08:35a	318
Reinf.fin	11/3/1999	04:58a	1,612
setup.fis	8/30/2004	01:29p	11,278
Str.fin	1/24/2000	08:08a	4,290
Support.fin	11/23/1999	04:29a	1,674
test.dat	8/9/2004	02:07p	330
times.fis	3/25/2004	12:46p	1,004
udec.lnk	8/30/2004	01:26p	777
Zmat.fin	11/3/1999	05:12a	3,971

ATTACHMENT A

COMPACT DISK 1 0F 1 OF FILES FROM UDEC KINEMATIC ANALYSIS

INTENTIONALLY LEFT BLANK

ATTACHMENT A

COMPACT DISK 1 0F 1 OF FILES FROM UDEC KINEMATIC ANALYSIS

INTENTIONALLY LEFT BLANK